Multimedia Analysis

Over 3G Wireless Interface

Jeremy Yee Chiat TAY

B.E. (Electronics) (Hons) / B.Inf.Tech
Queensland University of Technology

School of Electrical and Electronic systems Engineering
Queensland University of Technology
G.P.O. Box 2434, Brisbane, QLD, 4001, Australia

Abstract

Recent rapid advancements in mobile communication and emerging demands for complicated multimedia content and services over mobile systems have caused a dramatic increase in research interest in this area. Among the topics covering multimedia service performance over the wireless interface, the quality of received multimedia content is an important issue. With the increase of visual media in mobile services, user opinion acquired through perception of received image quality will play an increasingly important role in determining the effectiveness of such services.

The work documented in this thesis is motivated by the general lack of published work on software test beds for Third Generation Mobile Network (3G) and in particular for investigating mobile environment multimedia quality degradation. A 3G multimedia quality analysis system is presented, subjecting the input multimedia stream to the simulated 3G radio activities and measuring its degradation in terms of human perception. This approach takes a new and different model of multimedia quality measurement in a wireless communication domain, showing the possibility of a more effective approach that can be applied in many cases for assisting service quality assurance research across this area.

The development of this software system is covered in detail together with in-depth analysis of multimedia image quality over a simulated 3G radio interface. Universal Mobile Telecommunications System (UMTS) is the 3G standard chosen for study in this work. The suggested test bed simulates a single Frequency Division Duplex (FDD) downlink UMTS Territorial Radio Access (UTRA) channel, where the received media's image analysis is performed using a Human Vision System (HVS) based image quality metric. The system aims to provide a multipurpose and versatile multimedia 3G test bed for use in testing of various solutions for protecting multimedia data across a 3G radio interface. Furthermore, it produces effective human vision oriented feedback on visual

media degradation, providing a new and efficient method to address effectiveness of solutions in multimedia delivery over a mobile environment.

This thesis shows the ability of HVS-based image quality metric in analyzing degradation of visual media over a noisy mobile environment. This presents a novel direction in the area of telecommunication service multimedia quality analysis, with potential user quality perception being considered on top of data or signal-based error measurements. With such a new approach, development of multimedia protection solutions can be made more effective. Effective feedback provided by considering quality measurement with strong correlation to human perception allows close analysis of user visual discrimination across an image. An example of the usefulness of this information is especially visible if considering development of a content-based multimedia data protective system that provides different levels of protection, depending on the importance of visual media.

An apparent potential application of this thesis is in the testing of a multimedia/image protection protocol in a downlink channel. Future work might aim to extend the current system by adding network level traffic simulations and further addition of dynamic network control components, further considering network traffic conditions.

Contents

List of Figures

List of Tables

Acronyms and Units

Acronyms

3G	Third Generation Mobile Network
AICH	Acquisition Indicator Channel
AN	Access Network
AP-AICH	Access Preamble AICH
ATM	Asynchronous Transfer Mode
AuC	Authentication Centre
AWGN	Additive White Gaussian Noise
BCCH	Broadcast Control Channel
BCH	Broadcast Channel
BER	Bit Error Rate
BG	Border Gateway
BS	Base Station
BSS	Base Station System
BTS	Base Transceiver Station
CAMEL	Customized Applications for Mobile Network Enhanced Logic
CBC	Cell Broadcast Centre
CC	Call Control
CCTrCH	Coded Composite Transport Channel
CD/CA-ICH	Collision-Detection/Channel-Assignment Indicator Channel
CDMA	Code Division Multiple Access
CN	Core Network
CPCH	Control Physical Channel
CPICH	Common Pilot Channel
CS	Circuit Switch
CSCF	Call Session Control Function

CSF	Contrast Sensitivity Function
CSICH	CPCH Status Indicator Channel
DCH	Dedicated Channel
DL	Downlink
DPDCH	Dedicated Physical Data Channel
DPCCH	Dedicated Physical Control Data Channel
DS-CDMA	Direct Spread CDMA
DSCH	Downlink Share Channel
DTX	Discontinuous Transmission
EIR	Equipment Identity Register
EV	Early Vision
FACH	Forward Access Channel
FDD	Frequency Division Duplex
FACH	Forward Access Channel
FR	Frame Relay
GCR	Group Call Register
GGSN	Gateway GPRS Support Node
GMLC	Gateway Mobile Location Centre
GMSC	Gateway Mobile Switching Centre
GPRS	Generic Packet Radio Service
GPS	Global Positioning System
GSM	Global Systems for Mobile
HLR	Home Location Register
HSS	Home Subscriber Server
HVS	Human Vision System
IM	Importance Map
IMEI	International Mobile Equipment Identity
IMSI	International Mobile Station Identity
IP	Internet Protocol
IPDM	IM enhanced PDM
IPM	IP Multimedia
IPQR	IM weighted PQR
ISDN	Integrated Service Digital Network

ITU	International Telecommunication Union
IWF	InterWorking Function
JND	Just Noticeable Difference
LAC	Link Access Control
LBC	Local Band-limit Contrast
LCS	Location Service
LMU	Location Measurement Unit
LMSI	Local Mobile Station Identity
MAC	Medium Access Control
MAP	Mobile Application Part
ME	Mobile Equipment
MGW	Media Gateway Function
MM	Mobility Management
MMsk	Mutual Masking
MS	Mobile Station
MSC	Mobile Switching Centre
MSE	Mean Square Error
MSISDN	Mobile Station International ISDN Number
MSRN	Mobile Station Roaming Number
MT	Mobile Termination
N-ISDN	Narrowband ISDN
OSI	Open System Interconnect
OVSF	Orthogonal Variable Spread Factor
P-SCH	Primary Synchronization channel
PCCPCH	Primary Common Control Physical Channel
PCH	Paging Channel
PCPCH	Physical Common Packet Channel
PDCP	Packet Data Convergence Protocol
PDM	Perceptual Distortion Map
PDP	Packet Data Protocol
PDSCH	Physical Downlink Shared Channel
PhCH	Physical Channel
PGM	Portable Gray Map

PICH	Paging Indicator Channel
PLMN	Public Land Mobile Network
PQR	Perceptual Quality Rating
PRACH	Physical Random Access Channel
PS	Packet Switch
PSNR	Peak Signal-to-Noise Ratio
PSTN	Public Service Telephone Network
QoS:	Quality of Service
QAM	Quadrature Amplitude Modulation
QPSK	Quadri-Phase Shift Keying
R-SGW	Roaming signaling Gateway Function
RA	Routing Area
RACH	Random Access Channel
RF	Radio Frequency
RLC	Radio Link Control
RNC	Radio Network Controller
RNS	Radio Network System
ROI	Region of Interest
SCCPCH	Secondary Common Control Physical Channel
SCH	Synchronization Channel
SGSN	Serving GPRS Support Node
SICH	Acquisition Indicator Channel
SIM	Subscriber Identity Module
SM	Service Manager
SMSC	Short Message Service Centre
SMS-GMSC	Short Message Service GMSC
SOHO	Small Office Home Office
SS	Subscriber Server
SWIF	Shared InterWorking Function
TA	Terminal Adapter
TD-CDMA	Time Division CDMA
TDD	Time Division Duplex
TE	Terminal Equipment

TFCI	Transport Format Combination Indicator
TFI	Transport Format Indicator
ThE	Threshold Elevation
TMSI	Temporary Mobile Station Identity
TPC	Transmit Power Control
TrBk	Transport Block
TrCH	Transport Channel
TTI	Transmission Time Interval
UE	User Equipment
UL	Uplink
UMTS	Universal Mobile Telecommunications System
UTRA	UMTS Territorial Radio Access
UTRAN	UTRA Network
VDP	Visible Differences Predictor
VLR	Visitor Location Register
W-CDMA	Wideband CDMA

Units

c/deg	cycle per degree
db	Decibel
Hz	Hertz
kbit/s	kilo bit per second
k symbols/s	kilo symbols per second
M symbols/s	Mega symbols per second
Mbit/s	Mega bit per second
Mbps	Mega bit per second
MCPS	Mega chip per second
MHz	Mega Hertz
Ms	Millisecond
μs	microsecond

Publications[*]

These are the publications on topics associated with the thesis, which have been produced by, or in conjunction with, the author during his Master by Research candidacy:

Conference Papers

1. J. Tay and J.Chebil, "A Software Test Bed for Analysis of Image Quality over UTRA (UMTS Territorial Radio Access) Wireless Interface," WOSPA 2002, Brisbane, Australia, 17-18 October 2002.

[*]Note: The early stages of this Masters Degree program is associated with an industrial program which precludes any earlier publication

Authorship

The work contained in this thesis has not been previously submitted for a degree or diploma at this or any other higher education institution. To the best of my knowledge and belief, the thesis contains no material previously published or written by another person except where due reference is made.

Signed:…………………………………………………….

Date:…………………………

Acknowledgements

My journey through this Master Degree is no doubt full of obstacles and hurdles. As it has finally come to an end, I would like to take this opportunity to express my sincere gratitude and appreciation to all those who have lent me a hand one way or another in supporting me through this rough journey of mine.

Firstly, I would like to thank my family: my mother, my father and Chauses. I thank them with all my heart for it is them that build the prime driving force for me to overcome multiple impossibility and continue where numerous failure were encountered. To my mother who never stops believing in me, thank you for all your support and your devotion for none of this is possible without you. To my father who always encourages me, thank you for your advice and affirmation when things are rough and very little seems achievable. To Chauses who under all circumstances supported me and believed in me, it is you who gives me the will to reach the finishing point. Thank you, my family.

Secondly, numerous sincere and special thanks goes to my supervisors, friends and colleagues from the academic domain. I would like to thank Prof. Anthony Maeder, who supervised me during the last few months of my candidature, for giving me constant support, helpful advices and showing me skills, mindset and paradigm required to be competence in both industrial and academic domain. Special thanks to Dr. Adriana Bodnarova for being my associate supervisor and for your countless help that I cannot do without. I would especially like to acknowledge and thank Dr. Wilfried Osberger for his technical advice and for giving me in-depth technical details on his PHD work. Thank you also to my friends and colleagues, Arvin Lamana, Dr. John Williams, Haris Pandzo, Birgit Planitz, Greg Hislop, George Mamic, Jason Baker, Clinton Fookes, Alex Pongpech and Judith Planitz, who all "did time" with me in the RCCVA dungeon, for your wisdom, friendship and support. Last, but not least, my thanks to Dr. Mohammed Bennamoun, who is my initial principle supervisor, for giving me a chance to be a Master candidate.

Lastly, I would like to thank all my friends and associates that I failed to mention. I thank you all, sincerely for your friendship.

Chapter 1. Introduction

Recent advancements in mobile communication, especially the introduction of the Third Generation mobile network (3G) [1, 2] standard, has caused a dramatic increase of research interest in this area. Among the topics which have received concentrated attention, multimedia services and their performance over a wireless interface stands out as an important issue. Due to the versatile nature of the new generation of mobile infrastructure, the user can now transfer a high volume of data in a short time frame. Consequently, a small error over the wireless interface inflicts a large amount of quality loss among delicate operations such as multimedia delivery. Usage of a protection protocol can assist error recovery and minimize such losses; however, the effectiveness of the many protocols may not be fully tested due to the lack of availability of a versatile 3G software test bed. Furthermore, the differences in efficiency of two protocols on multimedia content may well depend on their effectiveness to protect image quality in addition to minimizing Bit Error Rate (BER).

This thesis presents the development of a universal 3G software test bed of UMTS standard, coupled with an image quality metric for media image quality analysis. The system is an expandable module package with the capability to be constructed into a fully functional multimedia application or packet data protection protocol testing unit.

The study concentrates on the popular Universal Mobile Telecommunications System (UMTS) [3] with UMTS Territorial Radio Access (UTRA) radio standards for the software test bed and a model for early vision in the Human Vision System (HVS) for the image quality analysis. This system is designed to mimic the processing of DCH into UTRA level signal and passing the physical layer signal through a physical channel model. An implementation of HVS system response is used to grade the quality degradation, the results of which are presented and analyzed. The scenarios considered are limited to UTRA's Frequency Division Duplex (FDD) in downlink mode.

The main motivation for this work is the general lack of published material on software test beds for lower service layers of mobile network, especially 3G. In addition, the analysis of mobile network multimedia service is mainly performed in terms of Quality of Service, with has little consideration of the human perception quality loss. Developed form this viewpoint, this research work aims to address this short fall in literature by producing a versatile 3G test bed, with the ability to analyze degradation in multimedia image quality.

An extended literature review has been conducted in search of published works on UTRA/UMTS test beds, analytical models and also multimedia quality analysis over 3G. However, minimal work on degradation in multimedia image quality can be found. The relevant published works found usually focus on areas such as:

- Multi user detection and channel estimation (e.g. [4] etc…);
- Channel modeling (e.g. [5-8] etc…);
- Dynamic channel allocation (e.g.[9] etc…); and
- Network level traffic modeling (e.g. [10] etc..).

However, a limited number of works can be found that completely describe a test bed and network simulation implementation to emulate UTRA transmission and receiving operations, as listed in [11] and [12]. Furthermore, in terms of quality analysis and outlining multimedia service requirements, the majority of literature focuses primarily on traffic level [13] or service level [14] Quality of Service (QoS) and network-based measurements (e.g. Bit Error Rate (BER) and latency) or primitive image measurement of PSNR. Examples of such literature includes [6, 14-23].

The problem covered in this research can be formulated as follows: The majority of quality analyses performed on multimedia communications are network solutions, which seldom take into account the user response. The novelty of this research is to take a new and more effective approach to analyzing visual quality degradation in 3G multimedia communications that correlates closely to human understanding and perception of visual media content. As the audience is usually the primary user of multimedia services, it is therefore appropriate that the response of such a user relative to quality degradation is investigated. QoS and network solutions will provide numbers to quantify loss of

multimedia data but such solutions fail to consider the level of impact such events have on the user. Examples where such inefficiency is especially clear include:

- Development of a content-based media protection protocol for 3G radio interface; and
- Dynamic multimedia content delivery adaptation for change in network conditions.

Therefore, using HVS-based error quantification not only helps to provide a more effective measure of visual media degradation, it can also act as a feed back mechanism to allow more accurate indications for direct use in executing operations to control the transmitting multimedia.

The primary contribution of this research centres on constructing a HVS image metric and integrating it onto a simulated 3G test bed module. Using the 3G test bed module as a platform, HVS can then provide quantitative analysis on the image media exposed to various mobile channel conditions. While many HVS image quality metrics are well documented, the author has not found a system that describes close coupling with a mobile environment simulation module. This research contributes in this area by fusing HVS image quality analysis with simulated 3G activities and illustrates the usefulness of such a combination by presenting quantifiable, consistent and effective image quality measurement in the developed system. By taking this step, a more ergonomic error quantification methodology is developed to provide effective and human-oriented feedback to assist in many areas of multimedia research.

The main objective of this work is to construct a seamless 3G multimedia quality analysis testing platform (commonly referred to in this thesis as the system). This system addresses the contribution by using a HVS-based approach to analyze visual content quality degradation while providing a detailed simulation of lower level 3G activities. The majority of work centres on constructing a working UTRA simulator test bed component, a working HVS-based image quality metric and verification of the functionality of the said system. System development employs published 3G standards and a published robust HVS image quality metric as system design. Methodology of the system is justified further in Chapter 5.

Designed to be versatile, the system demonstrates the novelty of using HVS methods to analyze visual media distorted using a detailed simulation of 3G radio interface activities. The system is configurable to perform operations from a multiple spectrum, based upon user specifications (addressed further in Chapter 5). Reliable methods are used to develop the major modules. The 3G test bed is developed directly from the UMTS specification, using a reliable development tool (Advance Design System 2001 by Agilent Technologies). Furthermore, the HVS module is implemented from a model of HVS behavior for quantifying degradation of quality in visual media.

The system can be further considered as a first stage of an expandable system that is extendable by modeling UMTS network behavior and UMTS connection with HiperLAN2 [24, 25] using the OPNET package. This future system is aimed to act as a testing base, assisting the development of a dynamic media quality adaptation protocol for routing multi-media service components over fast changing available channel capacity. Discussion on this aspect will be carried out further in the discussion and conclusion.

This thesis can be logically broken down into the following sections: namely, the UMTS background information (Chapter 2), system theory and design of system modules (Chapters 3-4), system development and implementation (Chapters 5-7), system testing and verification (Chapters 8-9) and conclusion (Chapter 10).

The chapter on UMTS background information covers the basic specifications for UMTS, giving a general overview of the 3G standard and related infrastructure of its operation. This aims to provide the reader with a conceptual understanding on the background operation of 3G technologies, allowing them to appreciate the significance and internal workings of 3G. This is necessary for the author to justify the contribution brought forward by the work presented in this thesis. The chapter on system theory and design of system modules conveys technical knowledge and specifications used during the development of various major components of the system.

The chapter on system development and implementation presents the methodology behind the development of the system, together with the internal structures of the implemented system. The chapter on system testing and verification presents a series of tests and related

results for verifying the system and its internal modules. The conclusion relates the entire thesis presentation to the objectives stated here in the introduction and discusses possible future work. The author has also published a refereed paper, which briefly summarizes the theory and design behind the system and gives a number of related results.

Chapter 2. 3G Background Information

Third generation mobile network (3G) is the latest advancement in the field of mobile technology. Providing high bandwidth communication of 8kbit/s-2Mbit/s and a revolutionary introduction of multimedia services over mobile communication, it aims to make mobile devices into versatile mobile user terminals. The highlight of 3G is to make the handset act more like a networked computer terminal rather than just a simple phone in order to bring the long anticipated multimedia capability straight into the user's hand. With this, there comes the promise of online e-commerce transactions, video conferencing, seamless web connection and packet video services.

Because these new services demand both high bandwidth and packet-based data handling, 3G standards need to accommodate the newly surfaced wireless bandwidth and user network management problem. These are subsequently handled by the W-CDMA (Wideband Code Division Multiple Access) wireless technology, TD-CDMA (Time Division CDMA) wireless technology and the all-IP network infrastructure respectively. The all-IP network is beyond the scope of this thesis and will not be discussed any further. Various 3G standards using W-CDMA technology have been proposed to the International Telecommunication Union (ITU) among which Universal Mobile Telecommunications System (UMTS) led by 3GPP and CDMA2000 led by 3GPP2 is among the popular 3G standard.

This chapter provides an overview of UMTS standards in 3G technologies by building a general skeletal picture of the widely-accepted standard. Information shown here is mainly a general inclusion of UMTS technical knowledge, helping readers to grasp its concept and appreciate its technological complexity. The presentation takes on a network level point of view, where brief UMTS network architecture and service functions are presented. General areas covered in this chapter include core network architecture, network control entities, traffic management function and radio interface channel resources. The purpose of this chapter is to demonstrate the author's awareness of basic UMTS technical knowledge and to further clarify the areas of UMTS/3G this research fits into.

UMTS has been designed for deployment over GSM-MAP core network infrastructure while CDMA 2000 uses ANSI-41 mobile infrastructure [26]. GSM-MAP and ANSI-41 are both core networks for a second generation mobile network, with GSM-MAP servicing Global Systems for Mobile (GSM) digital cellular phone systems and ANSI-41 supporting IS-95 (CDMA based). Usage of the previous core network for support of third generation mobile is feasible after minor upgrade while leaving the majority of the core network intact. The reason for this is the fact that the evolution from second to third generation mobile technology happens mainly in the wireless interface and service/data handling area. The importance of 3G lies in its ability to interconnect with other networks. A simple illustration is listed below. Note the roles of the core and wireless/radio network (e.g. UTRA: UMTS Territorial Radio Access) in Figure 2.1.

This figure is not
available on line.
Please consult
the hardcopy
thesis available
from the QUT
library

Figure 2.1: UMTS/UTRA Architecture Illustration [26]

ATM: Asynchronous Transfer Mode (channel transmission protocol)
CAMEL: Customized Applications for Mobile network Enhanced Logic
FR: Frame Relay (channel transmission protocol)
GGSN: Gateway GPRS Support Node (3rd generation packet data service for efficient data service)
IN: Intelligent Network   **IP:** Internet Protocol (Internet defined terminals network)
N-ISDN: Narrowband Integrated Service Digital Network
PSTN: Public Service Telephone Network (normal telephony)
RNC: Radio network controller
SGSN: Serving GPRS (Generic Packet Radio Service) Support Node
SOHO: Small Office Home Office high-speed wireless network access

UMTS has been chosen as the 3G standard to be investigated in this thesis, because of its flexibility and increasing popularity among researchers. This is mainly due to its planned deployment over the existing GSM core network, which is already globally deployed. Furthermore, it also supports both GSM (2nd Generation Mobile technology) and UMTS (3rd Generation Mobile Technology) concurrently. The following sections attempt to give some background information that relates to this work.

2.1 UMTS General Specifications

UMTS utilizes a bandwidth of 5 MHz with a basic chip rate of 4.096 Mcps over the 1900-2200 MHz wireless spectrum. Orthogonal Variable Spread Factor (OVSF) is used to provide different Quality of Service (QoS) and user bit rate up to 2 Mbps. The general frequency band distribution can be seen as below:

W-CDMA (TDD)	W-CDMA uplink (FDD)	MS	W-CDMA (TDD)		W-CDMA Downlink (FDD)	MS

1900　　　　1920　　　　1980　　　　2010　　　　2025　　　　2110　　　　2170　　　　2200
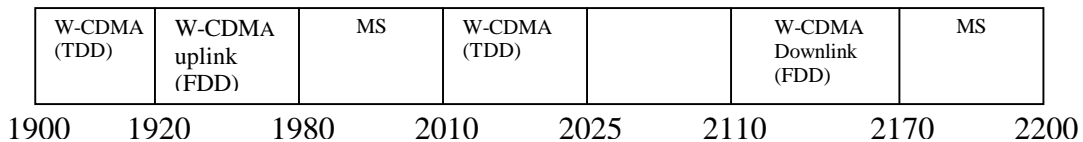
Figure 2.2 UTRA bandwidth distribution [27]

MS: Mobile Satellite application

FDD: Frequency Division Duplex (uplink and downlink has different frequency carrier (f_1 & f_2), separated by frequency guard

TDD: Time Division Duplex (uplink and downlink has same frequency f_c, this mode is better utilized for asymmetric services e.g. download/upload, video on demand)

Blank area: For other high bandwidth wireless applications currently in existence

As shown above, the radio access in the UMTS/UTRA has two duplex modes for effective utilization of the available radio spectrum: the Frequency Division Duplex (FDD) and Time Division Duplex (TDD). FDD uses different frequencies in downlink and uplink, while TDD uses time slot to synchronize between uplink and downlink (reciprocal transmission). FDD & TDD may share the same bandwidth if interference is acceptable

Employing coherent detection for better performance, UMTS has the ability to invoke dedicated pilot symbol embedded in user's data stream for support of adaptive antenna at Base Station (BS). Furthermore, it includes short spreading code to implement

performance enhancement techniques and requires no beacon or Global Positioning System (GPS) inter-cell operation in FDD mode, as it is asynchronous.

Table 2.1 summarizes the general technical details of UMTS to build a general understanding of the widely popular 3G standards.

Radio access technology:	FDD: DS-CDMA
	TDD: TDMA/CDMA (TD-CDMA)
Operating environments:	Indoor/Outdoor to indoor/Vehicular
Chip rate (Mcps):	UTRA: 4.906/8.192/16.384
Channel bandwidth (MHz):	UTRA: 5/10/20
Nyquist roll-off factor:	0.22
Channel bit-rates (Kbps):	FDD (UL): 16/32/64/128/256/512/1024
	FDD (DL): 32/64/128/256/512/1024/2048
	TDD (UL/DL): 512/1024/2048/4096
Detection scheme:	Coherent detection with time-multiplexed pilot symbols
Data Modulation and Spread Modulation:	Quadri-Phase Shift Keying (QPSK)
Frame Length:	10 ms
Time slot duration:	625 µs
No. of power control groups/time slots:	16
Pulse shape	Root raised cosine r=0.22
Spreading factor	FDD: Short codes, variable, 4-256
	TDD: 1,2,4,8,16 variable spreading

Table 2.1 UMTS Summary [26, 27]

The above details were obtained mainly from page 903 of [26]. To provide a better understanding of the usage of radio resources, the next section introduces the UTRA wireless channel, illustrating UTRA's radio channel infrastructures for user access.

2.2 UTRA Air Interface Radio Channels

This section describes some of the physical UTRA radio channels used for connection of Base Station (BS), the ending node of the UMTS network and the User Equipment (UE), also known as the Mobile Station (MS). Two major types of physical channel are available, the dedicated transport channel for data transportation and the common transport channel for system messages. These channels exist to service the upper layer transport channel. UTRA channels are logically divided into physical and transport channels in accordance with the Open System Interconnect (OSI) [28] system model definition.

The transport channel can be classed as either a dedicated transport channel or a common transport channel. The former consists of a bi-directional Dedicated Channel (DCH) for carrying user and control data between network and UE; it is mainly for user-oriented usage. The other is for common network management-oriented usage, which includes channels such as the Broadcast Control Channel (BCCH), Forward Access Channel (FACH), Paging Channel (PCH) and Random Access Channel (RACH). BCCH is a downlink channel that carries user and control information between network and UE (also known as mobile station (MS)). FACH is a downlink channel for carrying control information and a short user package. It comes into use when the BS serving the MS is known. PCH is a downlink channel for carrying control information during call alert when the serving BS of the MS being paged is not known. RACH is an uplink channel that carries control information and a short user package for call setup [29].

The physical channels consist of a Dedicated Physical Data Channel (DPDCH), Dedicated Control Physical Data Channel (DPCCH), Physical Random Access Channel (PRACH), Primary Common Control Physical Channel (PCCPCH), Secondary Common Control Physical Channel (SCCPCH) and Synchronization Channel (SCH) [27]. Both DPDCH and DPCCH are used for carrying DCH data, of which DCH is directly mapped onto the two channels. In the same context, RACH is mapped onto PRACH, BCCH onto PCCPCH and FACH with PCH onto SCCPCH. SCH is an independent channel for physical layer use and is not mapped onto by transport layer channels.

DPDCH and DPCCH are both bi-directional channels, of which DPDCH is for data transmission and DPCCH is for transmission sending of DCH information including the pilot symbols, Transmit Power Control (TPC) command and Transport-Format Indicator (TFI). Pilot symbols are used for facilitating coherent detection on both uplink and downlink, TPC is for the CDMA power control scheme and TFI carries information related to the instantaneous parameters of transport channels multiplexed on the physical channel [27].

PCCPCH is a downlink channel used by BS to continuously broadcast the BCCH to all MS in the mobile cell. SCCPCH is a downlink channel for carrying FACH and PCH information, where transmission is made only when data are available. PRACH is an uplink channel for random access of MS, where the MS needs to register itself on the network. SCH is a downlink channel used for synchronization of BS and MS.

Ending the brief description of major channels in UTRA used for connecting mobile phone and the fixed networks, the next section introduces the UMTS networking concept for the fixed network in managing mobile services.

2.3 UMTS Network Architecture

This section aims to give the overview on UMTS network architecture, showing the overall functional working and management of UMTS from a network prospective. As with earlier mobile networks, UMTS needs to introduce specific functions to provide various mobile services. These functional entities can be implemented using different functional equipment or groups of equipment. The network architecture also varies in its configuration to support specific functions. Functions are grouped into classes and functional entities are created to deliver the specified function. These functional entities in a UMTS Public Land Mobile Network (PLMN) can be divided into three separate groups, namely the Core Network (CN) entities, Access Network (AN) entities and MS entities.

CN is the switching network for overall provision of mobile service, line management and connection to fixed line networks (e.g. land telephone line, data network etc...). AN is the radio/wireless interface between MS and CN, while MS is the end node for the entire network. In terms of OSI model, AN can be presented into Layers 1-3 as per Figure 2.3. Layer 1 is the physical layer while layer 2 divided into two sub-layers of Link Access Control (LAC) and Medium Access Control (MAC) while layer 3 and LAC are divided into Control and User Planes. Layer 3 is divided into Radio Resource control (RRC, interface with layer 2), with higher layer of Mobility Management (MM) and Call control (CC) [29].
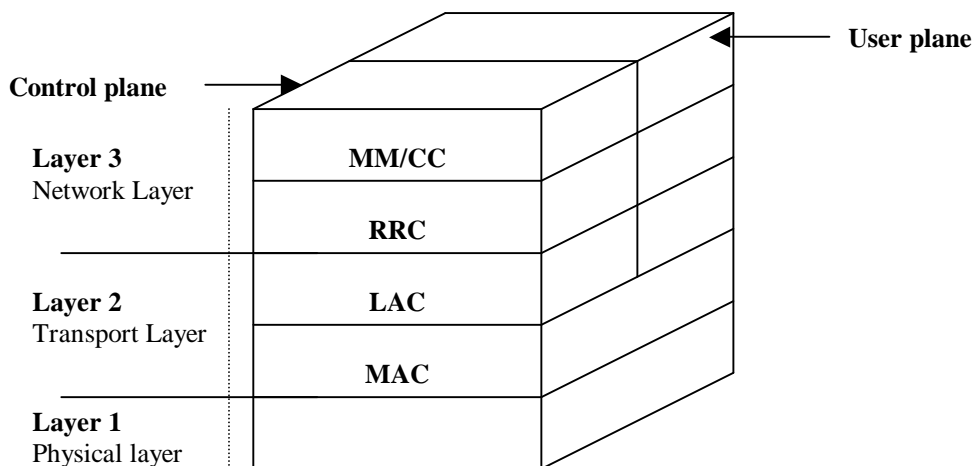
Figure 2.3 UMTS AN OSI Illustration

Some other specific mobile system entities are also available for dedication towards support of specific services. However, their absence should have limited impact on other entities of

the PLMN. These entities are: Group Call Register (GCR) entities, Shared InterWorking function (SWIF) entity, Location Service (LCS) entities, Customized Applications for Mobile network Enhanced Logic (CAMEL) entities, Cell Broadcast Centre (CBC) entities, Number Portability Specific entities and IP Multimedia (IPM) Subsystem entities.

Note that Figure 2.4 illustrates the basic network architecture for the UMTS PLMN configuration. It mainly consists of the basic mobile communication entities with configuration that can support both GSM (2G) and UTMS (3G) radio access as shown in the block configuration of UMTS showing the relationship of CN, AN and MS. The following sections aim to provide a functionally-based description of UMTS, to further revise the internal processes of UMTS. These sections (2.4-2.5) provide detailed insight into the 4 major groups of entities namely the CN, AN, MS and other miscellaneous entities, as described above.

This figure is not available online. Please consult the hardcopy thesis available from the QUT library

Figure 2.4 Basic UMTS PLMN Configuration [30]

2.4 Core Network Entities

The Core Network (CN) entities include entities for both Packet Switched (PS) and Circuit Switched (CS) domains. PS is a service mode intended for pure data communication (e.g. internet browsing) and CS mode for constant traffic services such as conventional phone calls. Functional entities in CN can be classified into the PS domain, CS domain or can be common to both domains. The following subsections describe the three groups of CN functional entities in detail, with the technical information sourced from [30].

2.4.1 CN Entities Common to PS and CS

Entities that are common to both PS and CS include Home Location Register (HLR), Home Subscriber Server (HSS), Visitor Location Register (VLR), Equipment Identity Register (EIR), Short Message Service Gateway Mobile Switching Centre (SMS-GMSC), SMS Interworking MSC and Roaming Signaling Gateway Function (R-SGW).

Home Location Register (HLR) is a database for mobile subscribers (user of service) management. It stores subscription information such as:

- Location information of subscriber equipment for MSC usage;
- Location information for SGSN usage (for GPRS support);
- Location Service (LCS) privacy exception list (for LCS support);
- Gateway Mobile Location Centre (GMLC) list (for LCS support); and
- MO-LR list (for LCS support).

HLR also stores various mobile subscription identity attachments, for example:

- International Mobile Station Identity (IMSI): for use as key to identify Mobile Station (UE)/User Equipment (UE);
- Mobile Station International ISDN Number (MSISDN): one or more of this is stored to be used as a key to identify MS/UE;
- Packet Data Protocol (PDP) address (for GPRS support) – 0 or more; and
- Location Measurement Unit (LMU) indicator (for LCS support).

HLR may be used to store other information as well, including:

- Teleservice and bearer services subscription information;

- Service restrictions (e.g. roaming limitation);

- Parameters attached to supplementary;

- List of all group IDs usable by subscriber to establish voice group or broadcast calls; and

- Information about GGSN (for GPRS support) – to allocate Packet Data Protocol (PDP) address for a subscriber dynamically.

Home Subscriber Server (HSS) is used to substitute the HLR when IP Multimedia (IPM) sub-network is implemented for delivery of multimedia over a UMTS All-IP network. It is a master database that holds subscription information to support network entities that handle calls or sessions. Some of its functions support call control in completing the routing/roaming procedure by solving ambiguity in authentication, authorization, naming/addressing resolution and location dependencies. As with HLR, it directly interfaces with other functional entities such as the Mobile Switching Centre (MSC) Server, Gateway MSC (GMSC) Server, Serving GPRS (Generic Packet Radio Service) Support Node (SGSN), Gateway GPRS Support Node (GGSN), Roaming Signaling Gateway Function (R-SGW) and Call Session Control Function (CSCF).

Some user information is held by HSS, including:

- User Identification, Numbering and addressing information;

- User Security information (Network access control information for authentication and authorization);

- Inter-system level user location information (e.g. handling user registration, stores inter-system location information etc.); and

- User profile (services, service specification information).

The HSS is responsible for supporting Call Control (CC)/ Service Manager (SM) entities of various control systems (CS Domain control, PS Domain control, IP Multimedia control etc.) offered by a service operator. It can also integrate heterogeneous information and offers enhanced features in core network to applications and services domains, while maintaining transparency of the heterogeneity to application and services domains. It does not have to deal with the complex heterogeneous variety of the information.

The various functionalities offered by HSS include:

- User control functions as required by the IPM subsystem;

- Subset of HLR functions as required by the PS Domain; and

- CS part of HLR (for subscriber access to CS Domain or legacy GSM/UMTS CS Domain networks roaming).

This figure is not
available online.
Please consult
the hardcopy
thesis available
from the QUT
library

Figure 2.5 Generic HSS Structure [30]

Figure 2.5 illustrates the generic conceptual view on HSS's protocol structure and various interfaces to other functional entities. These interfaces include Mobile Application Part (MAP) termination, addressing protocol termination, authentication, authorization protocol termination and IPM Control termination.

MAP termination is the procedure HSS uses to terminate MAP protocol. In MAP termination, those are:

- User Location Management procedure;

- User Authentication Management procedure;

- Subscriber profile Management procedure;

- Call handling support procedure (routing information handling); and

- Subscriber Server (SS) related procedure.

As illustrated in Figure 2.5, addressing protocol termination is where HSS terminates a protocol to solve addressing issues by using appropriate protocol. This is used primarily for user name/numbers/addresses resolution. Authentication & authorization protocol termination takes place after HSS terminates authentication and authorization protocols according to appropriate standards. This is used primarily for user authentication and

authorization procedures in IP-based Multimedia services. IPM Control termination is used when HSS terminates the IP-based multimedia call control protocol, according to appropriate standards. This is used primarily for User Location Management procedure for IP-based multimedia service and includes IP-based Multimedia call handling support procedure.

Visitor Location Register (VLR) is the functional entity used to control Mobile Station (MS) roaming in an MSC controlled area. When the area's MSC receives MS's registration procedure for entering a new location area, it transfers the identity of MS current location area to VLR for storage. VLR and HLR exchange information to allow proper handling of calls if MS is not yet registered on VLR. VLR may be in charge of several MSC areas simultaneously, storing information elements for call setup-up/receive by MS (supplementary service may require additional information obtained from HLR). The elements included are:

- International Mobile Subscriber Identity (IMSI);
- Mobile Station International ISDN Number (MSISDN);
- Mobile Station Roaming Number (MSRN);
- Temporary Mobile Station Identity (TMSI);
- Local Mobile Station Identity (LMSI);
- MS's registered location ;
- Identity of SGSN with MS's registration (for GPRS support which has Gs interface between MSC/VLR and SGSN); and
- Initial and last known location of MS.

VLR also contains supplementary service parameters applicable for registered mobile subscribers.

Authentication Centre (AuC) stores data for each mobile subscriber, allowing authentication of International Mobile Subscriber Identity (IMSI) and communication over radio path between MS and the network to be ciphered. It transmits authentication and ciphering data to VLR, MSC and SGSN via HLR for their authentication purpose. AuC also stores an identification key in association with HLR for each mobile subscriber. The key is used to generate IMSI authentication data and key for cipher communication between MS and

network over the radio path. AuC communicates only with its associated HLR over the H-interface.

Equipment Identity Register (EIR) is the GSM system logical entity that is responsible for storing International Mobile Equipment Identity (IMEI) in the network using self-contained one or several databases. Mobile equipment needs to be classified into three separate lists of "white listed", "gray listed" and "black listed", in EIR. However, IMEI may still be unknown to EIR.

SMS Gateway MSC (SMS-GMSC) acts as an interface for Short Message Service Centre (SMSC) to MSC for delivery of messages to MS. SMS Interworking MSC acts as an interface for Short Message Service Centre (SMSC) to MSC for submission of messages from MS.

Roaming Signaling Gateway Function (R-SGW) performs bi-directional signaling conversion between SS and based transport signaling in older Pre release 4 (release standard of IMT-2000) network and IP-based transport signaling of release 1999 network. It inter-works with Sigtran SCTP/IP signaling protocol and SS7 MTP signaling protocol. This includes interfacing pre release 4 network MSC/VLR to IP transport of MSP-E and MAP-G. This section has provided an overview on functional entities common to both CS and DS domains. The next section continues with an overview of core network entities specific to the CS domain.

2.4.2 CN Entities Specific to CS Domain

This section continues with the functional entities that are specific to the CS domain. The functional entities that fall under this group include the Mobile-service Switching Centre (MSC), Gateway MSC (GMSC) and Interworking Function (IWF).

Mobile-service Switching Centre (MSC) is the interface between a radio access system and a fixed network, which performs all required functions to allow Circuit Switched (CS) service to and from MSs. It acts as a switching exchange to handle all switching and signaling functions for MS in the location area designated for individual MSCs. Furthermore, the other factors that need to be considered are the impact of radio resources

allocation on a network, action appropriate for the mobile nature of the subscribers, performance of the procedure required for location registration and performance of the procedure required for handover (from BS to BS, MSC to MSC etc.). MSC can be implemented in two modules, the MSC Server and the Media Gateway Function (MGW).

MSC server mainly comprises of Call Control (CC) and mobility control parts of the MSC. It terminates user-network signaling and initiates appropriate network-network signaling. It contains a VLR to hold mobile subscriber's service data and CAMEL related data. It handles the connection control part of a call state for media channels in a MGW.

Media Gateway Function (MGW) has the role of defining the PSTN/PLMN transport termination point in the mobile network, while interfacing UTRA Network (UTRAN) with core network (mobile network backbone). It may also terminate bearer channel from switched circuit network and media streams from a packet network (e.g. RTP streams in IP network) and may support media conversation, bearer control, and payload processing (e.g. MPEG-4 codec processing). Furthermore, it exhibits the characteristics of interacting with the Media Gateway Control Function (MGCF), MSC server and GMSC server for resource control, owning and handling resources (e.g. echo cancellers) and may at times need to have appropriate codec for media processing. Resource arrangement allows MGW to be provisioned with necessary resources, for support of UMTS/GSM transport media.

Gateway MSC (GMSC) performs a routing function (interrogate appropriate HLR and then route call to MSC holding MS's registration) to MS on behalf of external network that cannot interrogate HLR directly (barred by network operator). Network operator may choose to appoint MSC to become GMSC to handle voice group/broadcast call directly, routing it to VBS/VBGS Anchor MSC based on call reference contained in the dialed number. GMSC can be implemented in two different entities: Gateway MSC Server (GMSC Server) and MGW. GMSC Server handles only signaling and comprises mainly of call control and mobility parts of the GMSC.

Interworking Function (IWF) is a functional entity associated with the MSC that provides interworking between a PLMN and fixed networks (e.g. ISDN, PSTN, PDNs), with the functionality dependent on service and fixed network type. It is required to interchange protocol between both networks of Public Land Mobile Network (PLMN) and fixed lined

network. Where PLMN service implementation is directly compatible with the interfacing network, this function is omitted.

This ends the section on functional entities specific to the Circuit Switch (CS) domain, running through the functionality of the various entities within the CS domain. The next section continues on related topics by covering the functional entities specific to the Packet Switch (PS) domain.

2.4.3 CN Entities Specific to PS Domain

UMTS Packet Switch domain (or GPRS) consists of the interface between the radio access system and fixed networks (ISDN, PSTN etc) for Packet switch service. It is responsible for performing functions that allow packet transmission to and from a MS. The entities associated with this domain are Serving Generic Packet Radio Service (GPRS) Support Node (SGSN), Gateway GPRS Support Node (GGSN) and Border Gateway (BG).

Serving GPRS Support Node (SGSN) has a location register that stores two types of subscriber data for the handling of the packet data transfer originating and terminating operation. This includes subscriber information and location information. The former contains the International Mobile Subscriber Identity (IMSI), one or more temporary identities and zero or more Packet Data Protocol (PDP) addresses. The later has information on the cell or Routing Area (RA) where MS was registered (selection depends on operational mode of MS) and Gateway GPRS Support Node (GGSN) number of all GGSN that maintains active Packet Data Protocol (PDP) context with current SGSN.

Gateway GPRS Support Node (GGSN) has a location register that stores two types of subscriber data for the handling of the packet data transfer originating and terminating operation. The subscriber data as received from HLR and SGSN has subscriber information that contains IMSI and zero or more Packet Data Protocol (PDP) addresses. Available together with the subscriber data are location information, storing SGSN address of SGSN where MS was registered and GGSN number of all GGSN that maintains active PDP context with current SGSN.

Border Gateway (BG) acts as the gateway PLMN, which supports GPRS and external Inter-PLMN backbone (backbone network to interconnect PLMNs) that supports GPRS. It provides an appropriate level of security for PLMN and its subscriber and is needed in PLMN to support GPRS only. This point concludes the entire section on Core Network (CN) functional entities, which provided a detailed overview of the functional entities within the UMTS CN. The next section continues with a description of the functional entities within the other two networks, Access Network (AN) and Mobile Station (MS).

2.5 Access Network Entities and Mobile Station Entities

AN entities provide access technology support (to access MS) for core network using two different types of access network, Base Station System (BSS) and Radio Network System (RNS). The MSC has the option to connect to either or both of the access networks.

Base Station System (BSS) offers TDMA-based access technology (i.e. for GSM). This is the system of base station equipment (e.g. transceivers, controllers etc.) responsible for communicating with Mobile Stations in a defined area. It is accessed by MSC through A interface and SGSN through Gb interface, supporting one or more mobile cells. If Abis-interface is implemented, then BSS consists of one Base Station Controller (BSC) and several Base Transceiver Stations (BTS). BSC is used for controlling an area of radio coverage consisting of one or more cells in GSM and it can control one or more BTS. BTS is the network component that serves a single cell in the GSM environment [30].

Radio Network System (RNS) offers W-CDMA-based access technology for UTRA air interface. It is also a system of base station equipment responsible for communicating with Mobile Stations in a defined area. Accessed by MSC through Iu-CS interface and SGSN through Iu-PS interface, RNS may support one or more cell. It consists of one or more base stations, one Radio Network Controller (RNC) and one or more Nodes. RNC is used to control an area of radio coverage consisting of one or more cells in UMTS, so it controls one or more Node B. Node B is a network component that serves a single cell [30].

Mobile Station (MS) functional entities consist of physical user equipment usable by a subscriber of the PLMN. It includes Mobile Equipment (ME) and Mobile Termination

(MT) for supporting various TA and TE functions, depending on application and services parameters. Terminal Adapter (TA) is any network device, which TE uses to interface with the network. Terminal Equipment (TE) is actual service equipment used by user, e.g. mobile phone, Personal Digital Assistance (PDA) etc. [30].

Subscriber Identity Module (SIM) for GSM or UMTS Subscriber Identity Module (USIM) for UMTS is the functional entity residing on the MS and used for accessing services with appropriate security [30].

This ends the section on AN and MS functional entities to illustrate their functional roles within the mobile network. It also concludes the sub-section of UMTS network architecture and the entire section on UMTS background as well. These sections have introduced the general definition of UMTS, the main components of UTRA radio channels and how the network architecture delivers UMTS.

The research presented in this thesis is conducted on the transport and physical layer of UMTS, specifically the interface between AN and MS. Overall, this research concentrates on quality of multimedia content at application level, while considering the impairment injected by operations at the lower level of UMTS, namely the transport and physical layer. It is assumed that the reader now possesses the basic information on the roles of various components and the internal working of UMTS and UTRA, and thus can identify how the work presented in this thesis relates to the UMTS technology.

The remainder of the thesis progresses through the development of the main contributions and related essential information, namely covering the UMTS radio specification and image quality metric background information.

Chapter 3. UMTS Radio Interface

This section pursues a direction closer towards defined objectives by investigating the topic directly related to building the 3G/UMTS test bed. The UMTS radio interface [31] in the access network is described, probing the issue of providing multiple access of Mobile Stations (MS) by Base Stations (BS) and data processing from transport to physical channel. The aspects discussed in this section are limited to Layer 1 (Physical Layer) and Layer 2 (Transport Layer) of the UMTS radio access interface.

To provide effective multiple high data rate (up to 2 MBit/s) access for multiple users, UTRA utilizes the multiple access technology in the limited bandwidth (1900 MHz – 2200 MHz) by using Wideband Code Division Multiple Access (W-CDMA) technology [26, 27]. More details on W-CDMA can be found in [32]. The radio access in the UMTS/UTRA has two duplex modes for further effective utilization of the spectrum: the Frequency Division Duplex (FDD) and Time Division Duplex (TDD).

FDD uses different frequencies in each downlink and uplink channels, where a separate band with distinct separation is assigned for the downlink and uplink channels. TDD uses time slots to synchronize between uplink and downlink, while using the same radio frequency. Time slots are divided into transmission and reception parts and information is transmitted reciprocally. A typical radio frame is 10 ms long and is divided into 15 slots (2560 chip/slot at 3.84 Mcps rate). As defined by CDMA, a distinct code is defined as a physical channel. The base technology used can be either a 5MHz wide spread bandwidth Direct Spread CDMA (DS-CDMA) in FDD (i.e. W-CDMA) or 3.84 Mega Chip Per Second (Mcps) in TDD, or the 1.6 MHz spread DS-CDMA (narrowband CDMA) for 1.28 Mcps TDD[12].

For 3.84 Mcps physical access, channel information rate varies with symbol rate derived from 3.84 Mcps chip rate and spreading factor. It ranges from 4 to 256 with FDD uplink and 4 to 512 with FDD downlink and 1 to 16 for TDD uplink and downlink. Modulation symbol rate varies from 15 k symbols/s to 960 k symbols/s in FDD uplink and downlink

and 3.84 M symbols/s to 240 k symbols/s for TDD. TDD in 1.28 Mcps uses 10 ms radio frame that divides into two 5 ms sub-frames, which each contain seven normal time slot and three special time slots. Modulation symbol rate varies from 80.0 K symbols/s to 1.28M symbol/s, as the spreading factors vary from 1 to 16 [12].

Whichever duplex mode is chosen, a common procedure (with different details) applies to process input bits into transmittable data (physical layer signal). Starting from the data link layer, the four common steps involved are multiplexing, channel coding, spreading and modulation. This section concentrates on the procedure specific in FDD Duplex.

Multiplexing and channel coding are among the processes of providing Media Access Control (MAC) from the physical layer to the upper layer. Channel coding is for randomizing transmission errors, with options including convolution coding, turbo coding or no coding. The modulation scheme used by UTRA is QPSK (8PSK for 1.28 Mcps TDD), with spreading and scrambling closely associated with modulation. A different spread code family is used for different spreading situations. For separating different cells (downlink):

- FDD: 10 ms period gold codes (38400 chips at 3.84 Mcps) with code length of 2^{18}-1 chips [11]; and
- TDD: Scrambling code with length 16 [33].

For separating different UE (uplink) [12]:

- FDD: 10 ms period gold code or S(2) codes with 256 chip period; and
- TDD: 16 chips period codes and midamble sequences of different length, environmentally dependent.

The general process is illustrated in Figure 3.1, where multiplexing and channel coding involve a combination of error detection, error correction, rate matching, interleaving and mapping transport channel into the physical channel. The spreading and modulation operation is applied to the signal produced from the process shown [12].

The area chosen to be investigated for this thesis is UTRA FDD downlink. The following subsections give more specific details on the four major functions mentioned, specifically those related to the Dedicated Channel (DCH).

Receiver
(reverse the above processes)

This figure is not
available online.
Please consult
the hardcopy
thesis available
from the QUT
library

Spread and Scrambled data

Channel mapped data symbol blocks

Figure 3.1 Transport/Physical Channel Downlink Structure [11, 12]

3.1 Multiplexing and Channel Coding

This section concentrates on the multiplexing and channel coding aspects of UTRA transport layer processing. The processes covered are transport layer procedures that process transport layer data into an acceptable form for the physical layer. The transport channels are hereby mapped onto physical radio channels as well. A simplistic breakdown of the overall process is provided below, followed by a more detailed analysis of the individual processes.

Incoming data are packaged into a series of Transport Blocks (TrBk) of which CRC [34] is the error detection provided upon each of them. In a Transmission Time Interval (TTI), transport blocks are serially concatenated but are code block segmented if the number of bits in the code blocks exceed the maximum size limit Z. Channel coding is then performed, with a choice of convolutional coding, turbo coding and no coding, with its corresponding coding rate. Rate matching is applied to repeat or puncture transport channel bits, to match the appropriate rate. Indication of Discontinuous Transmission (DTX) is added prior to first interleave, where block interleave with inter-column permutation is used.

To fit the blocks within an appropriate time frame, the blocks are segmented and mapped into 10 ms radio frames. Upon each 10 ms interval, a radio frame from Transport Channel (TrCH) is sent into the TrCH multiplexing process, where frames from multiple channels are multiplexed serially into a Coded Composite Transport Channel (CCTrCH). The second DTX indicated is then added, follow by physically segmenting the data stream into the Physical Channel (PhCH). If more than one PhCH is in use, the bits are divided among the different PhCHs. This is followed immediately by the second interleave, which uses a block interleaver in 3 steps. First, one places the input bits into the matrix and applies padding, then applies column permutation to the matrix and output bits from the matrix and applies pruning. The bits are then mapped onto the Physical Channel (PhCH). The DTX indication bits are used to fill up the radio frame, indicating when the transmission should be turned on or off. First DTX insertion is inserted only if the position of the TrCH in the

radio frame is fixed. Second insertion is at the end of the radio frame. Physical channel mapping follows before the handing over to spreading and modulation. These will be covered in more detail in the subsections below, while further details can be located in [35].

3.1.1 CRC Attachment

CRC is used as error detection on transport blocks, of which parity bit size can be 24, 16, 12, 8 or 0 bit. The parity bit block L_i is applied upon transport block m of Transport Channel (TrCH) I of size A_i. The polynomials of the cyclic generator are [35]:

- $g_{CRC24}(D) = D^{24} + D^{23} + D^6 + D^5 + D + 1$;
- $g_{CRC16}(D) = D^{16} + D^{12} + D^5 + 1$;
- $g_{CRC12}(D) = D^{12} + D^{11} + D^3 + D^2 + D + 1$;
- $g_{CRC8}(D) = D^8 + D^7 + D^4 + D^3 + D + 1$.

3.1.2 Transport Block Processing

The representation for tranport block concatenation is as listed below[35]:

- $b_{im1}, b_{im2} \ldots b_{imBi}$ represent the tranport block;
- i is the TrCH number;
- m is transport block number;
- B_i the number of bits in each block (CRC included);
- $x_{i1}, x_{i2} \ldots x_{ixi}$ represent the pro concatenation bits.

The relation is defined as:

- $x_{ik} = b_{i1k}$ (k=1,2,…,B_i);
- $x_{ik} = b_{i,2,(k-Bi)}$ (k= B_i +1, B_i +2,…,2B_i) ……;
- $x_{ik} = b_{i,Mi,(k-Bi)}$ (k= (M_i-1)B_i +1, (M_i-1)B_i +2,…, M_iB_i.

Code block segmention is performed on the transport block if the size of the block X_i is larger than maximum allowable code block size Z. Z is determined by the channel coding method used, where convolution coding [36] gives $Z = 504$; turbo coding [37] gives $Z = 5114$ and no channel coding yields $Z =$ unlimited.

3.1.3 Channel Coding

Representation for channel coding block is as listed below [35]:

- $0_{ir1}, 0_{ir2} \ldots 0_{irki}$ represents the channel coding block;
- *r* is the code block number
- K_i is the number of bits in each code block
- *Yi* is the number of encoded bits

The choices of channel coding available are convolutional coding *k*, turbo coding and no coding, Table 3.1 showing the coding scheme and rate for the various transport channels while the coding scheme is described below:

- Convoluntional coding: with rate 1/2 yields $Y_i = 2*K_i + 16$; rate 1/3: $Y_i = 3*K_i + 24$;
- Turbo coding: with rate 1/3: $Y_i = 3*K_i + 12$;
- No coding: Yi = Ki.

Type of TrCH	Coding Scheme	Coding rate
Broadcast Channel(BCH)	Convolutional Coding	1/2
Paging Channel(PCH)		
Random Access Channel(RACH)		
Control Physical Channel(CPCH), Dedicated Channel(DCH), Downlink Share Channel(DSCH), Forward Access Channel(FACH)		1/3, 1/2
	Turbo Coding	1/3
	No Coding	

Table 3.1 Channel Coding Scheme

3.1.4 Radio Frame Equalization & First Interleaving

Radio Frame Equalization is the process of padding the input bit sequence ensuring that output can be segmented into a size required in rate matching. This is only performed in the uplink as downlink rate matching output block length is always conformed to the required criteria.

A block interleaver with inter-column permutaions is used to perform the first interleaving. $x_{i,1}, x_{i,2} \ldots x_{i,xi}$ denotes the input bit into block interleaver. i is the TrCH number and X_i the number of bits. The number of columns needed for permutation is listed in Table 3.2 [35].

Transmission Time Interval (TTI)	Number of columns (c1)	Inter-column permutation paterns $<P_{1c1}(0) \ldots P_{1c1}(c1\text{-}1)>$
10 ms	1	<0>
20 ms	2	<0,1>
40 ms	4	<0,2,1,3>
80 ms	8	<0,4,2,6,1,5,3,7>

Table 3.2 Inter-column permutation patterns for 1ˢᵗ interleaving

The procedure is as follows:

1. Construct a matrix X with column number c1 as selected from Table 3.2 and number it 0..c1 from left to right.
2. Number of rows of the matrix is calculated as X_i/c1.
3. Write input bit sequence into matrix row by row from left to right and top to bottom.
4. Shufflle columns (inter-column permutation) as per specified in the inter-column permutation table to form new matrix Y.
5. Read output bit sequence from Y column by column, top to bottom and left to right.

3.1.5 Radio Frame Segmentation, Rate Matching and Transport Channel Multiplexing

In radio frame segmentation, the input bit sequence is segmented when Transmission Time Interval (TTI) is longer than 10 ms. Given radio frame block length F_i, the input bit sequence length is semented into a series of bits in segments of F_i length [35].

Rate matching is a process by which bits on a transport channel are repeated or punctured to match the attributes of the assigned rate. Number of bits to be repeated or punctured are calculated based on TTI. This is done to ensure total bit rate after TrCH multiplexing is identical to total channel bit rate of allocated dedicated physical channels.

Transport Channel (TrCH) multiplexing is performed when a multiple transport channel is available. Given multiple (more than one) Transport Channel (TrCH), a radio frame from each TrCH is delivered for TrCH multiplexing every 10 ms, where it is serially multiplexed into a Coded Composite Transport Channel (CCTrCH).

3.1.6 Discontinuous Transmission Indication Insertion

Discontinuous Transmission Indication (DTX) is the downlink process of filling the radio frame with bits. It indicates when the transmission should be turned off and when it is not transmitted. Two insertions of DTX indication bits are performed. The insertion point of DTX indication bits is dependent on the fixation option in TrCHs (fixed or flexible position) [35]. First DTX insertion is used if the position of the TrCHs in the radio frame is fixed. Insertion of the 2nd indication bits is placed at the end of the radio frame. However, the DTX is distributed over all slots after the second interleaving.

The first insertion of DTX indication bits fills up the TTI with the following format:

- $h_{ik} = g_{ik}$ k = 1,2…,G_i;
- $h_{ik} = \delta$ k = G_{i+1}, G_{i+2}…D_I,

where:

- h_{ik} is the bits output from the DTX insertion;
- g_{ik} is the input bits;
- G_i is the number of bits in one TTI of TrCH *i*;
- D_i is the number of radio frames multiplied by the number of bits in a radio frame minus bits that have been punctured; and
- δ is the DTX inserted.

The second insertion of DTX indication bits has the following format:

- $w_k = s_k$ k = 1,2…,S;

- $w_k = \delta$ $k = S_{+1}, S_{+2}...P.R,$

where:

- w_k is the bits output from the DTX insertion;
- s_k is the input bits;
- S is the number of bits from TrCH multiplexing;
- P is the number of physical channels;
- R is the number of bits in one radio frame, including DTX bits for each physical channel; and
- δ is the DTX inserted.

3.1.7 Physical Channel Segmentation and Second Interleaving

When multiple physical channels (more than one) is used to transport data, physical segmentation is needed to divide bits among different physical channels. The bit distribution is noted as follows [35]:

- $u_{1,k} = x_{f(k)}$ $k = 1..U;$
- $u_{2,k} = x_{f(k+U)}$ $k = 1..U;$
- $u_{P,k} = x_{f(k+(P-1)xU)}$ $k = 1..U,$

where:

- x_X is the input bits;
- $u_{P,k}$ is the output bits;
- P is the number of physical channels;
- U is the ratio between the number of input bits and the number of physical channels; and
- F is conditional. During non-compressed mode f(k) = k. But when compression by puncturing:
  - ➢ $U_{1,1}$ corresponds to bit x_k, with k being the smallest index if bits p are not counted; and
  - ➢ $U_{1,2}$ corresponds to bit x_k, with k being the smallest index if bits p are not counted and this continues for $u_{1,3}$ until $u_{P,u}$.

In the second interleaving, a similar operation to the first interleaving is used, but 30 columns are used this time, where the permutation pattern is:

Number of columns (c2)	Inter-column permutation pattern $<P2(0), P2(1)…P2(c2-1)$
30	$<0, 20, 10, 5, 15, 25, 3, 13, 23, 8, 18, 28, 1, 11, 21, 6, 16, 4, 14, 24, 19, 9, 29, 12, 2, 7, 22, 27, 17>$

Table 3.3 Inter-column permutation patterns for 2nd interleaving

3.1.8 Physical Channel Mapping

Physical mapping is done by mapping bits v_{pk} onto the Physical Channels (PhCHs). The bits for each PhCH are to be transmitted over the air interface in ascending order, following k. Notation in this section is denoted as follows [35]:

- $v_{p1}….v_{pU}$ are the input bits;
- p is the physical channel number; and
- U is the number of bits in one radio frame in one physical channel.

Downlink physical channels do not need to be completely filled with bits. The association of transport channels with physical channels is as listed below:
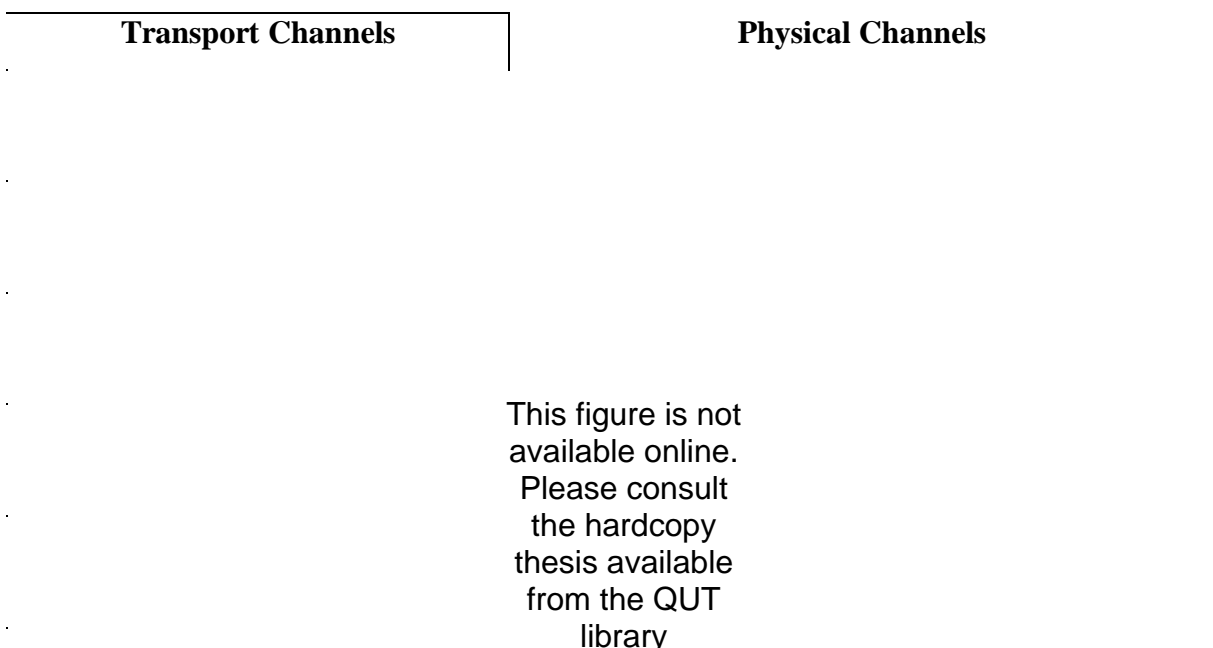
Transport Channels   **Physical Channels**

This figure is not available online. Please consult the hardcopy thesis available from the QUT library

This figure is not available online. Please consult the hardcopy thesis available from the QUT library

Table 3.4 Transport Channel to Physical Channel Mapping [35]

This section describes the operations involved in multiplexing and channel coding, processing transport level data into a form suitable for conversion into a physical signal. The next section covers the remainder of the transport data conversion process, providing details with spreading and modulation in the preparation of the physical layer data for radio transmission.

3.2 Modulation and Spreading

This section covers the modulation and spreading technique used by the UTRA FDD downlink channel. This technique is used for the Primary Common control Physical channel (P-CCPCH), Secondary Common Control Physical Channel (S-CCPCH), Common Pilot Channel (CPICH), Acquisition Indicator Channel (AICH), Page Indication Channel (PICH), Physical Dedicated Shared Channel (PDSCH) and Downlink Dedicated Physical Channel (DPCH), which is the common phrase referring to the Dedicated Physical Data Channel (DPDCH) and the Dedicated Physical Control Channel (DPCCH). See the details derived from [11].

This figure is not available online. Please consult the hardcopy thesis available from the QUT library

Spreaded signal

Figure 3.2 Downlink spreading [11]

The downlink data are first serial-to-parallel converted and mapped onto I and Q arm (each symbol pair converts to even and odd numbers respectively) as shown in Figure 3.2. The two notable processes of channelization ($C_{ch,SF,m}$) and scrambling ($S_{dl,n}$) are visible. The channelization is used to spread the real value code $C_{ch,SF,m}$ to the actual chip rate. The chips are then scrambled via complex chip-wisemultiplication using complex-valued scrambling code $S_{dl,n}$. The channels are then individually weighted and convolved. The spreaded channels are complex added, before being complex added again with the non spreaded channels, and then handed to the modulator. Note that the physical channels feed into the spreading process (except Acquisition Indicator Channel (AICH)) and can have value of +1, -1 and 0 (0 indicates DTX). The various downlink physical channels are multiplexed as shown in Figure 3.3.

Downlink Physical Channels from Spreading in Figure 3.2-1

This figure is not
available online.
Please consult
the hardcopy
thesis available
from the QUT
library

▼

Figure 3.3 Multiplexing of Multiple Physical Channels [11]

The channelization code used in spreading is called the Orthogonal Variable Spreading Factor (OVSF, maintains orthogonality between channels of different rates and spreading factors). P-CPICH and P-CCPCH are fixed with channelization codes $C_{ch,256,0}$ and $C_{ch,256,1}$ respectively, while the remaining channel is dynamically assigned into another channelization code by the UMTS access network UTRA Network (UTRAN). OVSF is defined as per Figure below, noting the format is $C_{ch,SF,k}$ where k is the code number and $0 \leq k \leq SF-1$.

Figure 3.4 Channelization Code Definition [11]

A total of 262143 separate and distinctly different scrambling codes are utilized from the 2^{18}-1 combination. It is divided into 512 sets of primary scrambling codes and each has 25 secondary scrambling codes. It is generated by combining two real sequences into a complex sequence. The real sequence is constructed as position-wise modulo-2 sum of 38400 chip segments of two binary m-sequence generated by a two-polynomial generator of degree 18. The resulting sequence is a set of gold sequence, which is repeated every 10 ms radio frame. Suppose x and y are the two real sequences, x sequence is constructed using polynomial $1 + X^7 + X^{18}$ and y sequence constructed using polynomial $1 + X^5 + X^7 + X^{10} + X^{18}$. Taking the m-sequence as $Z_n(i) = x((i+n)$ modulo $(2^{18}$-1$)) + y(i)$ modulo 2, where $I = 0\ldots.. 2^{18}$-2. The scrambling code $S_{dl,n}(i)$ is thus $= X_n(i) + jZ_n(i+131072)$ modulo $(2^{18}$-1$))$, $i = 0,1,\ldots,38399$. [11]

The spread complex-valued chip sequence is then modulated using a QPSK [38] modulator, illustrated as below (downlink modulation chip rate is 3.84 Mcps):

This figure is not
available online.
Please consult
the hardcopy
thesis available
from the QUT
library

Figure 3.5 QPSK Modulator [11]

This ends the section on spreading and modulation, and also the entire section on the UMTS radio interface. This section has provided a conceptual but technical overview of the actual process of the wireless connection between UTRA network and UE. It is assumed now that the reader has acquired enough information about UTRA to allow an understanding of the section on the UTRA simulation test bed module. This section has formed the conceptual design for the building of the UTRA module in the test bed, as shown in later sections. The next section is concerned with the other element, which is equally important in this thesis, the HVS-based image quality metric.

Chapter 4. HVS-Based Image Quality Metric

With the incremental advancement of mobile communication technology, the presence of a multimedia component in the communication services is forever on the increase. Example applications of the heavy usage of a multimedia component include web browsing, video streaming, video conferencing etc. Such user services are already commonplace within the wired network but are gradually being introduced onto the mobile network, following the ongoing deployment of technology that enables such high demand applications. UMTS standards currently define several classes of services covered by the standard [16], this includes conversational classes (e.g. voice), streaming class (e.g. video streaming), interactive class (e.g. web browsing) and background class (e.g. email download). Quality assurance can be establish via a Quality of Service (QoS) contract, where the parameters listed are ensured to stay within an acceptable level. Examples of measurements of quality in terms of QoS are, for example, the guaranteed bit rate, maximum bit rate, transfer delay and bit error ratio [39].

At present, it is the only early stages of 3G/UMTS deployment, and the majority of communications task will concentrate on delivering connectionless data-oriented services (e.g. web browsing). Mobile networks have wireless behavior which is dramatically different from the wired network as it operates in an open-air environment within which a greater injection of error is inevitable. Without proper communication protocols at both application and service level, much of the contents may be rendered useless. Upon failure of protocols to protect such impairment, the content will need to be reconstructed at the user end. Graphic and text content are still easy to reconstruct; however, pictures or still images in web page contents are a much more difficult task. Therefore, when measuring quality of user end service, it is important to consider the deformation and impairment of still images. Furthermore the subsequent effect on the human subject is important, as the purpose of 3G is to bring multimedia content closer to the user.

An effective visual media quality measurement can provide constructive feedback towards measuring the accuracy and effectiveness of solutions many researchers have proposed to

improve multimedia delivery. Note from before that the quality measurements at UMTS service and traffic level are in terms of QoS parameters, which do not effectively represent quality of visual media. Consequently, it is common to quote physical data quality measurement (e.g. bit error rate, packet error rate) or video signal measurement (e.g. PSNR) when testing for multimedia quality over the wireless network although the quality of the multimedia content is actually the main concern. QoS parameters do not necessarily reflect the perceptual quality of the visual content; a more advanced and ergonomic perceptual quality metric is needed for a different yet effective approach to measuring media visual content quality [40].

This chapter aims to investigate an effective and ergonomic method of measuring the quality of multimedia visual content, especially for still images. The following is divided into three sections, with the first discussing the basic concepts of HVS-based image quality measurements. This is closely followed by presentation of two major in-depth concepts of this area, in two separate sections.

4.1 A Question of Measuring Image Quality

Image and picture quality has become an increasingly important issue in the incremental usage of multimedia in our daily routine. However, unlike physical and analog signals where quality is effectively determined using traditional signal processing methods, a good specialized picture quality measurement is needed to comprehend the likely response of a human viewer.

As recommended by ITU-R Recommendation BT.500-6 [41], images may be assessed using subjective or objective methods. Subjective methods involve using human subjects to judge the quality of a picture or image, while objective methods use mathematical algorithms that correlate well with the human perceptual response. It is obvious that an automated image quality assessment metric needs to be of an objective nature. A wide number of objective methods have been proposed and documented; however, many still use the simple calculation of Mean Square Error (MSE), Peak Signal-to-Noise Ratio (PSNR) and subjectively correlative parameters such as blurriness, blockiness, noisiness and jerkiness [42]. However, these monotonic methods seldom correlate well with the response of the Human Visual System (HVS), which is very complicated and non linear.

Among many proposals to solve the problem, HVS-based techniques have fueled a series of new models that accurately measure image fidelity and are robust enough to withstand subjective testing. HVS theory involves the factors of early vision, by means of which human visual attention is modeled. A scalar quantification is produced for accurate subjective testing, and is generally applicable upon a large range of images. HVS-based models normally mimic operations of the early vision system (including primary visual cortex) using five main factors of [42]:

- Luminance to contrast conversion (for example in [43]);
- (Multiple) Channel decomposition (for example in [44]);
- Contrast Sensitivity Function (CSF) (for example in [45]); and
- Masking (for example in[45, 46]).

These five factors are the important properties of human early-vision. Luminance to contrast conversion is the process that mimics the ability of the human eye to code changes in the spatial domain, where the spatial domain refers to the aggregate of pixels composing an image [47]. This is done by accessing the ratio of the luminance of the visual stimulus with its background, thus determining its contrast. A particular example is the use of Local Band-limited Contrast (LBC) [48] which can define a value of contrast at each point in the image for each spatial frequency band. Note from Figure 4.1 that spatial frequency is the measure of sine-wave grating changes per degree field of vision, in order of cycle per degree (c/deg). Channel decomposition is needed to break down the images into spatial channels for application of LBC. CSF is a function which emulates HVS relationship to detect contrast threshold, which is the contrast needed for detection of stimulus on a flat background. Normally, a human observer exhibits the property of a low pass or band pass filter CSF behavior in terms of spatial frequency. By cautiously assuming that HVS is linear, this provides a powerful method for visually determining complex visual stimulus.

High Spatial Frequency   **Figure 4.1 Spatial Frequency**   **Low Spatial Frequency**
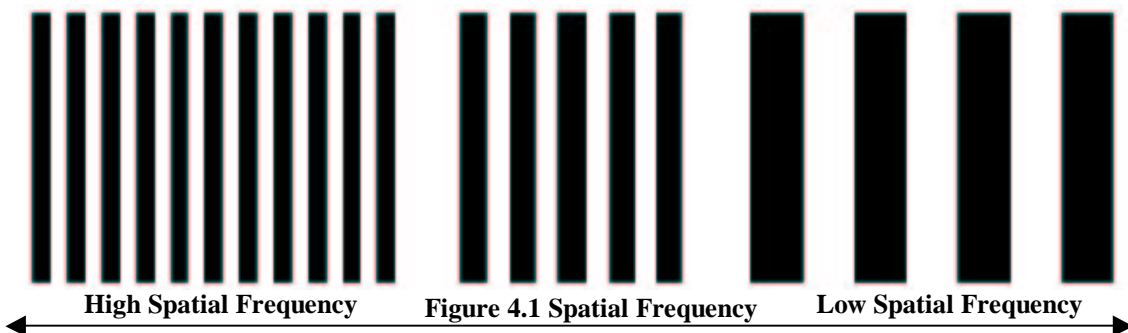
The image quality metric is for measurement of the distortion of the original image relative to the received/coded images. Quality metric based on HVS techniques measures the perceptual importance of an image by discounting its psychophysically redundant features. Please note that beyond this stage, the term "stimulus" is referred to as the distortion of the received/coded image relative to the original image and the original image is identified using the term "background". Masking is the phenomenon where reduction in visibility is brought about when stimuli are viewed on a non-uniform background, relative to viewing in a uniform background. This affects the CSF as the masker increases, causing the CSF threshold to rise. The effect is known as Threshold Elevation (ThE) [49]. Summation is the weighted inclusion of all the four mentioned components to produce a more complete HVS model.

Among all perceptual image quality metric with HVS-based fidelity models, two important factors must be observed:

- Model parameters: Chosen to reflect the viewer visual response to both complex natural scenes and simple artificial stimuli; and
- Quality rating: It is important for model to convert the visual error map into a single number for determining overall quality distortion. Therefore, higher level cognitive factors need to be carefully employed.

Numerous HVS based quality metrics have been proposed. Among the notable models are those developed by Daly [50]; Karunasekera and Kingsbury [51]; Lubin [52]; Osberger [42]; Teo and Heeger [53] and Watson [46]. These are summarized briefly below.

Daly proposed the Visible Differences Predictor (VDP) algorithm in [50]. This is a multi-channel (decomposition) image quality metric for assessing image fidelity. It can be calibrated for specific viewing characteristics such as viewing distance, pixel spacing etc. Luminance values of the original and distorted image are pass through a luminance non-linearity process, followed by a robust CSF. The image is then decomposed into multiple frequency and orientation sensitive channels and passes into the masking process to adjust each channel's visible threshold. A process termed Mutual Masking (MMsk) is then performed to account for different type of artifact. The resulted differences are compared

to the thresholds to produce a map of visually notable differences, which traces the extent and location of the errors.

Karunasekera and Kingsbury present a single channel decomposition model in [51] for detection of image distortion, particularly blocking artifacts. This model is extendable to include other image distortion artifacts such as ringing and blurring. HVS modeling used here is based on parameters derived from measurement of subject reaction time to various clearly visible (suprathreshold) stimuli. Luminance non-linearity and spatial activity masking stages is also included, followed by determining magnitude of the image artifacts by averaging errors around artifact edge. Results with good correlation with subjective rankings have been achieved. However, image quality metrics built using this technique cannot be applied generally, as the quality grading is highly dependent on types of image artifact present.

In [52], Lubin presents another multi-channel model, which again calibrates for viewing characteristics. The raw luminance signal is effectively converted to local contrast in this model and decomposition into separate spatial frequencies occurs. Orientation selectivity, contrast sensitivity and spatial masking follow, where the intra-channel masking effect is simulated using a sigmoid non-linearity. Summation across all channels using a Minkowski metric is applied following thresholding to produce a visually notable difference map. A single quality figure is then obtained by summation across the map, which allows comparison of quality between images. Lubin's model achieves result with close correlation with subjective testing.

The model proposed by Osberger in [42] and [54] includes multiple channel contrast conversion, frequency sensitivity and masking. It also includes the Importance Map (IM) concept in the model for a more accurate access to quality by identifying the relative importance of various areas in an image. Osberger uses the IM of an image to scale the fidelity found to obtain a more complete error assessment. A quality grading is produced to enable comparison between different results. This model is specifically tuned for natural images and Osberger presents strong verification testing with favorable result [42] to show that his system is robust, efficient and accurate.

Teo and Heeger [53] based their model on the response of a cat's vision system. In their system the original and distorted images are first decomposed into spatial frequency and orientation sensitive channels using a linear transform. Contrast masking is then applied using squaring and normalization. Summing response differences between both images (over small patches of the images) completes the detection process. Although Teo and Heeger present a sound system, they did not produce comparison of their results with that obtained using subjective opinion. Therefore it is difficult to verify the accuracy of this model.

Watson presents a video quality metric in [46], which can be adapted to process images. The model first converts image illumination values to local contrast form, where a sequence of noticeable visual difference is then obtained by dividing the contrast values with spatial thresholds of respective spatial frequencies. A nett difference sequence is further produced by subtraction of the two sequences from the two images. Contrast masking is then applied, followed by Minkowski pooling to sum the result over difference frequency channels, yielding a summary measurement of visual error.

Osberger's model stands out among the others listed above, providing techniques that are both accurate and extendable. Therefore, this model is selected for implementation in this thesis. The remainder of this chapter covers the two major concepts in Osberger model, the HVS-based fidelity system and the Importance Map.

4.2 HVS Fidelity System

The early vision model proposed by Osberger in [42] and [54] is for assessing both the fidelity and the quality of natural images, based on the operation of neurons in the primary visual cortex of the human eye. This Early Vision (EV) model is tuned for natural images and is of an adaptive and non-linear nature. Figure 4.2 illustrated the EV model (2 images).

This figure is not
available online.
Please consult
the hardcopy
thesis available
from the QUT
library

Figure 4.2 HVS Early Vision Model [54]

The model accepts the luminance values at the same location of both images then converts it into band-limited contrast, using a Local Band-limited Contrast (LBC) function. The function decomposes the contrast into 1-octave bandwidth channels, which are further decomposed into orientation selective channels (using fan filters). The result and its difference is then processed using the Contrast Sensitivity Function (CSF) [45], determining the frequency-dependent threshold of detection. Threshold Elevation (ThE) models the spatial masking process to raise the detection threshold. Visibility of difference between the original and distorted image is determined using the new threshold. This process repeats for each channel at each location by subtracting the original LBC signals from the coded LBC signals. The method of identifying the visibility difference is by dividing the individual difference for each channel at each location by the detection threshold [42].

Minkowski summation is performed across multiple channels to produce a single fidelity map for indication of the visible distortion locations. This map is the same size as the original image and is known as the Perceptual Distortion Map (PDM). It indicates the number of Just Noticeable Differences (JND) [46, 55, 56] of the distorted image that is above detection threshold. A further Minkowski summation across the PDM space produces a single number known as the Perceptual Quality Rating (PQR), which is in the range of 1.0-5.0. PQR is the ranged number produced from PDM to rank the distorted image and it correlates well with validation tests. Note that a higher number corresponds to lower distortion, hence higher quality.

Individual factors from channel decomposition to summation are discussed in the section below.

4.2.1 Channel Decomposition and Band-limited Contrast

The model accepts luminance values as input. Therefore, a set of image gray levels needs to be converted into luminance using determined parameters from the display device. The model described here is from [42]. Parameters of importance include viewing distance, pixel spacing, image dimensions, ambient luminance and display luminance response (monitor gamma level). The default value in the implemented model should carries the values that correlate with the physical properties of the equipment used to subjectively verify the model.

As mentioned before, LBC algorithm [48] is used to decompose the input image luminance into multiple channels, of which the images are represented as local band-limited contrasts. Cosine log filters with 1-octave bandwidth are used to implement the spatial frequency decomposition in LBC. Original image is recoverable via simple addition. The filter has a 1-octave bandwidth and centred at frequency 2k-1 c/deg, with r being the radial spatial frequency, the expression becomes:

$$G_k(r) = 1/2\{1 + \cos(\Pi \log_2 r - \Pi(k-1))\},$$
(4.1)

of which the representation can be seen in Figure 4.3 (a):

This figure is not
available online.
Please consult
the hardcopy
thesis available
from the QUT
library

(a)   **(b)**
Figure 4.3 Filter Structure [42]
(a) Spatial frequency response of cosine log filters (with 1-octave bandwidth)
(b) Orientation response of fan filter with 30degree bandwidth

Fourier transform F(r,θ) is performed upon the image f(x,y) then filtered using a cosine log filter, producing a band-limited image:

$$A_k(r,\theta) = f(r,\theta)G_k(r). \tag{4.2}$$

Channel orientation sensitivity is implemented using a fan filter, observe Figure 4.3(b), of which the equation of the fan filter [50, 57] with orientation is:

$$fan_l(\theta) = \begin{cases} \frac{1}{2}\{1+\cos[\frac{\pi|\theta-\theta_c(l)|}{\theta_{tw}}]\} & if \ |\theta-\theta_c(l)|<\theta_{tw} \\ 0.0 & \text{otherwise,} \end{cases} \tag{4.3}$$

note that θ_{tw} is the angular transition width and $\theta_c(l)$ is the orientation of the peak fan filter l as represented by:

$$\theta_c(l) = (l-1)\vartheta_{tw} - \pi/2 \tag{4.4}$$

Typically, four (using orientation bandwidth 45 degree) or six (30 degree bandwidth) fan filters are used. This corresponds with the mean bandwidth in the cortical neurons of the monkey and the cat. To ensure filtering is fully reversible, the θ_{tw} or angular transition width is set to the angular spacing between adjacent fan filters. However, as implementation of orientation sensitivity (i.e. fan filtering) increases, the computational

cost increases significantly. Because this does not give much improvement in result accuracy, it is therefore omitted.

Usually, six frequency channels are used, giving k=1..6. Individual spatial frequency band $A_k(r,\theta)$ is transformed back into the spatial domain using inverse Fourier transform, giving $a_k(x,y)$. Now, the local band limited contrast needs to be calculated as $c_k(x,y)$ by [42]:

$$c_k(x, y) = \frac{a_k(x, y)}{l_k(x, y)}, \tag{4.5}$$

given that $l_k(x,y)$ is the mean local luminance. Given that a_0 is the residual low frequency image, it is calculated by:

$$l_k(x, y) = a_0(x, y) + \sum_{i=1}^{k-2} a_i(x, y), \tag{4.6}$$

4.2.2 Contrast Sensitivity Function

CSF detailed in this model must be appropriate for the visual stimuli in the task of assessing fidelity and quality of natural images. The spatial extent of the grating patch identifiable by the CSF must be small (1 cycle) with temporal presentation of l.0 seconds. The question of lighting level also needs to be considered. Typically, high light levels dim a stable CSF (typically > 10 cd/m^2) while at lower levels it reduces in proportion to the square root of the luminance (DeVries-Rose law). Given that l is local luminance, CSF$_{base}$ is the base threshold for high luminance values [58-61] and l_{th} is the cut-off luminance, which is consistent with DeVries-Rose law, CSF can be defined as [42]:

$$\text{CSF}(l) = \begin{cases} \text{CSF}_{base} & l \geq l_{th} \\ \sqrt{\dfrac{l}{l_{th}}} CSF_{base} & l < l_{th}, \end{cases} \tag{4.7}$$

4.2.3 Spatial Masking

As mentioned before, contrast of the background and the uncertainty created by the background are the main factors that influence the amount of masking taking place. This model uses a threshold elevation process to model spatial masking. Typically, low

uncertainty stimuli exhibit ThE curve with log-log of gradient 0.7 while high uncertainty (complex) stimuli exhibit gradient of 1.0 [42]. This is as shown in Figure 4.4.
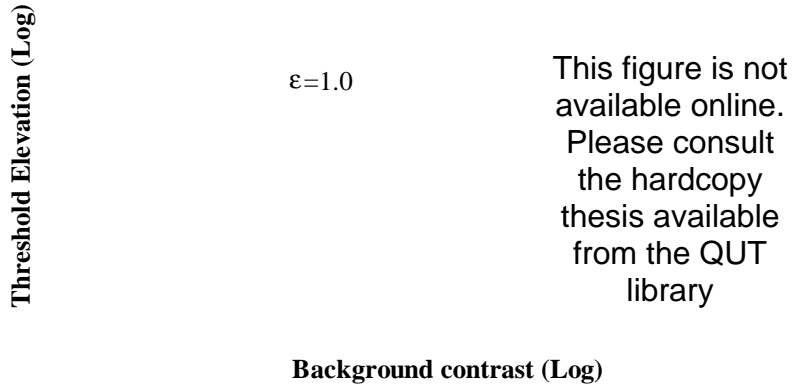
Threshold Elevation (Log)

$\varepsilon=1.0$

This figure is not available online. Please consult the hardcopy thesis available from the QUT library

Background contrast (Log)

Figure 4.4 Log-Log relation of ThE VS Background Contrast [42]

In short, human viewers tolerate greater error in textured areas (high complexity) than among edges (low complexity). In this model, the spatial masking effect is emulated by classifying images into flat, edge and texture regions. Point is classified as flat if local contrast of the region is below the threshold needed to induce masking (contrast $<C_{th0}$). In contrast, where an orientation is dominant, the point is classified as an edge, while the rest is classified as being a texture. The ThE is used to implement masking, as stated in page 112 of [42]:

$$C_{thk} = \begin{cases} C_{th0k} & \text{If } C_{mk} < C_{th0k}, \\ C_{th0k}(\dfrac{C_{mk}}{C_{th0k}})^{\varepsilon} & \text{otherwise} \end{cases} \qquad (4.8)$$

Note that:

- C_{thk} is the detection threshold, where a masker is present for frequency k
- C_{th0k} is the base threshold for *k* (frequency band from CSF)
- C_{mk} is the contrast of the masker for *k*
- Use $\varepsilon = 0.7$ for edge and $\varepsilon = 1.0$ for textured.

The masking process for this model is for single frequency band only, not across multiple channels. Now that masking dynamically changes the detection threshold for scene error using local scene content, the difference between original and coded images $V_k(x,y)$ is now represented as in page 113 of [42]:

$$V_k(x,y) = \frac{c_k(x,y) - c_k^{'}(x,y)}{C_{thk}(x,y)} \qquad (4.9)$$

Note that c_k is the original image contrast while $c_k^{'}(x, y)$ is the coded image contrast. It goes without saying that when $V_k(x,y) = 1.0$, the difference is equal to the threshold of detection.

4.2.4 Summation

After division of the error signal by detection threshold in each channel and location, the visible distortion is spread in a multi-resolution way. A single map is needed to effectively show the visibility of distortion, where summation across different channels is needed. Minkowski summation is used across different channels to produce the Perceptual Distortion Map (PDM) where the error at each point is effectively represented. The location and magnitude of visible distortion is clearly visible, representing the image fidelity. The PDM equation is shown below, where β_1 is the probability summation exponent with a typical value of 4.0, as in page 114 of [42].

$$PDM(x, y) = (\sum^{k} V_k(x, y)^{\beta_1})^{1/\beta_1}$$

(4.10)

A single number to present the overall picture quality is required for ease of comparison. Minkowski summation is again used for summation of N pixels PDM to produce a fidelity to quality conversion. The Quality rating is termed Perceptual Quality Rating (PQR) and is calculated as in page 114 of [42]:

$$PQR = (\frac{1}{N}\sum^{N} PDM(x, y)^{\beta_2})^{1/\beta_2}$$

(4.11)

Note that $\beta_2 = 1.0$ gives the quality that is proportional to the error average over the entire image, while $\beta_2 = 3.0$ gives the most accurate result according to page 114 of [42]. To scale it into a range of 1.0-5.0 for ease of referencing, the following equation is used with p = 0.8:

$$PQR_{1-5} = \frac{5}{1 + p \cdot PQR}$$

(4.12)

This ends the section on the HVS-based fidelity system for determining distortion across two images. The next section focuses on the Importance Map concept for identification of the spread of the importance area across an image.

4.3 Importance Map System

The Importance Map (IM) technique used in this thesis is outlined in both [62] and [54]. It is a region-based attention model, with its main approach based upon combining multiple feature maps into an overall map that grades attention. The approach is to first segment the image into homogeneous regions, then derive a series of intermediate feature maps using factors known to influence visual attention [63]. Next, these maps are fused together with individual weighting upon each feature map to generate an overall IM.

Factors that influence attention can be either regional based properties like size and shape, or object oriented based properties like contrast and texture. The success of generating IM depends on the image segmentation, which is an active research area of its own. In this model, a recursive split and merge technique is used, as it is efficient as well as low in computational cost. The recursive split and merge technique is based upon local region variance. Split process is performed via comparison of an image block's variance to the split variance threshold. While exceeding the threshold, the block is divided into four sub-blocks, and recursively splitting the individual sub-blocks until the blocks either satisfy split criteria or the block size is smaller than the pre-determined minimum (e.g. 1 pixel). Upon completion of the splitting process, the result is then merged. Adjacent regions are merged into a single region if the merged region has a lower variance than the merge variance threshold. The minimum region size threshold is set at 16 pixels to avoid accumulation of regions that are too small. Both the split variance threshold and the merged variance threshold are recommended to be 250 to provide good results for most natural scenes [42].

Figure 4.5 describes the overall process of the IM processing proposed by [62] and [54].

This figure is not
available online.
Please consult
the hardcopy
thesis available
from the QUT
library

Figure 4.5 IM Processing [64]

As shown, the segmented area is analyzed by different factors that influences attention, the area of interest as shown below [54, 62]:

- Contrast of region with its surroundings: Area with high contrast relative to local surrounding regions is a strong visual attractor. This is due to the behavior of the human eyes, converting luminance to contrast at the early stage of processing, as described in a previous section.

- Size of the region: larger regions are stronger visual attractors, relative to smaller regions. However, there is a saturation point.

- Shape of the region: unusual (e.g. multiple corners and angle) or long and thin shapes are attractors of attention, over smooth and homogenous region.

- Location of region: the region around the centre is stronger, and so attracts more visual attention.

- Foreground/Background region: the foreground region is a stronger visual attractor than the background region.

- Others: Color, skin tone etc…

The following outlines the various relations that govern the calculation of the five individual feature maps. Given that an image is recursively split and merged into a series of regions termed R_i ranged from 1 to X, and X is the number that is determined to be the end of the recursive split merge process. Five individual feature maps are produced, based upon the calculated importance value of the individual features of the region. Therefore, for a region R_i that covers pixel (x_i,y_i) to (x_j,y_j) and graded value A for the importance factor I_m, the pixels covered by R_i on the feature map for I_m will all be given the importance value A. All the results are combined with weight factors, discriminating between the more attractive attributes and the others, producing a complete IM.

Contrast important I_{cont} is calculated using the equation below [62].

$$I_{cont}(R_i) = \frac{\sum_{j=1}^{J}\left(\left|\overline{R_i(gl)} - \overline{R_j(gl)}\right| \cdot \min\left(k_{border} \cdot B_{ij}, size(R_j)\right)\right)}{\sum_{j=1}^{J} \min(k_{border} \cdot B_{ij}, size(R_j))} \tag{4.13}$$

Note that:

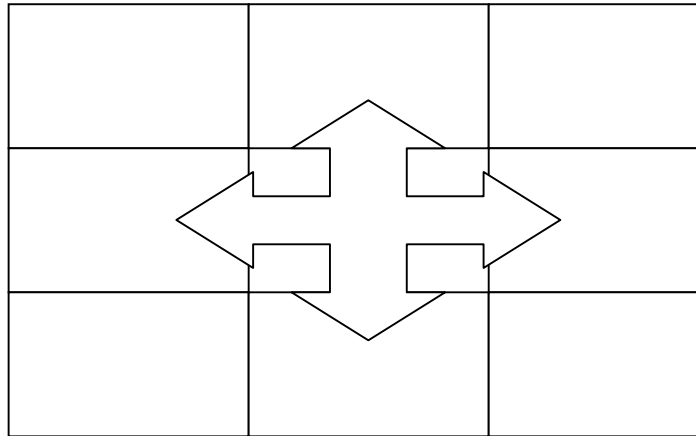- j=1..J are regions with a 4-connected border with R_i, as outlined below

Figure 4.6 Illustration of 4-connected Relationship

- k_{border} is a constant for limiting extent of neighbor influence
- B_{ij} is the number of pixels in R_j which share 4-connected border with R_i
- I_{cont} is scaled in the range 0-1

Size importance I_{size} is calculated based upon the size of the region, as given in Figure 4.6 [62]. The I_{size} value is calculated based on the size of R_i using the relationship of:

- $I_{size}(R_i) = 0$ if $size(R_i) \leq th_{size1}$;

- $I_{size}(R_i) = \dfrac{1}{th_{size2} - th_{size1}}$ if $th_{size1} < size(R_i) \leq th_{size2}$;

- $I_{size}(R_i) = 1$ if $th_{size2} < size(R_i) \leq th_{size3}$;

- $I_{size}(R_i) = 1 - \dfrac{1}{th_{size4} - th_{size3}}$ if $th_{size3} < size(R_i) \leq th_{size4}$; and

- $I_{size}(R_i) = 0$ if $size(R_i) > th_{size4}$.

Note that the threshold is selected as $th_{size1} = 0$, $th_{size2} = 0.01$ $th_{size3} = 0.05$ and $th_{size4} = 0.50$.

This figure is not
available online.
Please consult
the hardcopy
thesis available
from the QUT
library

Ratio of Size of Region Ri to size of image

Figure 4.7 I_{size} Calculation [62]

Important of region shape I_{shape} is calculated as below [62]:

$$I_{shape}(R_i) = k_{shape} \cdot \frac{bp(R_i)^{pow_{shape}}}{size(R_i)} \tag{4.14}$$

Note that:

- $bp(R_i)$ is the number of pixels in R_i that shares a 4-connected border relation with another region
- pow_{shape} is a factor used for increasing size-invariance of I_{shape}
- k_{shape} is a scaling constant (adaptive) for reducing shape importance for regions with many neighbors
- I_{shape} is scaled to range 0-1

Importance of region location is calculated using the equation below [54]:

$$I_{location}(R_i) = \frac{\sum_{z=1}^{4} w_z \cdot numpix(R_{iz})}{size(R_i)}$$

(4.15)

Note that:

- $numpix(R_{iz})$ is the number of pixels in region Ri that locates in zone z
- w_z are the zone weightings as shown below:

This figure is not
available online.
Please consult
the hardcopy
thesis available
from the QUT
library

Figure 4.8 Location zones weightings [62]

The foreground/background region importance is based on the assumption that fore-ground objects do not locate on the borders of the scene. Regions are assigned to be in the foreground or the background by considering the number of pixel the region has on the frame border. High frame border pixel count distinguishes the region to be in the background and vice versa. The generalized equation used is shown below [62]:

$$I_{FGBG} = 1 - \min\left(\frac{borderpix(R_i)}{0.3 \cdot \min(borderpix(frame), perimeterpix(ri))}, 1.0\right)$$

(4.16)

Note that:

- $borderpix(R_i)$ is the number of pixels in R_i that are also on the edge of the frame

- perimeterpix(R_i) is the number of pixel in R_i, which shares a 4-connected border with another region.

To produce an overall IM, the various factors for the various regions must be effectively added together, using the following equation [62]:

$$I_{spatial}(R_i) = \sum_{f=1}^{5}(w_f^{pow_w} \cdot I_f(R_i)^{pow_f})$$

(4.17)

Note that:

- f is a particular importance feature;
- w_f is the feature weight, which is assigned as the following for maximum effectiveness:
  - ➢ Location: 0.270,
  - ➢ Foreground/background: 0.246,
  - ➢ Shape: 0.182,
  - ➢ Contrast: 0.169, and
  - ➢ Size: 0.133;
- pow_w is the feature weighting exponent for control relative impact of w_f of which in this thesis it is taken as 1 for all features;
- power$_f$ is the IM weighting exponent, which is also taken as 1 for all features in this thesis's implementation; and
- Furthermore, the highest importance region is scaled to have a value of 1.0.

This ends the section on Importance Maps and thus concludes the section on HVS-based image quality metrics. This Chapter has run through the concepts used for implementing the image quality metric chosen for use in the system. The following chapters describe the implementation of the entire 3G multimedia software test bed, as stated in the introduction. The information on HVS-based system is visited again in a later section describing its implementation. The next chapter identifies the methodology used in the design of the software test bed.

Chapter 5. Test Bed Methodology

This section details the implementation of the working system. As mentioned, the system consists of two major units: the 3G/UTRA software test bed and the HVS-based image quality analysis module. This chapter concentrates on the system specification, followed by the system development details in Chapters 6 and 7. A top down waterfall approached [65] is employed as the main development method, with the overall structure as shown below:
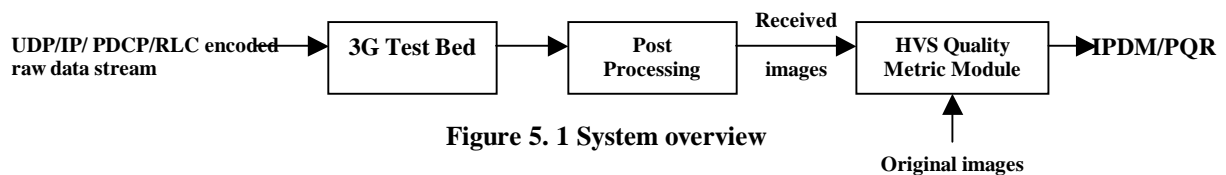

Figure 5. 1 System overview

The protocol coded data stream is sent through the 3G test bed and received at the output. Post processing converts the received data stream with the protocol to produce the received media as a series of images to be fed into the image quality module. A rating is then obtained to reflect the distortion of the received media relative to the original.

The test bed is designed to accept coded data for the transport layer channel, the Dedicated Channel (DCH). Note that the DCH is commonly mapped onto the Dedicated Physical Data Channel (DPDCH) and the Dedicated Physical Control Channel (DPCCH).

Upon a network simulation, the data stream needs to be coded with a protocol to complete the basic protocol requirement prior to streaming into the 3G test bed. Protocol under immediate consideration includes:

- UDP and IP [28] for network routing; and
- Packet Data Convergence Protocol (PDCP) and Radio Link Control (RLC) for radio resource control [66-68].

It is therefore clear that the UTRA/3G module of the test bed implements physical channels DPDCH. The design is based entirely upon Chapter 3, of which only a subset is implemented. The test bed accepts the transport channel DCH as input. The primary aim is

to implement a single channel FDD downlink user channel, with variable channel conditions that can be controlled to reflect different situations which the physical signal can be exposed to. Some basic environmental parameters include speed and signal arriving angles, which are presented in the next section. Furthermore, the information/data rate and physical traffic rate, together with other variables, are also available for selection. Two models of the 3G test bed are implemented, with one using a variable rate downlink and the other using a fixed rate downlink. The model presented in this thesis uses a variable rate downlink, as time and resources allow only effective presentation of a single model.

HVS-based quality metric is implemented using the design stated in Chapter 7 by molding the HVS-based fidelity system together with the IM system, of which design details are stated in Chapter 4. An implementation of this quality metric is currently limited to processing Portable Gray Map (PGM) files. Adaptation to process color images is feasible. Post-processing is the process of extracting transmitted media into the form able to be processed by the HVS-based quality metric. In this case, the accepted format is a series of PGM files or, in a later implementation, PPM files for color images.

The system structure module is developed in a module format for ease of structural and functional expansion and maintenance. Objectively collected functionality has controlled the natural breakdown of functions to be grouped into the 3G test bed, image quality metric and post-processing module, as mentioned. The purpose of the 3G test bed and image quality metric differs greatly, and although strong cohesiveness is built into the system, it is logical to develop the test bed and quality metric separately, using tools more suitable for telecommunication and image processing, respectively. These two modules are the common part of this system, where, at its minimum, it allows the system to serve as a simple 3G test bed for the testing of raw images.

This system is designed to be flexible and versatile, to dynamically fulfill the user's requirements, as controlled by the post-processing module. An example of this is use of the system to perform an efficiency test for a new multimedia application protection protocol. In the case where the input into the system is the transport level coded signal of the said media, post-processing is required to extract a series of images from the received data to be fed into the image quality metric. The system then produces a HVS oriented

quality evaluation on the received images, providing a guide for improving the tested protection protocol.

This chapter concerns mainly system methodology and functional specification. Chapters 6 and 7 further extend the general functional model presented here by bringing in domain specific design architectures. The 3G test bed module is presented in an object oriented manner, dividing up individual functional modules for detailed analysis, progressing using a general data flow direction. The image quality metric module is presented as an integration of the HVS fidelity module and the Importance Map module, illustrating the relationship between the two modules and the method used to integrate them. The development method of this module is different from the 3G test bed, where the architecture is generally functionally-based and is not objectively grouped. To effectively present this module, a functional flow model has been employed, describing the model by stepping through all the individual processes involved in data processing.

Following an explanation of the purpose of the individual functional modules, the remainder of this chapter presents brief specifications of the individual modules, and a brief discussion of the approach taken and validation tactics used for the system.

5.1 3G/UMTS Test Bed Methodology

The 3G/UMTS test bed aims to emulate the processing of DCH data into a physical layer signal (transmission), and the 3G physical channel condition and processing of the physical layer signal back into DCH data (receiving). Transmission and receiving processing is implemented directly from the specifications in Chapter 3, following UMTS multiplexing, channel coding, spreading and modulation outlines, as described. The physical channel condition is modeled to reflect the distortion experienced by the physical signal in a channel subject to multi-path fading effect, Doppler effect [69], channel delay and impregnated with Additive White Gaussian Noise [70] (AWGN).

This test bed models the actual process in 3G physical layer signal transmission, including transforming the transport layer data into a physical signal (transmitting) and processing the physical signal into transport layer data (receiving). The purpose of using this physically

precise model rather than a compact mathematical model that would statistically corrupt the data stream, is to enable closer approximation of the conditions the data stream is likely to be subjected to. Hence, this provides a more accurate and far more useful approach, allowing the system to be used in multiple applications, even those that require delicate modeling of the 3G physical layer functional processes (e.g. complex multimedia downlink applications).

The implementation of this module is a complex process, of which the selection of effective development tools and deployment platform is an important issue. Versatility should be preserved, allowing deployment of the 3G test bed onto both Linux and Windows-based PCs with minimal effort. Therefore, the development tools chosen should laterally use the translation language concept, with the language interpretation virtual machine available in both Linux and Windows platforms.

An in-depth search was carried out for possible tools, with the candidate being immediately narrowed down subjectively with the availability of resources to host them. The likely options include Ericsson's RedWine package [71], Matlab [72], Matlab Communication Blockset [72], OPNET [73], Agilent's Advance Development System (ADS) 2001 or direct development using C/C++. Red Wine is a private system used by Ericsson that is not within the author's access. Developing the test bed using C/C++ or Matlab using code written purely by the author will consume a large amount of time, not to mention the large amount of complicated testing that would need to be performed on every piece of code before the system could be validated. The likely candidate was narrowed down to Matlab Communication Blocksets, OPNET and ADS.

Each of the three remaining tools has been carefully tested for suitability. Matlab Communication Blocksets proved to be versatile, but lacked a large number of 3G functionalities, crippling its usefulness. OPNET has proved to be useful, providing the ability to simulate low-level 3G activities while also considering network level traffic management. However, the internal workings of OPNET are off-limits to the user, causing extreme difficulty in input and output of data for the system developed. Finally, the test bed implemented uses Agilent's ADS 2001, where selection was based largely on its versatile nature for telecommunications data processing system development. It consists of multiple 3G components, based upon UTRA, but ADS too experienced a large number of

input/output interfacing problems but these have been overcame. A large number of basic 3G functional components have been implemented, allowing the user to concentrate on developing the infrastructure of the system. Although the available basic components from ADS 2001 are at times inflexible, this package remains the most suitable developing environment used by the author to date.

The implementation process logically follows the specification in Chapter 3. The basic structure is collectively explained in correspondence to the four major functional processes of multiplexing, channel coding, spreading and modulation, as mentioned before. Additional consideration has been given to modeling the effect of transmission of multiple user signals and physical channel loses. These are presented in detail in Chapter 8.

Post-processing is primarily responsible for extracting a series of images from the received media. This process includes extracting the coded multimedia data from the received protocol coded data stream, followed by recovering the impaired data into the form closest to the original as possible. Next, extraction of image inputs to be fed into the image quality metrics is done with a dynamic process, which depends on the media type being tested. For example, if the media being tested is a JPEG image, the post-processing module is responsible for extracting an image of acceptable form for the metric. However, if the media handed is a MPEG stream, a series of images will be extracted and serialized for input into the metric.

Development of the 3G test bed module is among the most complex in this system. As shown, the methodology behind this module involves the implementation of the published 3G standards using an incremental developing software engineering model. The purpose and requirements of this module have been justified, including the role of the post-processing module. The next section continues with methodology of the image quality metric.

5.2 Image Quality Metric Methodology

The image quality metric in this system is used to provide an effective quality analysis indicator for the visible portion of the tested media. For image quality, it is one thing to say that the image has been corrupted using a subjective rating, but another to provide a valid metrical evaluation system that provides quality, with results correlating to relative grading by human subjects. As previously mentioned, objective methods like MSE and PSNR can be used to provide numbers for measurement of quality; however, these seldom correspond well to the grading provided by human subjects. This module combines the two major human vision emulation techniques described in Chapter 4 to provide a complete HVS-based image quality metric that is capable of providing quantitative measurements of quality degradation that are correlative to human subject ratings. Data obtained in this manner are not only comparative but they also reflect more accurate detection of image quality degradation as the behavior of the HVS is taken into account. Therefore, the image quality metric is integrated into the overall system to further extend the versatile nature of the system, allowing effective testing for degradation in multimedia quality.

The development model chosen for this module is a top down functional-based model, where the functions are grouped together according to their logical relations. Chapter 7 presents the implementation of the HVS-based fidelity sub-module and Importance Map (IM) sub-module with specifications outlined in Chapter 4, followed by overall integration of the two modules into the image quality metric. The merging enhances the result from the HVS-based fidelity sub-module using the IM sub-module, giving a more accurate HVS-based quality rating.

The two sub-modules are implemented separately and integrated together, with the HVS-based fidelity sub-module being implemented using Matlab, and the IM sub-module using C. This is the case, as the base code available for the author to use was originally in those formats, and this will be addressed in detail later. The first sub-module is functional-based, in reference to the development model chosen. The basic processes are built in a bottom up fashion with the logical grouping of small processes into repetitively used functions. The second sub-module is slightly more compact, due to the strong cohesive nature of the

processes involved. This module is implemented largely as a single function to yield stronger efficiency. Following presentation of the details of the implementation method, testing and verification approaches are shown in the next section.

5.3 System Testing and Validation Strategy

The system was tested using a black box testing strategy overall, as it is too complex to be fully tested function by function in a functional verification manner. Various functionality tests were performed during the building of the system but these tests are not presented as they do not enhance the purpose of this thesis which is to effectively present a system that addresses the objective stated in the introduction. Modules are tested individually for behavior to consolidate the specification outlined in relevant chapters. Upon satisfactory completion of the individual modules, overall system testing will be carried out on the intergradations of every modules, by subjecting the overall system to a continuous test run.

During individual testing, the 3G test bed module, the HVS fidelity module (commonly known as the HVS module) and the IM module will be tested. The 3G test bed module takes various images as input, while varying various adjustable parameters within the module that are significant (e.g. velocity, channel condition etc.).

The HVS module will take various images and their impaired images to test for fidelity of the damaged area. The IM module will take various images and constructs a series of IM based upon the single influencing factors and also the summation of all the influencing factors. Overall system testing will take the same path as the testing of the 3G test bed module. However, it will produce quality ratings, related fidelity map and IM map.

Testing and presentation in this thesis is limited to proving the feasibility and workability of the entire system. Therefore, no protocols (i.e. RLC, PDCP etc.) are implemented. Raw PGM files are processed by the system to produce individual modules and overall system result for presentation in Chapters 8 and 9.

This chapter has presented the system methodology, together with the infrastructure of the individual modules. All modules and infrastructure have been justified, followed by an explanation of the development strategy used. The testing and validation technique is also presented. The next two sections follow by presenting and outlining the progress and design prospective used in the implementation of the two main modules.
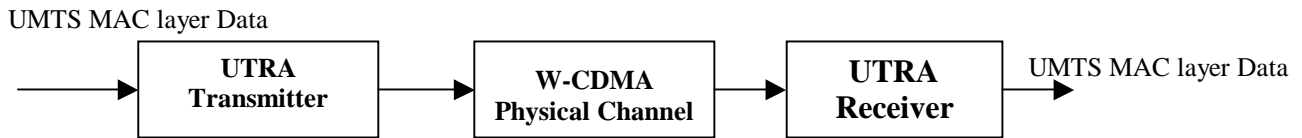
Chapter 6. ADS Implementation

UMTS MAC layer Data

| UTRA Transmitter | → | W-CDMA Physical Channel | → | UTRA Receiver | UMTS MAC layer Data |

Figure 6.1 UTRA Block Diagram

The system implements a single user downlink channel as shown above, which includes the Base Station (BS) source, 3G traffic channel and the User Equipment (UE) receiver. The basic physical channel Dedicated Physical Data Channel (DPDCH) is implemented to carry the transport channel Dedicated Channel (DCH), while assuming that the input into the system is readily coded DCH data. For an all-IP network enhanced UMTS, a DCH data stream should basically be the actual raw data being coded into UDP/IP [28] subsequently with header by Packet Data Convergence Protocol (PDCP) and BS's Radio Link Control (RLC).

System implementation is done via the 3G/UMTS component library and a strategic modification to the major components. The structural portions of the test bed design are carried out with some components being omitted (e.g. RLC). A major problem with implementing the test bed is due to ADS's lacking in I/O interface. This hurdle was overcame by using the MATLAB server interface. The input streams are placed in a binary file, to be read by ADS via the Matlab server interface, while the output is handled in the same fashion. The sub-images shown are the internal modified parts of the source components, for reading the input stream fusing Matlab server. The system default model set DPCH at 960 kbps and effective information data rate of 256 kbps. Simulation is non real time, and begins with a long setup time, where simulation of 30 data frames (1kb) takes around 11 minutes on a CPU with AMD 1800 XP processor and 256 MB RAM.

The following sections present the three major schematics of the implementation. Note that the diagrams in these sections are enlisted from [74]. Section 6.1 is the main schematics implementation for the test bed and is constructed using functional components provided by ADS with some modifications. The roles and functionalities of these individual

components are described in section 6.1. Section 6.2 and 6.3 provide further details into two major components used by the author to construct the main schematics. These schematics for the two major components were originally provided by ADS but were modified by the author by adding several special purpose additional modules. This modification was done using existing functional components provided by ADS. Note that ADS is a component based developing environment, with similar construction methods used in Visual Basic and Matlab Blockset: however, it contains more constraints and most basic components are not modifiable.

76.1 ADS Implementation Main Design Schematics
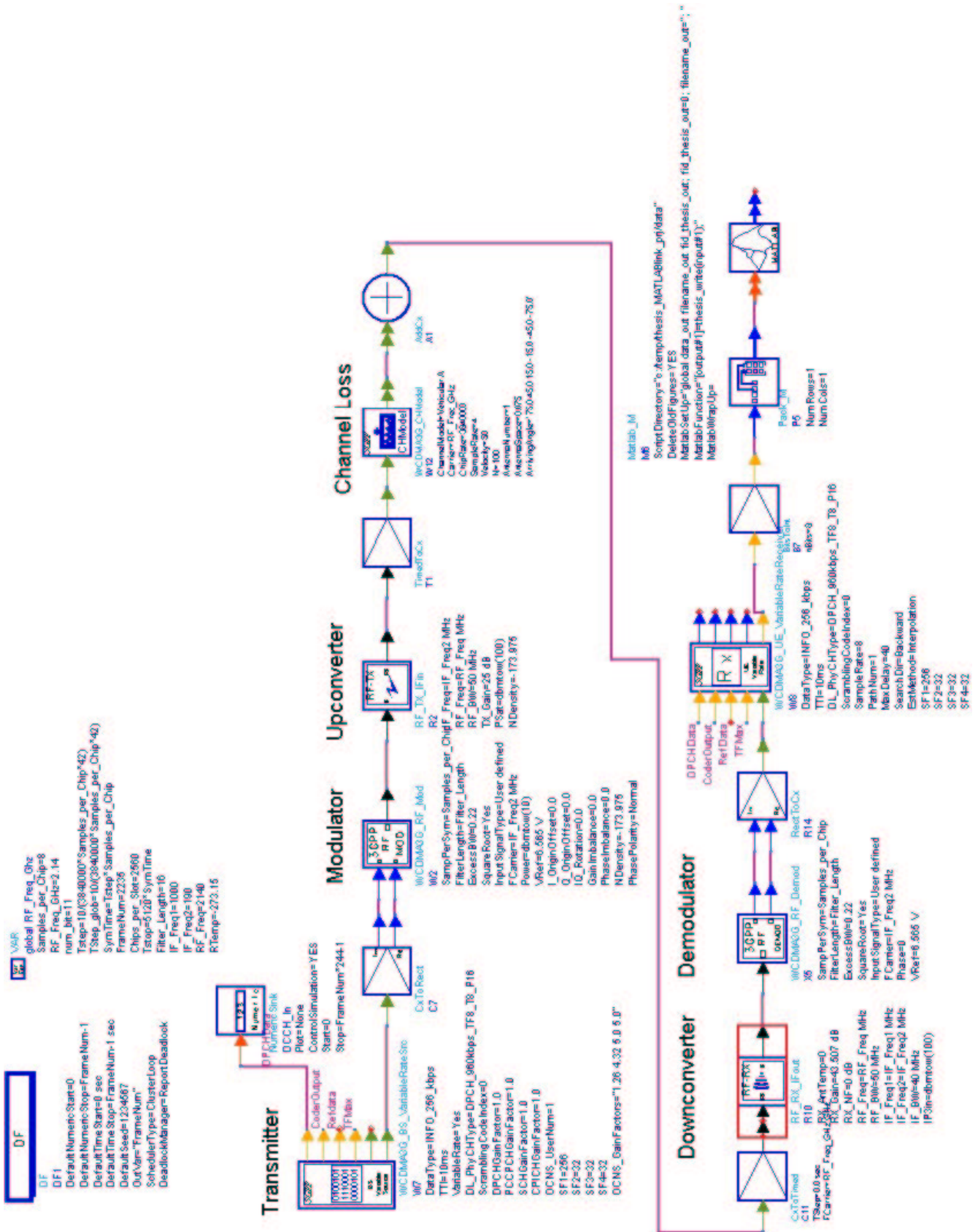
Figure 6.2 ADS Main Schematic Overview

Figure 6.2 illustrates the main schematics of the UTRA/3G test bed module implementation. As shown, a single user downlink channel is implemented with a single Base Station (BS) variable rate source, a 3G physical channel module and a User Equipment (UE) variable rate receiver. The main variables are controlled using DF and variable array as listed in the top left hand corner of the schematic. The physical layer signal data are output from the BS source, then modulated and handed to the up-converter Radio Frequency (RF) transmitter. The radio signal is then passed through the 3G physical channel before being received via the down-converter RF receiver and handed to the UE receiver. The receiver then processes the incoming signal back to transport layer Dedicated Channel (DCH) signal and handed to the Matlab server for recording. The following lists the major components.

3GPP

CoderOutput

0100101
1110001
0000101

TFMax

BS
Variable
Source

WCDMA3G_BS_VariableRateSrc
W7
DataType=INFO_256_kbps
TTI=10ms
VariableRate=Yes
DL_PhyCHType=DPCH_960kbps_TF8_T8_P16
ScramblingCodeIndex=0
DPCHGainFactor=1.0
PCCPCHGainFactor=1.0
SCHGainFactor=1.0
CPICHGainFactor=1.0
OCNS_UserNum=1
SF1=256
SF2=32
SF3=32
SF4=32
OCNS_GainFactors="1.26 4.32 5.0 5.0"
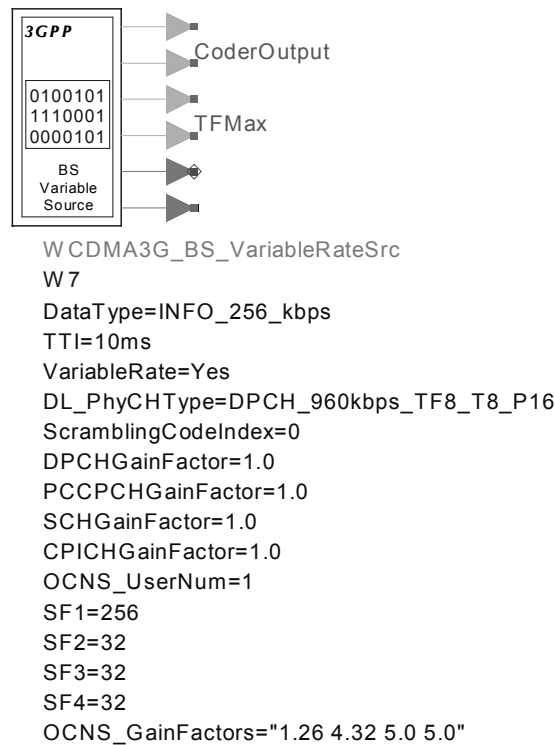
Figure 6.3 BS Variable Rate Source

Figure 6.3 shows the variable rate source that can provide a variable information signal rate range from 8 to 512 kbps for downlink. The transport channel interface for the data part of the Dedicated Channel (DCH) is provided on the physical channel being implemented here. The transport interface is hereby implemented as a Matlab server interface and this is discussed further in a later section. Channel coding, transport channel multiplexing, physical channel mapping, spreading and scrambling operations are also included for DPDCH and common control channels. The control channel includes a Primary Common

Control Channel (PCCPCH), Primary Synchronization Channel (P-SCH), Secondary Synchronization (S-SCH), and Common Pilot Channel (CPICH). An orthogonal channel is also included which simulates up to 4 users in orthogonal code channels.

Both the Transmission Time Interval (TTI) and downlink physical channel rate are controllable. SF1-SF4 controls the spreading factor for the 4 user orthogonal channels. This component implements the simulation of base station physical traffic. It covers the procedure in Figure 3.1 (CRC Attachment to Scrambling code) and the internal details are covered later.
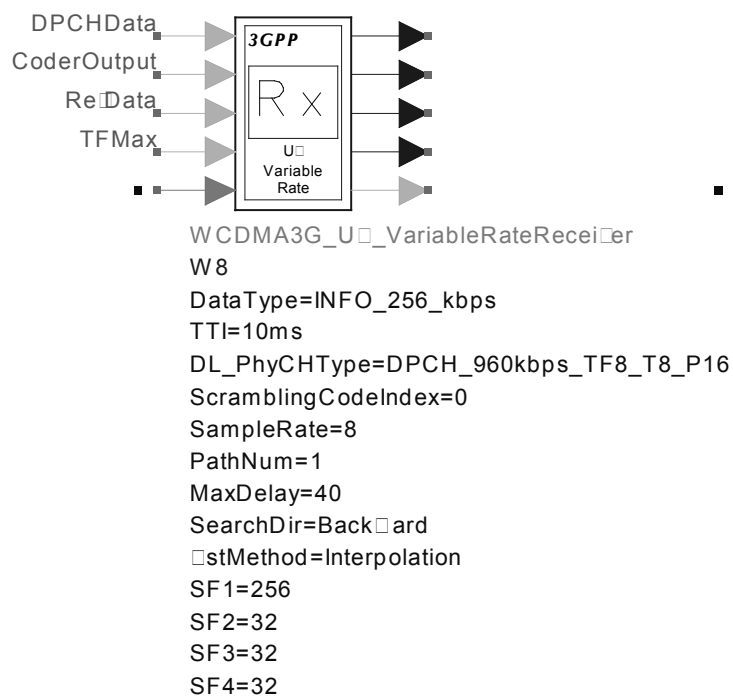
Figure 6.4 UE Variable Rate Receiver

Figure 6.4 show the UE variable rate receiver, with comparable information rate and related parameters with the BS variable rate source. For receiving the downlink channel signal, this component includes the rake receiver, spreading code and scrambling code generation, transport channel de-multiplexing, channel decoding and Bit Error Rate (BER) measurement. The component parameters should be the same as the BS source. Signal sample rate and arriving path as well as maximum anticipated delay is selectable. This component reverses the process applied in the previous component and the internal details of this component are described in later sections.

Figure 6.5 shows the 3G Physical Channel Model used in this simulation schematic. This component implements the AWGN and Multi-path channel in Figure 3.1 Six types of channel model are available, with varying delay, power and Doppler spectrum of the channel path.
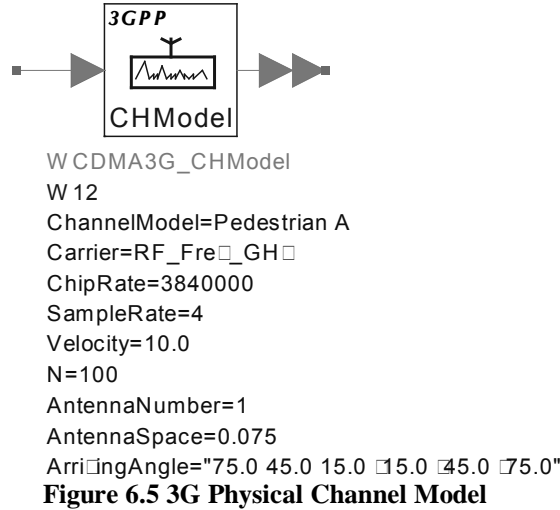


```
3GPP
CHModel

WCDMA3G_CHModel
W12
ChannelModel=Pedestrian A
Carrier=RF_Fre=_GH>
ChipRate=3840000
SampleRate=4
Velocity=10.0
N=100
AntennaNumber=1
AntennaSpace=0.075
Arri9ingAngle="75.0 45.0 15.0 ⋖15.0 ⋖45.0 ⋖75.0"
```

Figure 6.5 3G Physical Channel Model

The available channel model includes Indoor A, Indoor B, Pedestrian A, Pedestrian B, Vehicular A and Vehicular B. Special note must be taken that the carrier frequency must be synchronized between BS source and UE receiver. This component simulates a multi-path fading channel based on a tapped-delay line model. Varying delay is simulated using a delay component, power distribution simulated using the power amplifier while the Doppler spectrum is simulated using phase shifter and Jakes model. Antenna array is also considered, with the multi-path signal being summed and coupled prior to placing to output. The arriving angle detailed the arriving angle in degrees for each incoming path [74]. Note that the indoor environment uses a flat Doppler spectrum and the others use a classic Doppler spectrum. This component is replaceable with a customized user model using Matlab, with example models in [7], [8] and [5].
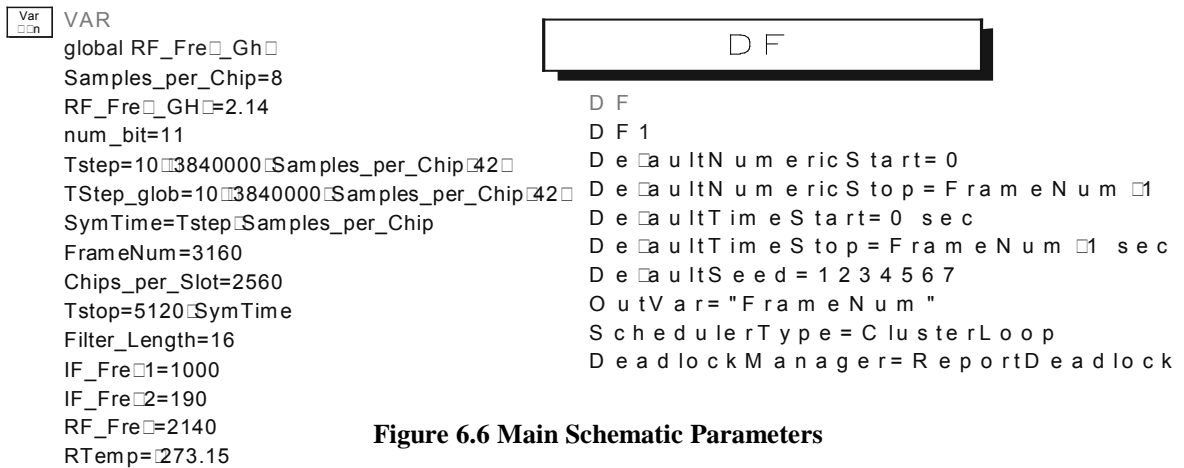
```
Var
8=n      VAR
         global RF_Fre=_Gh>
         Samples_per_Chip=8
         RF_Fre=_GH>=2.14
         num_bit=11
         Tstep=10@3840000?Samples_per_Chip?42B
         TStep_glob=10@3840000?Samples_per_Chip?42B
         SymTime=Tstep?Samples_per_Chip
         FrameNum=3160
         Chips_per_Slot=2560
         Tstop=5120?SymTime
         Filter_Length=16
         IF_Fre=1=1000
         IF_Fre=2=190
         RF_Fre==2140
         RTemp=⋖273.15
```

```
                    DF

DF
DF1
De;aultNumericStart=0
De;aultNumericStop=FrameNum⋖1
De;aultTimeStart=0 sec
De;aultTimeStop=FrameNum⋖1 sec
De;aultSeed=1234567
OutVar="FrameNum"
SchedulerType=ClusterLoop
DeadlockManager=ReportDeadlock
```

Figure 6.6 Main Schematic Parameters

Figure 6.6 shows the main schematic controllable parameters. Notable parameters are the RF frequency, the frame number (controls the amount of information to be sent through) and number of chips per slot.
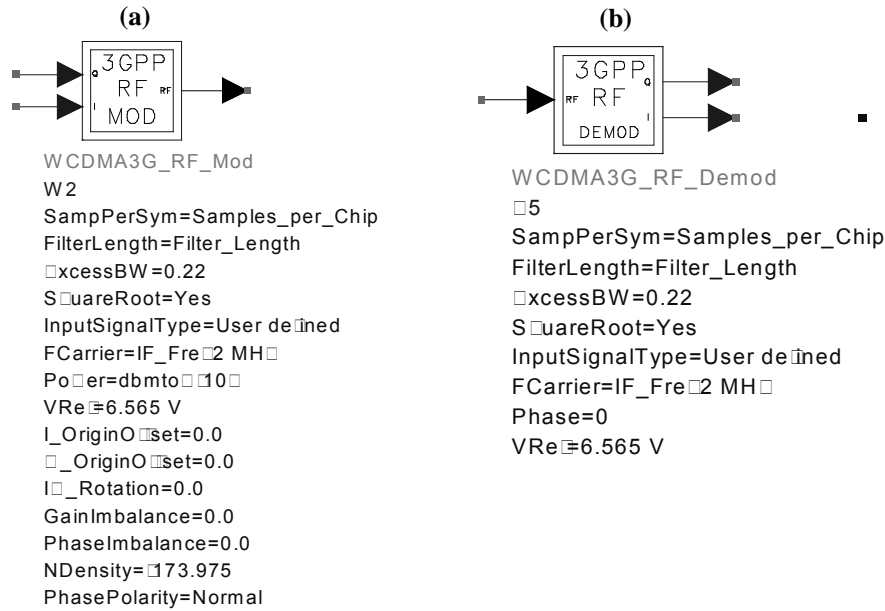
(a)   **(b)**

WCDMA3G_RF_Mod
W2
SampPerSym=Samples_per_Chip
FilterLength=Filter_Length
8xcessBW=0.22
S=uareRoot=Yes
InputSignalType=User de;ined
FCarrier=IF_Fre=2 MH>
Po: er=dbmto: A10B
VRe;=6.565 V
I_OriginO;;set=0.0
D_OriginO;;set=0.0
ID_Rotation=0.0
GainImbalance=0.0
PhaseImbalance=0.0
NDensity=⊲173.975
PhasePolarity=Normal

WCDMA3G_RF_Demod
C5
SampPerSym=Samples_per_Chip
FilterLength=Filter_Length
8xcessBW=0.22
S=uareRoot=Yes
InputSignalType=User de;ined
FCarrier=IF_Fre=2 MH>
Phase=0
VRe;=6.565 V

Figure 6.7 Modulation Components
(a) RF Modulator (b) RF Demodulator

Modulation and demodulation is done outside of both source and receiver components with the components shown above. The Modulator takes the I and Q arm data stream base band signals, then up-sampled, filtered and modulated them into the in-phase and quadrature phase carriers of a Quadrature Amplitude Modulation [70] (QAM) modulator. I_Original Offset, Q_OriginOffset, IQ_Rotation, GainImbalance parameters and Ndensity are used to add impairments to the otherwise ideal transmitted signal. Both the modulator and demodulator use square root raise-cosine filtering with the same excess bandwidth.

(a)   **(b)**

RF_TC_IFin
R2
IF_Fre==IF_Fre=2 MH>
RF_Fre==RF_Fre= MH>
RF_BW=50 MH>
TC_Gain=25 dB
PSat=dbmto: A100B
NDensity=⊲173.975

RF_RC_IFout
R10
RC_AntTemp=0
RC_Gain=43.507 dB
RC_NF=0 dB
RF_Fre==RF_Fre= MH>
RF_BW=50 MH>
IF_Fre=1=IF_Fre=1 MH>
IF_Fre=2=IF_Fre=2 MH>
IF_BW=40 MH>
IP3in=dbmto: A100B
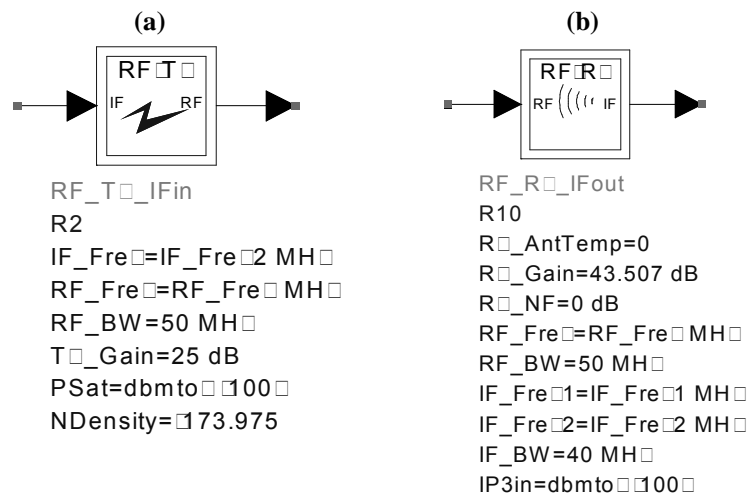
Figure 6.8 RF Component
(a) RF Transmitter (b) RF Receiver

Figure 6.8 illustrates the component for simulating RF activity. The transmitter converts input IF signal output from modulator into output RF signal with nonlinear distortion and additive noise. The PSat parameter determines the nonlinear distortion by modeling amplitude modulate (am) to am distortion. NDensity is the parameter that governs the noise.

(a) **(b)**

CxToRect
C7

RectToCx
R14

(c) **(d)** **(e)**

TimedToCx
T1

CxToTimed
C11
TStep=0.0 sec
FCarrier=RF_Fre=_GH> GH>

AddCx
A1
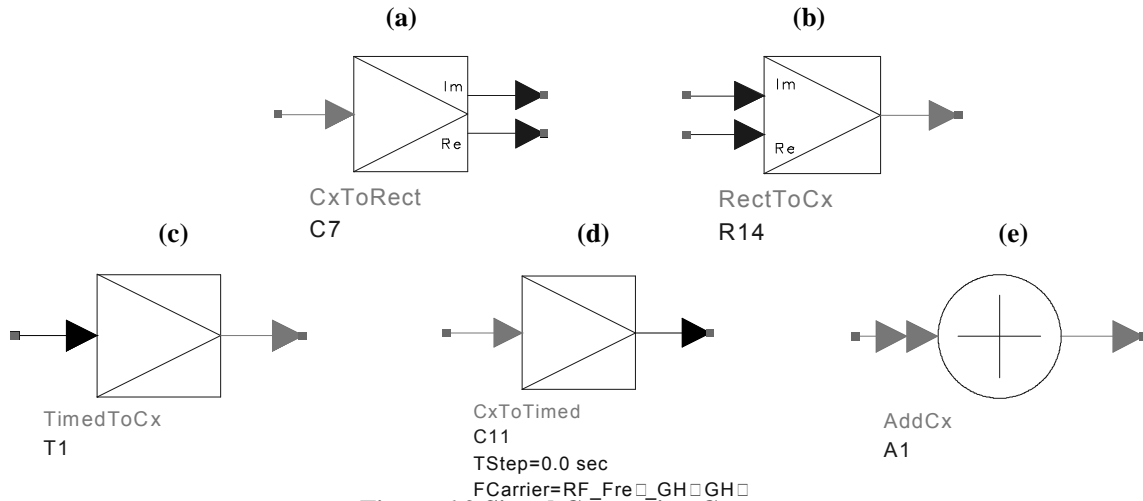
Figure 6.9 Signal Conversion Component

(a) Complex to Rectangular (b) Rectangular to Complex (c) Time to Complex
(d) Complex to Time (e) Adding multiple Channel Complex

Figure 6.9 illustrated the signal conversion component used in various schematics for conversion of signals between major components.

(a)

Matlab_M
M6
ScriptDirectory="cJ@emp@hesis_MATLABlink_prk@ata"
DeleteOldFigures=Y8S
MatlabSetUp="global data_out ;ilename_out ;id_thesis_outH;id_thesis_out=0H;ilename_out=IIH"
MatlabFunction="EoutputF1G thesis_: riteAnputF1BH"
MatlabWrapUp=

(b) **(c)**

Pack_M
P5
NumRo: s=1
NumCols=1

BitsToInt
B7
nBits=8
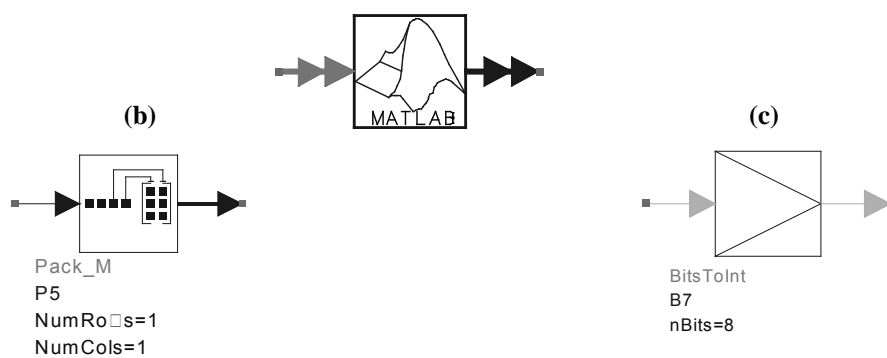
Figure 6.10 Matlab Server Output Components
(a) Matlab Output (b) Matrix Packaging (c) Bits to Integer Conversion

Figure 6.10 shows the various components used for outputting the processed data from ADS. Specific written Matlab code allows Matlab Server loaded separately from ADS to accept the output signal output using the Matlab Output component. The data are first converted from bits to integer and packed into a 1x1 matrix prior to outputting onto Matlab.

This schematic presented in Figure 6.2 is the first level view of the 3G test bed module, implementing the specification in Chapter 3. It is constructed using the main functional modules provided by ADS 3G module libraries. These modules are as presented in this and the next two sections. BS source and UE receiver modules in this section are high level modules that are built using more fundamental functional modules. The internal schematics of these two modules are modified from that obtained from the ADS library. The new schematics are presented in the next two sub sections.

This ends the section on the main schematic for the UTRA/3G test bed module where the main structure has been explained. The next two sections illustrate the BS and UE components.

6.2 ADS Implementation Base Station Design Schematics

Figure 6.11 ADS Base Station Internal Block Schematic

This section illustrates the BS variable source. The schematic is modified from the original design from [74]. Upon every eight firings of the simulated source, to Matlab server inputs a byte from the testing data file, which is converted back to bit before handing over to the next section. The input from the Matlab component is taken as transport channel Dedicated Channel (DCH) data at this stage. It is then transport channel coded and then multiplexed together again into a single Coded Composite Transport Channel (CCTrCH) prior to handing to segmentation into the Dedicated Physical Data Channel (DPDCH). Transport Format Combination Indicator (TFCI) mapping and encoding is done concurrently with the mentioned processes.

The data stream is then power allocated, then spread and scrambled using OVSF channel code before being multiplexed with Common Pilot Channel (CPICH), Primary Common Control Channel (PCCPCH) and simulated channel noise to complete the final output. Note that for easy functionality explanation, the schematic is divided into 5 blocks, which are presented in the following.

Matlab_M
M2
ScriptDirectory="cJ@mp@hesis_MATLABlink_prK@ata"
DeleteOldFigures=Y8S
MatlabSetUp="global data_in ;ilename1 ;id_thesisH;id_thesis=0H;ilename1=IIH'
MatlabFunction="EoutputF1G-thesis_readAnputF1BH"
MatlabWrapUp=

Pack_M   UnPk_M   FloatToInt   IntToBits
P2   U3   F1   I1
NumRo: s=1   NumRo: s=1   nBits=8
NumCols=8   NumCols=1
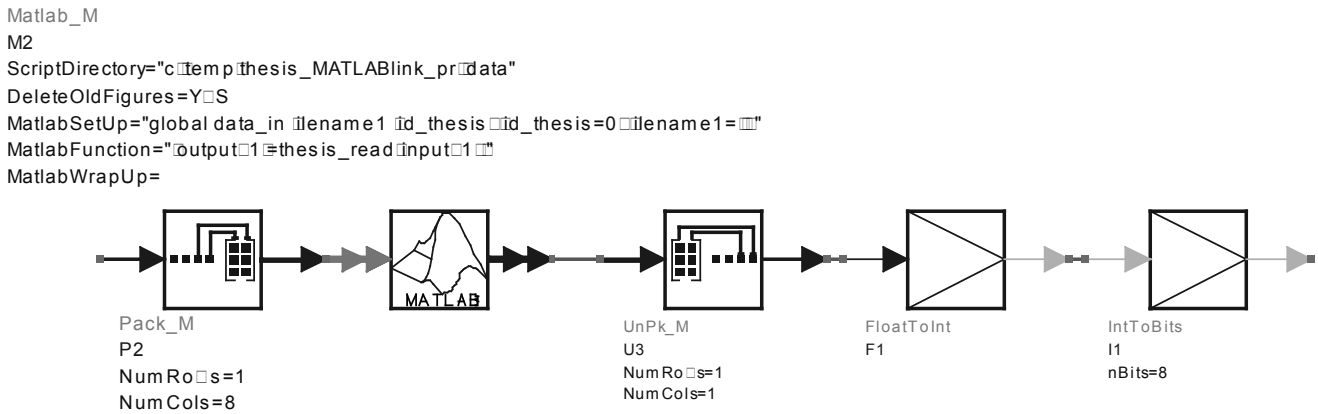
Figure 6.12 Matlab Server Data Input Section

Figure 6.12 illustrates block 1, the Matlab server data input block that allows input of the data file from the output ADS. The tokens from the variable sources are grouped using Pack_M components into a group of 8 to represent a byte. Then the Matlab input component is invoked, receiving a byte of data in the form of a matrix. The matrix is then unpacked and converts back into bits for further processing in following sections.
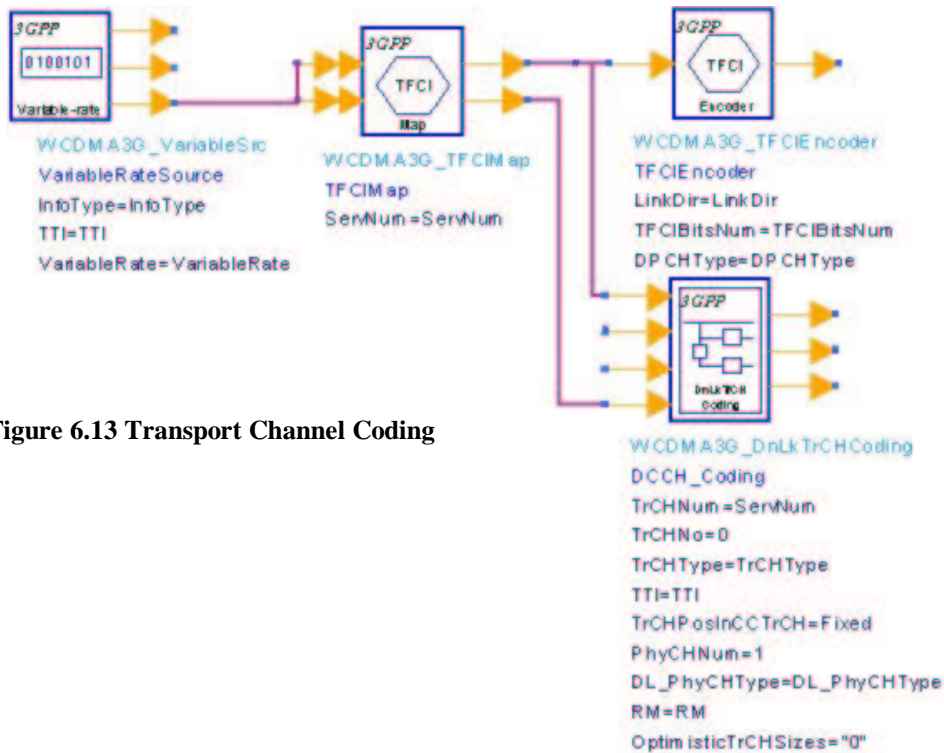
Figure 6.13 Transport Channel Coding

Figure 6.13 illustrates the major components in block 2, which relates to coding of the transport channels. The variable rate source mentioned before is listed here, as it provides the variable rate data source as well as the maximum transport format, which govern transport channel coding. The main component here is the DnLkTrCHCoding, which is responsible for CRC encoding, code block segmentation, channel coding, rate matching, first interleaving and radio frame segmentation. Convolutional coding is used if TTI count is greater than 504 and turbo coding if TTI count is greater than 5114. The details are as presented in section 3.1, covering the section on channel coding and related operations.

TFCIMap component is used for Transport Format Combination Indicator (TFCI) mapping of the transmission side and subsequently TFCIEncoder is used to encode the TFCI. TFCI is for indication of multiple transport channel in and CCTrCH. Although a single variable source is used here, it is compulsory for further extension. The encoded TFCI is used in the component in the later section.
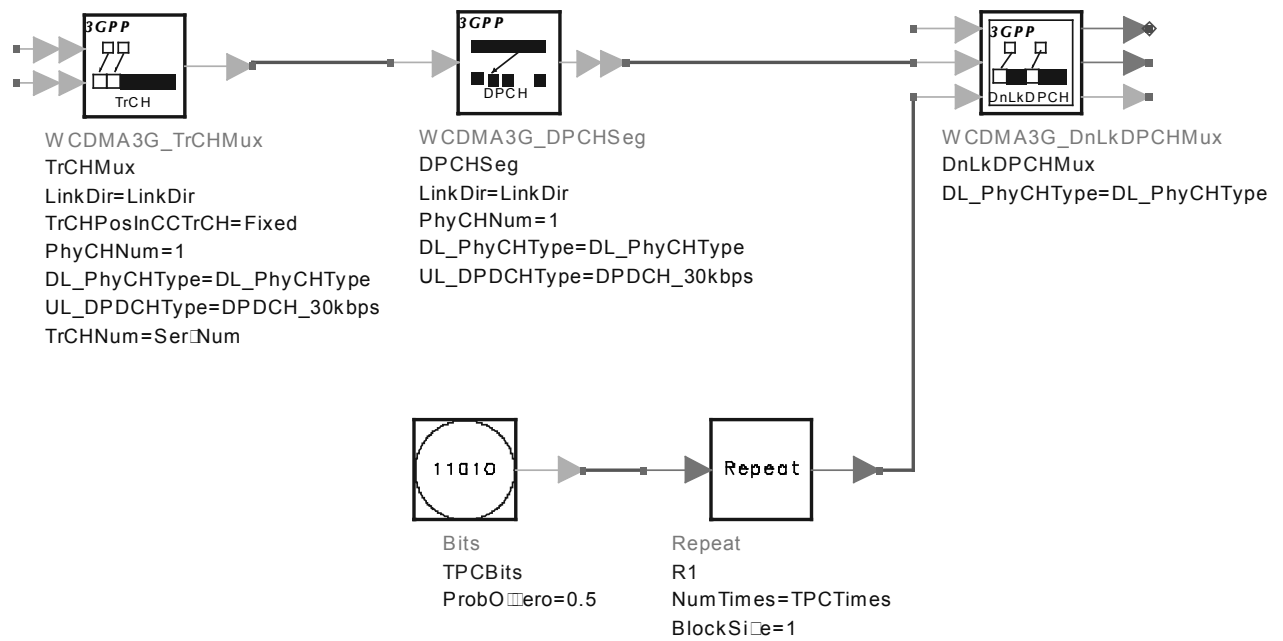
Figure 6.14 DPCH Processing

Figure 6.14 shows block 3, which immediately follows block 2 to carry out DPCH processing. TrCHMux component takes output from various DnLkTrCHCoding components and multiplexes it into a single CCTrCH transport channel. Discontinuous Transmission Indications (DTX) is also inserted upon flexible positions in the downlink transport channels. As mentioned, only one user data transport channel is implemented; therefore, only one transport channel is present but this component is still necessary for DTX addition. DPCHSeg component divides the CCTrCH data into multiple DPDCH. However, this model only supports a single DPDCH. DnLkDPCHMux component is then used to multiplex DPCH for downlink, perform second interleaving, QPSK data mapping and Space Time Transmit Diversity (STTD) encoding and multiplexing. DPCCH data are added to the data stream in this component.
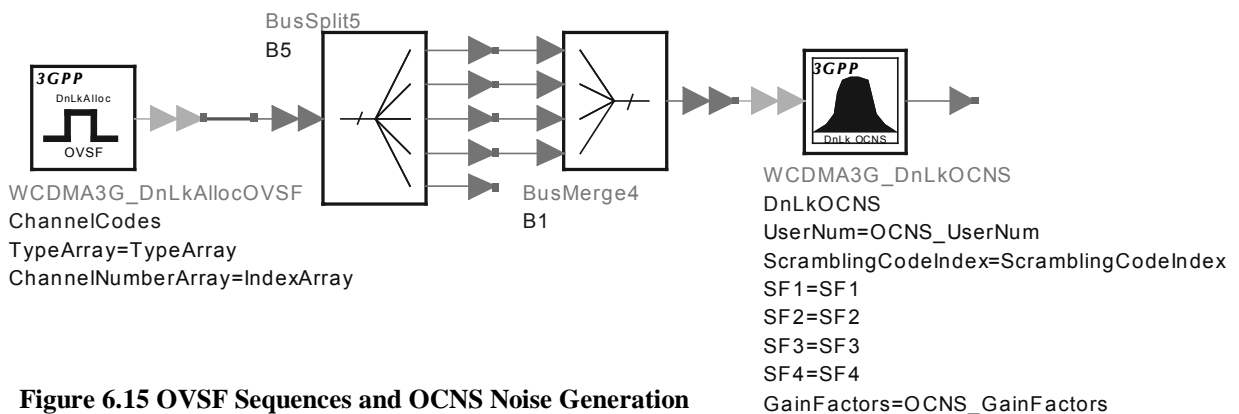
Figure 6.15 OVSF Sequences and OCNS Noise Generation

The above Figure shows block 4 for OVSF sequences generation and OCNS noise generation. DnLkAllocOVSF component is used to generate OVSF for use as downlink

75

spread code.   Using OVSF tree structure, orthogonality is maintained among all output sequences. Five sequences are generated of which one is used for downlink spreading and the other four are used by the DnLkOCNS component for noise generation. DnLkOCNS simulates the Downlink orthogonal channel noise, which generates four DPCH in the downlink using four separate random bit sources. The random bits are QPSK mapped and spread by the four spread codes mentioned and multiplied scrambling code generated by the downlink scrambling code generator within itself.

3GPP

Po: erAlloc

WCDMA3G_DnLkPo: erAlloc
DnLkPo: erAllocation
DL_DPCHType=DL_PhyCHType
TC_Di9ersity=Normal
ChannelNumber=1

3GPP
DnLkSpreading

WCDMA3G_DnLkSpreading
DnLkSpreading
SF=SF
Use8xtSpreadingCode=Yes
SpreadingCodeIndex=0
ScramblingCodeIndex=ScramblingCodeIndex

GainCx

DPCHGain
Gain=DPCHGainFactor

BusMerge4
B2

3GPP
DnLk
CPICH

WCDMA3G_DnLkCPICH
DnLkCPICH
ScramblingCodeIndex=ScramblingCodeIndex
CPICHGainFactor=CPICHGainFactor

11010

Bits
PCCPCHBits
ProbO;Lero=0.5

3GPP
DnLk
PCCPCH
SCH

WCDMA3G_DnLkPCCPCH_SCH
W2
ScramblingCodeIndex=ScramblingCodeIndex
PCCPCHGainFactor=PCCPCHGainFactor
PSCHGainFactor=PSCHGainFactor
SSCHGainFactor=SSCHGainFactor

Figure 6.16 Multiple Physical Channel Multiplexing

Figure 6.16 above shows the final block for the BS downlink source. DnLkPower-Allocation component takes the normalized power output from block 3 and transforms it into signal with proportional power across several physical channels. Signal is then handed to DnLkSpreading for spreading and scrambling using spread code generated from block 4. Component DnLkPPCCPCH_SCH generates PCCPCH modulated data that are time multiplexed with Synchronization Channel (SCH) data. DnLkCPICH component generates modulated CPICH channel. The various physical channels are then merged to produce as the output of the BS downlink source component.

This ends the section on a variable rate base station source/transmitter, covering the transmission operations. The next section presents the UE implemented design.

6.3 ADS User Equipment Implementation Design Schematics

Figure 6.17 ADS User Equipment Internal Block Structure
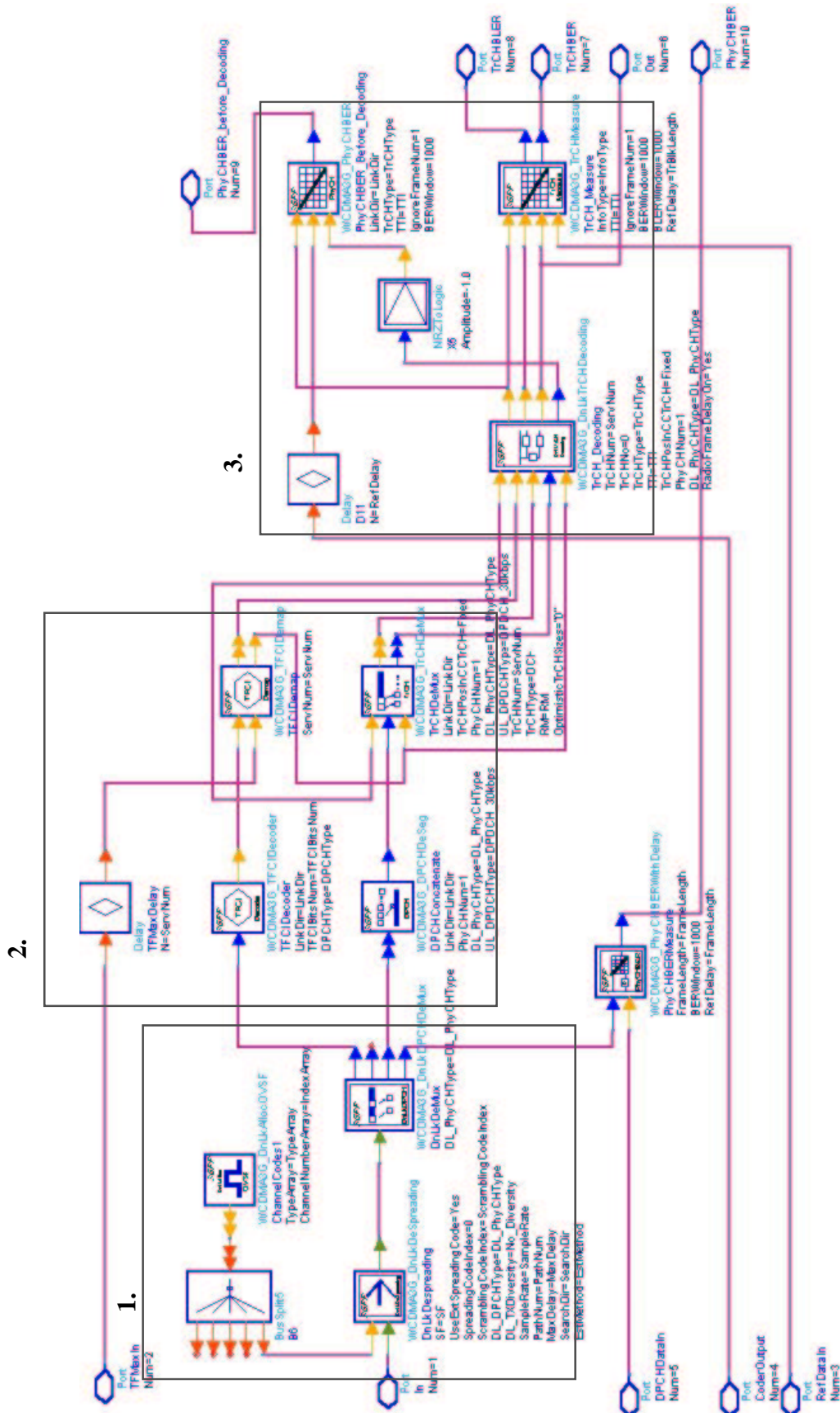
This section presents the internal design schematics of the UE variable rate receiver, with the schematics based on the internal design available in [74]. Presented in Figure 6.17, it contains the Rake receiver, spreading code and scrambling code generation, transport channel de-multiplexing, channel decoding and BER measurements. The incoming signal is received using a rake receiver and using a spreading and scrambling code generated via OVSF. The output signal from this is then de-segmented from DPCH and de-multiplexed into various transport channels. Transport channel decoding is then performed to extract DCH output data. As with the previous section, the schematic is divided into three blocks for ease of illustration.
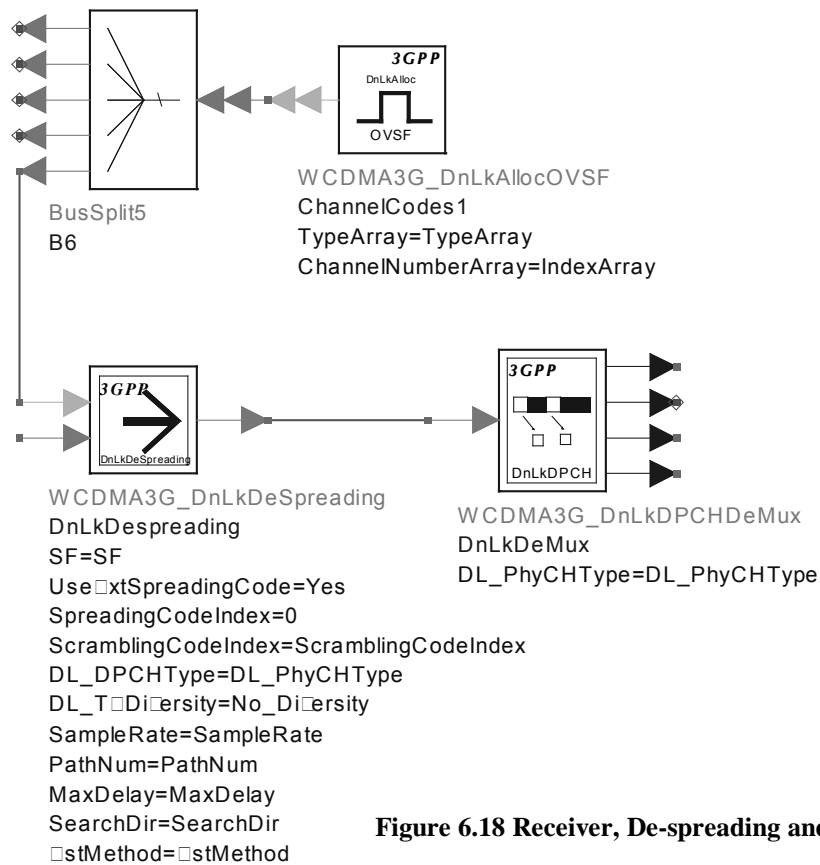
Figure 6.18 Receiver, De-spreading and De-multiplexing

Figure 6.18 illustrates the receiving process of the UE component. DnLkAllocOVSF is again used to generate the OVSF that is necessary for receiving the incoming signal. DnLkDeSpreading is the component processing the incoming raw signal by receiving, spreading and scrambling. Using the OVSF sequence generated as spread code and internal generated scrambling code, the internal Rake receiver de-scrambles and de-spreads the signal. The output signal is then handed to DnLkDPCHDeMux for de-multiplexing to produce DPDCH, Transmit Power Control (TPC) bits (added during power allocation in

BS) and TFCI bits. Note that DPDCH data are de-interleaved for the 2nd interleaving process (in Figure 3.1).

Delay
TFMaxDelay
N=Ser9Num

3GPP
TFCI
Decoder

WCDMA3G_TFCIDecoder
TFCIDecoder
LinkDir=LinkDir
TFCIBitsNum=TFCIBitsNum
DPCHType=DPCHType

3GPP
TFCI
Demap

WCDMA3G_TFCIDemap
TFCIDemap
Ser9Num=Ser9Num

3GPP
DPCH

WCDMA3G_DPCHDeSeg
DPCHConcatenate
LinkDir=LinkDir
PhyCHNum=1
DL_PhyCHType=DL_PhyCHType
UL_DPDCHType=DPDCH_30kbps

3GPP
TrCH

WCDMA3G_TrCHDeMux
TrCHDeMux
LinkDir=LinkDir
TrCHPosInCCTrCH=Fixed
PhyCHNum=1
DL_PhyCHType=DL_PhyCHType
UL_DPDCHType=DPDCH_30kbps
TrCHNum=Ser9Num
TrCHType=DCH
RM=RM
OptimisticTrCHSi>es="0"

Figure 6.19 Physical Channel De-segmentation and Transport Channel De-multiplexing

Figure 6.19 shows block 2, which involves TFCI operations, DPCH de-segmentation and transport channel de-multiplexing. The TFCIDecoder decodes the TFCI output from the DnLk-DPCHDeMux while the output data are handed to DPCHDeSeg for de-segmentation. Bits from different DPDCH are concatenated into a single CCTrCH. TFCI de-mapping is done in TFCIDemap while TrCHDeMux handles the Transport Channel de-multiplexing. This processes de-multiplex radio frames from all transport channels from a single CCTrCH and also punctures DTX with flexible transport channel positions.
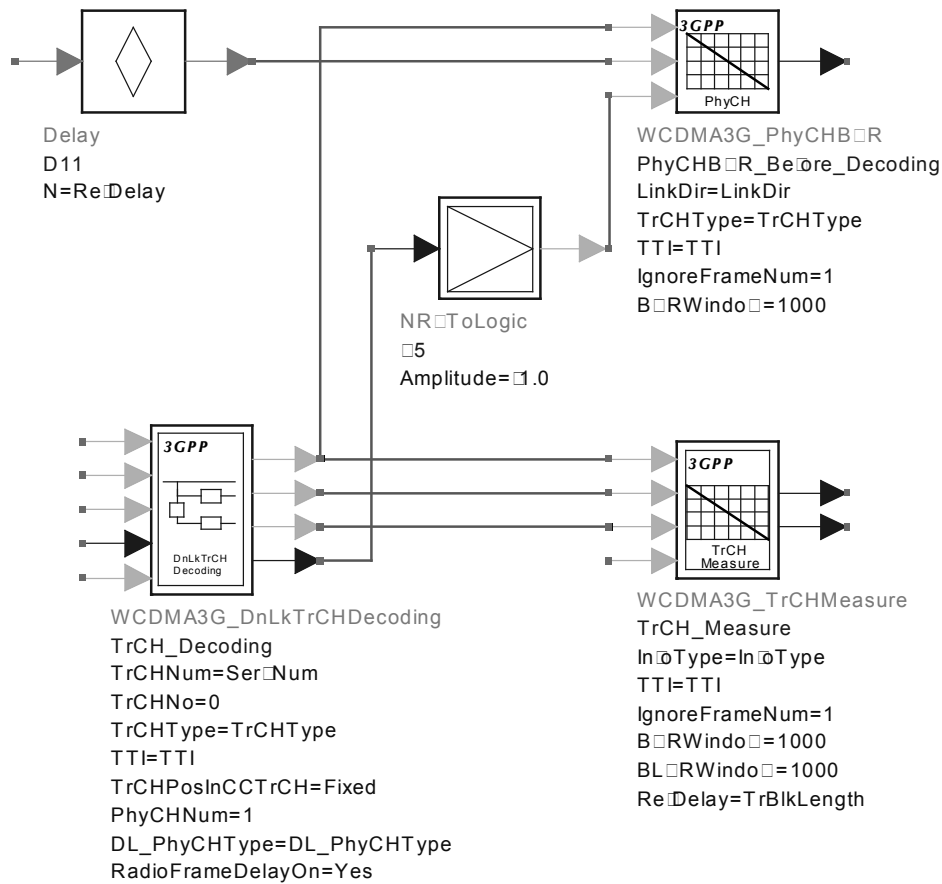
Figure 6.20 Transport Channel Decoding

The above Figure illustrates block 3 of the schematic. Components TrCHMeasure and PhyChBER are used for physical signal measurement. The delay component in this block and the previous block are used to compensate respective values with the amount of delay experienced by the physical layer signal. The main component in this block is DnLkTrCHDecoding, which performs downlink transport channel decoding. The major function includes radio frame delay, radio frame de-segmentation, first de-interleaving, rate de-matching, channel decoding, code block concatenation and CRC checking. The output is the DCH data entered via the BS variable rate source.

The section on UE variable rate receiver is concluded. This also ends the section on ADS UTRA/3G test bed module implementation. Overall, the major design schematics have been presented and dissected in detail, reviewing the operation of the transmitter, receiver and physical channel model. The next section presents the HVS-based image quality metric implementation.

Chapter 7. HVS-Based Quality Metric System Implementation

Relative to the test bed methodology and the objective stated in the introduction, this section describes the implementation of a HVS-based quality metric system. This involves fusing of the HVS fidelity system and Importance Map (IM) system to produce a complete HVS-based quality metric. This quality metric considers error/artifact induced picture quality in a different way, where image quality is depending on the image respond on HVS-based attention and perception model.
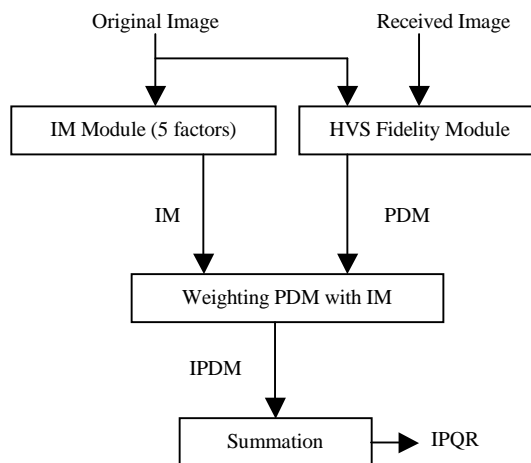
Figure 7.1 HVS Quality Metric [42]

Figure 7.1 shows the block structure of the overall quality metric. As shown, the HVS fidelity system takes the received image and the original image to produce a PDM. The IM unit accepts the original image and produces an image map, from which the IM enhanced PDM (IPDM) is produced. Further Minkowski summation is performed on the IPDM to produce the IM weighted PQR (IPQR).

A multiple channeled HVS fidelity system is implemented. As mentioned in a previous section, it converts luminance to contrast, multi channel decomposes the outcome using a Local Band-limit Contrast (LBC) process, followed by the application of a Threshold

Enhanced (ThE) Contrast Sensitivity Function (CSF) to determine the Just Noticeable Difference (JND) fidelity measurement; application of visibility threshold is followed by Minkowski summation to produce the output PDM. Note that the PDM is a fidelity map that indicates visible distortion between received and original picture.

Furthermore, IM is used to identify the Region of Interest (ROI), grading the regions from 0.0-1.0 with 1.0 given to area of most importance in the image. Therefore, IM grading is relative within individual images. PDM is weighted with IM, weighting the quantifying fidelity measure relative to its location and scaling the PDM accordingly with the IM grading. A simple approach for weighting is adopted from [64]:

$$IPDM(x, y) = PDM(x, y) \cdot IM(x, y)^{\gamma}$$

$$(7.1)$$

The IPDM map illustrates the distortion between the images relative to human perception. Where IPDM (x,y) is the IPDM value for pixel (x,y), respectively for PDM and IM. γ is a compensating index, where experiments shows the best value to be 0.5 [42]. In the final rating, the Importance weighted PQR (IPQR) is produced from the new PDM. IPQR is a number ranging from 1 to 5 which grades the distortion, where 5 is the highest (no distortion) and 1 is the lowest. The equation for producing both IPQR and IPQR range 1-5 is listed below [64]:

$$IPQR = (\tfrac{1}{N} \sum_{}^{N} IPDM(x, y)^{\beta})^{1/\beta}$$

$$(7.2)$$

$$IPQR_{1-5} = \frac{5}{1 + p \cdot IPQR}$$

$$(7.3)$$

Note that p is a scaling constant, β is used for output control, while low value gives correlation upon average pixel error and high value gives a correlation upon maximum IPDM value. $\beta = 3.0$ is usually used to get an accurate result.

It is important to note that different images produce different IM maps. Therefore, even if given two different images with very similar distortion, the IPQR produced is very likely to be diverse. This is because distortion has different impacts on image quality, depending on the location it situates, as different areas have different importance ratings.

Furthermore, IPQR is produced based on IM, which works well on natural images generally. In the case of artificial and specific images (e.g. medical images), the user may choose to use PQR over IPQR as IM is tuned for the natural image and may not be suitable for the images in question.

HVS image analysis is implemented using Matlab while the IM analysis is implemented using C, to improve the efficiency of the split and merge algorithm. Both currently process only gray scale images and accept the Portable Grey Map (PGM) format. The following describes the conceptual details of the implementation.

7.1 HVS Fidelity Module Implementation

The main structure of the fidelity system is based on a log cosine function with texture masking enhancement. The texture masking enhancement raises the threshold in textures sharply while along edges only moderately. The difference between the original and the received image is taken at each band and compared to the masking threshold, determining its visibility. The image is first read in and converts from gray level to luminance, depending on monitor characteristics. Matlab fft2 function is used for the Fourier transform needed, as mention in an earlier section. The radial frequency at each location is obtained and scaled to its maximum value. The log cosine filters are then configured and applied to each of these filters in term of the image matrix.

Matlab ifft function is used as an inverse Fourier transform to convert the visual frequency back to the luminance domain for further processing. Local point contrast is calculated next, using the equation listed in the previous section. Texture masking is done next, by classifying the image locality into flat, edge or textured regions. This is done as explained in the previous section, calculating mean absolute difference in blocks surrounding each pixel, reflecting activities in the local region. The threshold in various regions, band and channels for Contrast Sensitivity Function (CSF) is adjusted from spatial masking, prior to the application of CSF. Summation is done over channels, then over a small region of space, as specified in the previous section, producing the PDM.

The author would like to note that the implementation of this module is based largely on the codes provided by Osberger, the author of [42], with minor modification. The majority of the base functions written by Osberger are used with minimal modification, while the author writes the main program. It can be said that the author uses Osberger's code as a HVS fidelity module library. This concludes the section on the HVS-based fidelity system. The next section will be on IM implementation in C.

7.2 Importance Map Implementation

IM C code implementation starts by reading in the image, handling it differently depending on whether it is an ASCII or binary coded image file. Image data are held as individual pixels in a two dimension array (e.g. Image). Splitting is then done in a recursive procedure, where upon each recursion, the variance of the region is first calculated. Upon dissatisfaction of a condition, the process splits the image into four equal sections and invokes a splitting procedure for each. As mentioned in a previous section, the condition requires the variance of the region in processing to be lower or equal to the set threshold. Within the split algorithm, the merging process is done after the recursive splitting of the four divided blocks of the immediate region, then merging is done for all the pixels in the immediate region. Merging is done via comparing two neighboring pixels, and both regions are merged if the two regions are different and the combined variance is less than merging threshold.

During the operation, another array of equal size to the Image array, the Array_Image_Region, keeps track of the region a pixel belongs to. This record of region assignment is finalized upon the end of running each recursive thread of the split procedure. This gives an immediate region number to the newly formed region, after which a merge operation will occur as mentioned before. While at the end of the entire recursive split-merge run, individual pixels of the image are indexed with a region. Upon the finalization of each immediate region, the pixel count, sum of value of the region and summed squared value of the region is recorded individually into separate areas, termed Array_Region_Total, Array_Region_Count and Array_Region_Count2 for easing of the importance factor calculation later on. This will also be updated in the merge algorithm

and finalized at the end of the entire split merge run. Another array Array_Region_Parent is formed during the merging process, and keeps records of a region's parents. This array houses the entire merging process, by holding the parent of two regions; i.e. if region 2 and region 1 are merged, region 1 is region 2's parent. This is how the merging information is kept while leaving Array_Image_Region unchanged after it is first written.

Further merging is then performed, continuously trying to merge small regions with their close neighbors until successful. Array_Image_Region and Array_Region_Parent are used to go through all regions, searching for all 4 directions of the region to seek the possibility of merging. The difference in mean gray level of the region in question and its corresponding region is analyzed and will be merged free of variance influence if the difference is lower than a threshold. The array Array_Region_Merged is then generated reflecting the final assigned regions for further usage. The Array_Region_Merged is then used as the main index point for calculation of the five importance factors in the image. The parameters of the individual factors are collected independently from the mentioned arrays if needed, and then the calculation is performed as specified in an earlier section. The result is recorded into importance factor arrays, for the regions specified in Array_Region_Merged. Consequently, upon the end of the individual factor calculation, the summation process is again a looped process guided by Array_Region_Merged, producing the final IM values. The individual factor result and the summed IM values are output into individual image files respectively.

The author would like to note that the implementation of this module is based on the codes provided by Osberger, the author of [42], with extensive and major modification. Other than the main skeletal structure and input/output codes, the remaining codes have been extensively reconstructed and rewritten to implement the IM module as described in [42].

7.3 Combination of HVS-Based Fidelity and IM Results

With the results gathered from 7.1 and 7.2, the remaining system is implemented using Matlab. The PDM matrix from 7.1 is conserved while reading the IM map from 7.2 and processing it into a scale from 0.0-1.0. The remaining process is performed mathematically as specified in Chapter 7 without much complication.

The description of the implementation of the HVS-based quality metric is concluded. A general description of the infrastructure designs and innovative areas have been provided while many technical details have been omitted. The next section presents the results and analysis of the two main modules implemented.

Chapter 8. Individual System Testing

This section presents the results and corresponding analysis of the three most important areas of the overall test bed. These are the UTRA/3G test bed module; the HVS-based fidelity system and the Importance Map system. The results are presented to illustrate the working and behavior of the individual systems. The input data from processing are raw PGM files, as the aim of this thesis is to present the workings of the test bed implemented with minimal complication of the communication protocols or image compression technologies. The test images used in Chapters 8 and 9 are common testing images used by image processing application.

8.1 UTRA/3G Test Bed Module System Testing

Results presented here are divided into three sections: general image testing, images subject to variable environmental parameters and velocity and image subject to varying arrival angle. The aim of this section is to show that the UTRA/3G test bed module is working and is generally consistent with expected outcomes.

8.1.1 General Image Testing

This section shows results of sending various different images through the UTRA/3G test bed module. A different range of images is tested while the environment parameters are fixed to Vehicular A. Six separate group of images are shown with each subjected to channel conditions under velocities of 20 km/h, 50 km/h and 80 km/h. The new terminology used in this section is listed below [42]:

$$MSE = \frac{1}{MN} \sum_{i=0}^{M-1} \sum_{j=0}^{N-1} (x_{ij} - \hat{x}_{ij})^2 \qquad (8.1)$$

$$PSNR = 10 \log \frac{(2^n - 1)^2}{MSE} dB \qquad (8.2)$$

where:

- MSE is Mean Square Error;
- PSNR is Perceptual Signal to Noise Ratio;

- x_{ij} is the original pixel value at position (i,j);

- $\hat{x}_{ij}$ value of distorted pixel at position (i,j);

- M is number of horizontal pixels;

- N is the number of vertical pixels; and

- n is the number of pixels.

MSE and PSNR are used to illustrate the pixel level measurement of errors and signal to error ratio for an image. Figures 8.1 to 8.6 illustrate the results for a range of images subjected to channel motion of 20, 50 and 80 km respectively.
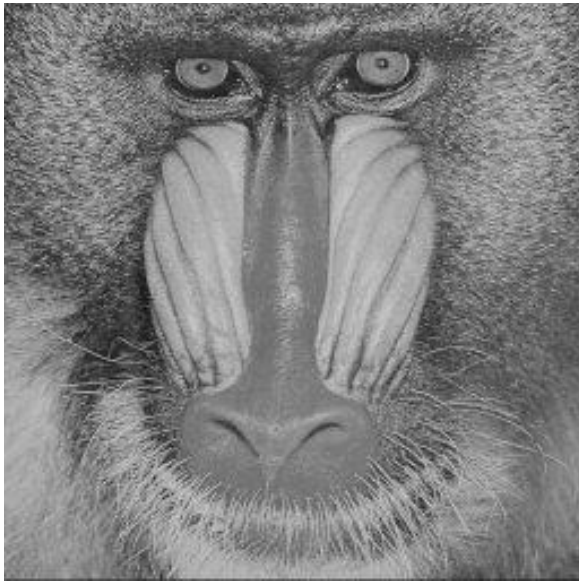
Figure 8.1 (a)
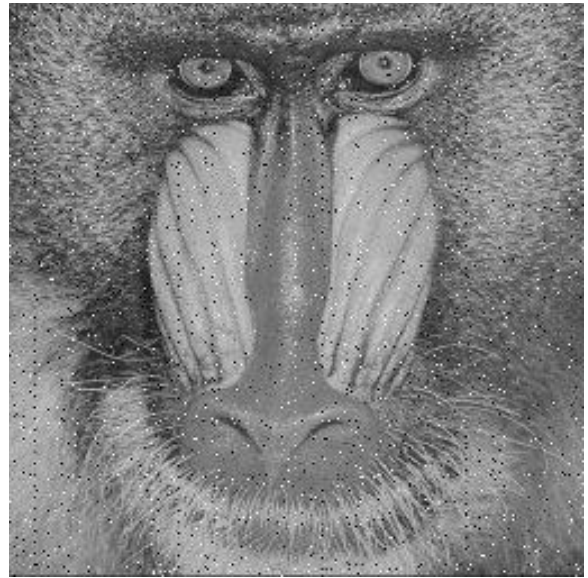
Figure 8.1 (b)
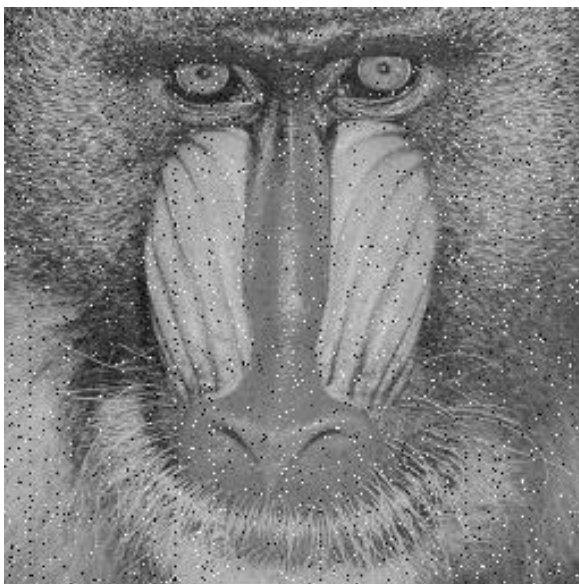
Figure 8.1 (c)
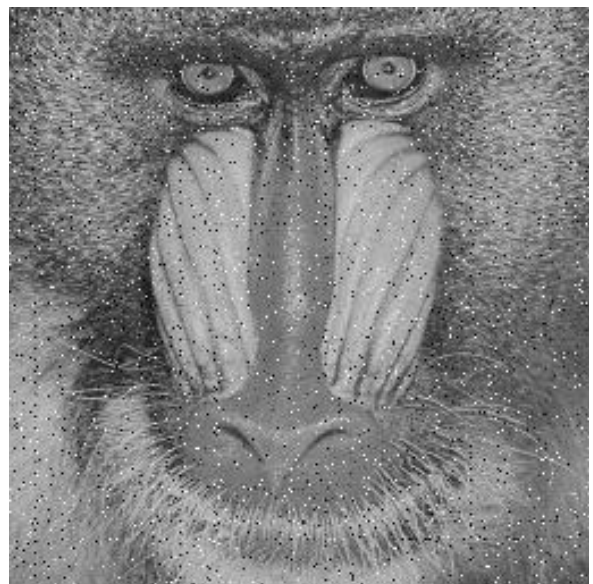
Figure 8.1 (d)

Figure 8.1 Image "Baboon" Subjected to Channel of Three Different Velocities
(a) Original   (b) 20 km/h (c) 50 km/h (d) 80km/h

Figure 8.2 (a)

Figure 8.2 (b)

Figure 8.2 (c)

Figure 8.2 (d)

Figure 8. 2 Image "Football" Subjected to Channel of Three Different Velocities
(a) Original   (b) 20 km/h (c) 50 km/h (d) 80km/h

Figure 8.3 (a)

Figure 8.3 (b)

Figure 8.3 (c)

Figure 8.3 (d)

Figure 8.3 Image "Lena" Subjected to Channel of Three Different Velocities

(a) Original   (b) 20 km/h (c) 50 km/h (d) 80km/h

Figure 8.4 (a)   **Figure 8.4 (b)**

Figure 8.4 (c)   **Figure 8.4 (d)**

Figure 8.4 Image "Soccer" Subjected to Channel of Three Different Velocities

(a) Original   (b) 20 km/h (c) 50 km/h (d) 80km/h

<div align="center">

Figure 8.5 (a)   **Figure 8.5 (b)**

Figure 8.5 (c)   **Figure 8.5 (d)**

Figure 8.5 Image "Bike" Subjected to Channel of Three Different Velocities
(a) Original   (b) 20 km/h (c) 50 km/h (d) 80km/h

</div>

<div align="center">

Figure 8.6 (a)   **Figure 8.6 (b)**

Figure 8.6 (c)   **Figure 8.6 (d)**

Figure 8.6 Image "Light house" Subjected to Channel of Three Different Velocities
(a) Original   (b) 20 km/h (c) 50 km/h (d) 80km/h

</div>

Image	Velocity	MSE	PSNR (dB)
"Baboon"	20 km/h	260.83	24.00
	50 km/h	323.54	23.03
	80 km/h	366.96	22.48
"Bike"	20km/h	257.06	24.03
	50 km/h	315.77	23.14
	80 km/h	374.46	22.40
"Football"	20 km/h	255.37	24.06
	50 km/h	323.86	23.03
	80 km/h	376.54	22.37
"Lena"	20 km/h	264.22	23.91
	50 km/h	335.37	22.88
	80 km/h	366.95	22.48
"Light House"	20 km/h	265.06	24.30
	50 km/h	316.89	23.12
	80 km/h	368.47	22.47
"Soccer"	20 km/h	259.20	23.99
	50 km/h	315.82	23.14
	80 km/h	365.42	22.50

Table 8.1 General Image Testing Result Summary
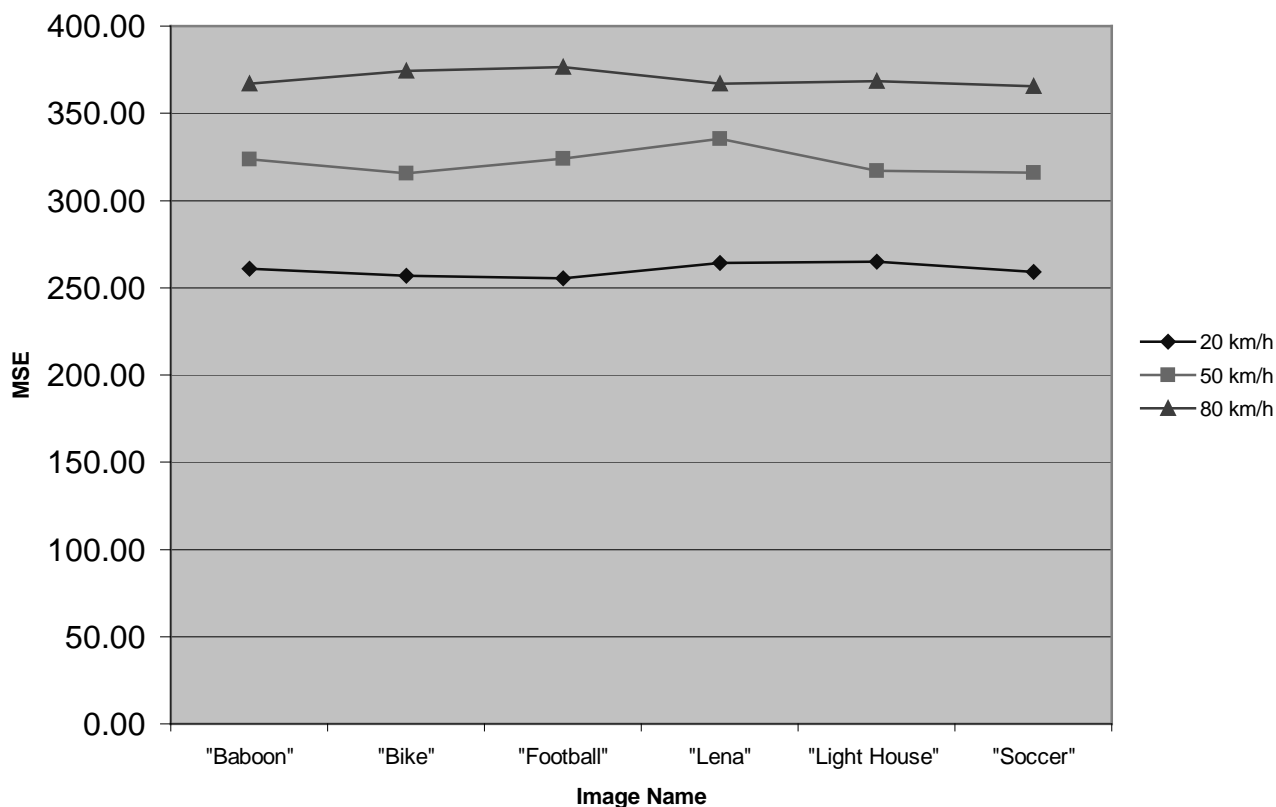
Figure 8.7 General Image Testing MSE Graph

General Image Testing PSNR
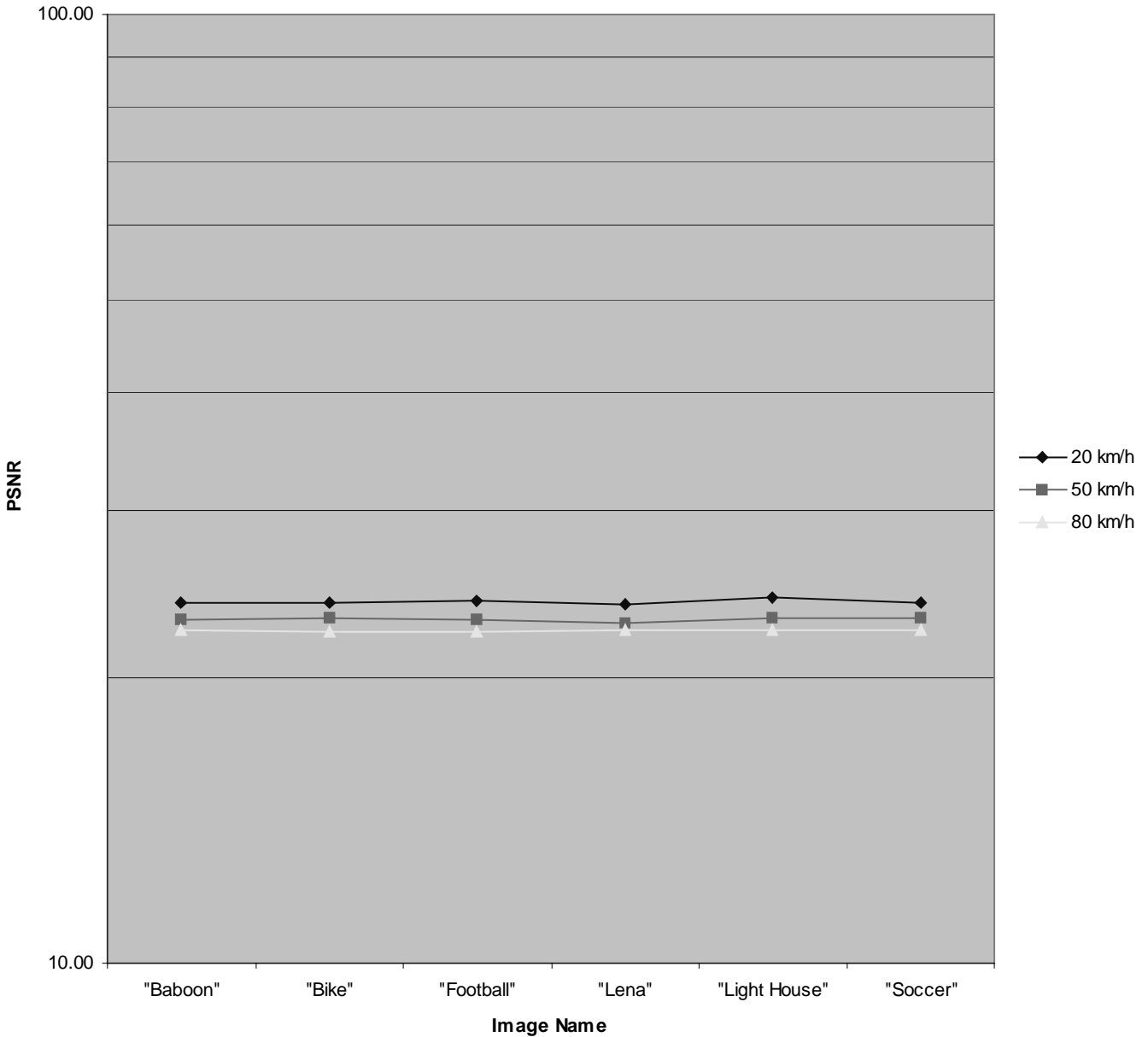
Figure 8.8 General Image Testing PSNR Graph

In these displayed experimental results, the test images consist of a sample of different types of image. Typical genres of "Nature", "Mechanical Object", "Action", "Face", "Landscape" and "Sports" are considered by choosing the corresponding test images of "Baboon", "Bike", "Football", "Lena", "Lighthouse" and "Soccer". From Table 8.1, the results have shown that with increasing velocity, while keeping the environment parameters fixed, the MSE error of the image increases, independent of the image type being tested. Visualization of the result in Figure 8.7 shows that MSE values across all images group into a pattern with different channel conditions (velocities). Figure 8.8 reflects the same

condition, although the grouping is less obvious. Different channel conditions induce different MSEs (and subsequently different PSNR), whose values for each condition collect into a limited range. Each result group for the channel conditions of 20, 50 and 80 km/h for both error (MSE) and quality (PSNR) measurement has conformed to within a variation of a limited range. This is consistent with expected outcomes.

Velocity	Mean (n = 6)	Mean Deviation (n= 6)
20 km/h	260.29	3.08
50 km/h	321.88	5.72
80 km/h	369.80	3.80

Table 8.2 MSE Result Statistics of Error Mean and Deviation

Using a light statistical analysis, Table 8.2 presents means and deviations for the MSE results grouped by channel velocities of 20 km/h, 50 km/h and 80 km/h. As shown in the Table, the standard deviation between the 3 sets of results is relatively small compared to data values. This further supports the integrity of the 3G/UTRA test bed component.

The experimental velocities of 20, 50 and 80 km/h were chosen as they reflect the various situations which a vehicular motive mobile device can experience. The parameter value of 20 km/h allows consideration of extremely slow moving traffic, and 50 km/h corresponds to average speed while a vehicle is in a low-speed built-up area. Keeping the same range difference as the two previous velocity selections, the higher speed of 80 km/h is chosen to conform to the general speed of a suburban motorway.

Furthermore, Figures 8.1 – 8.6 have shown that the error of the images does not have a rigid spread pattern for all tested images. This is proof that the errors injected are dynamic and are not image dependent. This is reflected by the randomly spread errors in all images, where corresponding images do not have a rigid error pattern. Furthermore, the error for a velocity is varied within a limited range, providing evidence that a stable rate of error injection has been obtained. The result has shown that the UTRA/3G module is working and is consistent in general with various types of images. The remainder of this chapter describes image quality in terms of PSNR, as this term directly correlates to image quality as opposed to MSE which measures error and displays an inverse relationship.

8.1.2 Image Subjected to Variable Environment Parameters and Velocity

This section exposes a fixed image to the six different available environment parameters at a selected velocity. The chosen test images are "Announcer" and "Football", as these images reflect the "News" and "Action" formats respectively. These formats are common image types in services rendered for UEs. Testing channel condition is fixed with arriving angle of "75.0 45.0 15.0 –15.0 –45.0 –75.0", Chip Rate = 3840000, Antenna number = 1, Antenna Spacing = 0.075 and frame number of 3160. Figure 8.9 (a) shows the original images while Figures 8.9 (b) to 8.13 illustrate the results. Comparison is done using PSNR so as to reflect the image quality instead of the error rate.

Figure 8.9 (a)
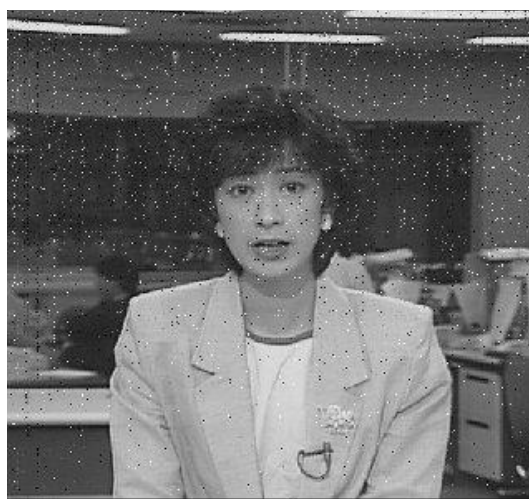
| **Figure 8.9 (b)** | **Figure 8.9 (c)** |
| **PSNR = 40.0 dB** | **PSNR = 24.72 dB** |

Figure 8.9 Image "Announcer" subjected to Indoor Environment Parameter

(a) Original (b) 0 km/h at Indoor A   (c) 0 km/h at Indoor B

Figure 8.10 (a)
PSNR = 44.66 dB

Figure 8.10 (d)
PSNR = 37.68 dB

Figure 8.10 (b)
PSNR = 45.53 dB

Figure 8.10 (e)
PSNR = 45.53 dB

Figure 8.10 (c)
PSNR = 45.66 dB

Figure 8.10 (f)
PSNR = 45.53 dB

Figure 8.10 Image "Announcer" subjected to Indoor Environment Parameter
(a) 0.5 km/h Indoor A (b) 1 km/h Indoor A (c) 1.5 km/h Indoor B
(d) 0.5 km/h Indoor B (e) 1 km/h Indoor B (f) 1.5 km/h Indoor B

Figure 8.11 (a)
PSNR = 46.97dB
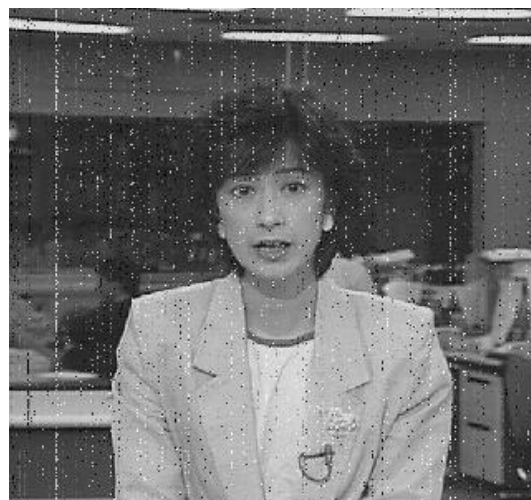
Figure 8.11 (e)
PSNR = 23.26 dB

Figure 8.11 (b)
PSNR = 46.08 dB

Figure 8.11 (f)
PSNR = 23.34 dB

Figure 8.11 (c)
PSNR = 32.14 dB
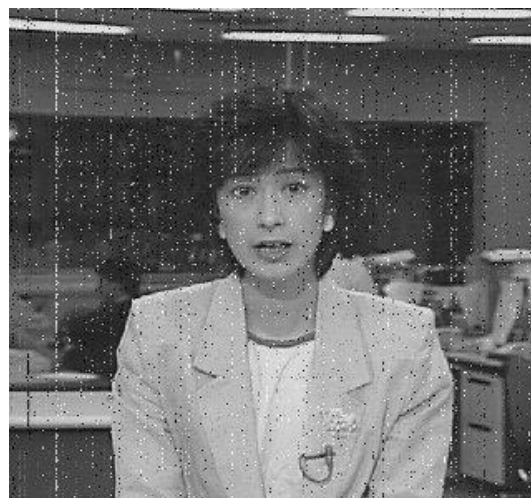
Figure 8.11 (g)
PSNR = 22.89 dB

Figure 8.11 (d)
PSNR = 29.85 dB

Figure 8.11 (h)
PSNR =22.51 dB

Figure 8.11 Image "Announcer" subjected to Pedestrian Environment Parameter

(a) 1.5 km/h Pedestrian A (b) 3 km/h Pedestrian A (c) 10 km/h Pedestrian A (d) 20 km/h Pedestrian A
(e) 1.5 km/h Pedestrian B (f) 3 km/h Pedestrian B   (g) 10 km/h Pedestrian B (h) 20 km/h Pedestrian B
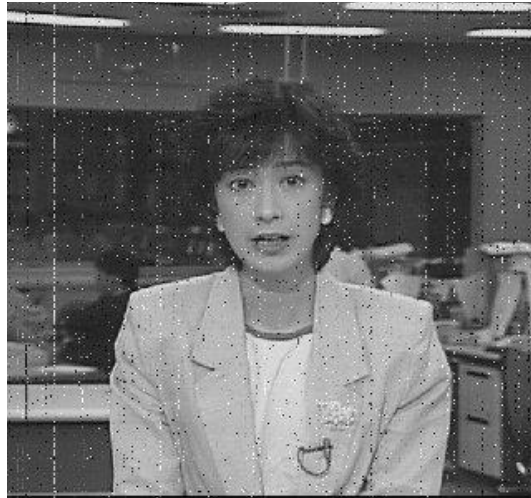
Figure 8.12 (a)
PSNR = 24.07 dB
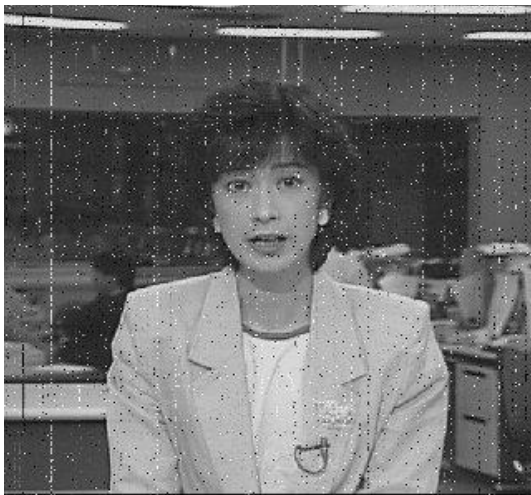
Figure 8.12 (b)
PSNR = 23.56 dB
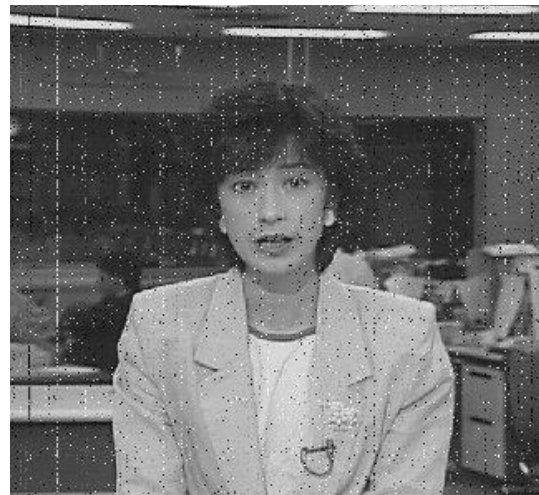
Figure 8.12 (c)
PSNR = 23.04 dB
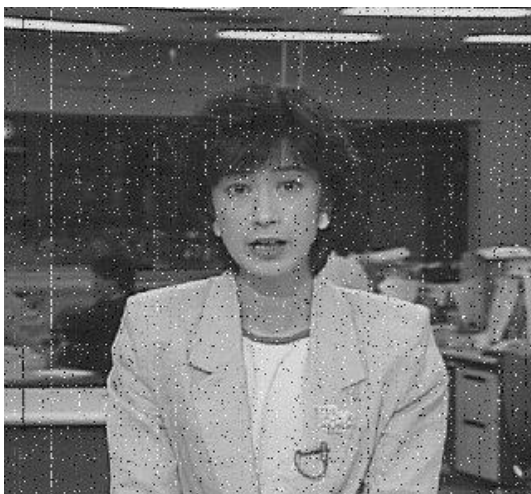
Figure 8.12 (d)
PSNR = 22.44 dB
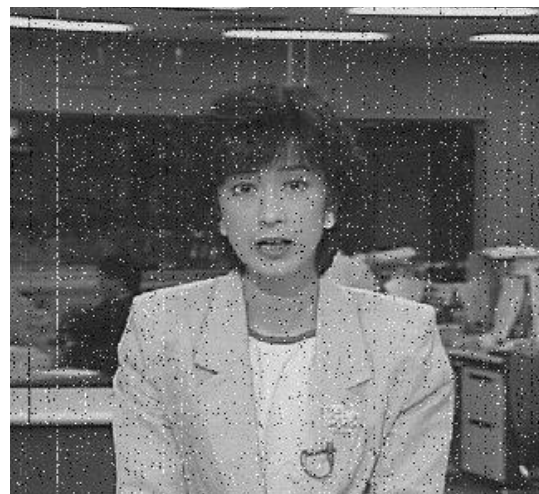
Figure 8.12 (e)
PSNR = 21.66 dB

Figure 8.12 Image "Announcer" subjected to Vehicular Environment Parameter
(a) 20 km/h Vehicular A (b) 40 km/h Vehicular A
(c) 60 km/h Vehicular A (d) 80 km/h Vehicular A (e) 100 km/h Vehicular A
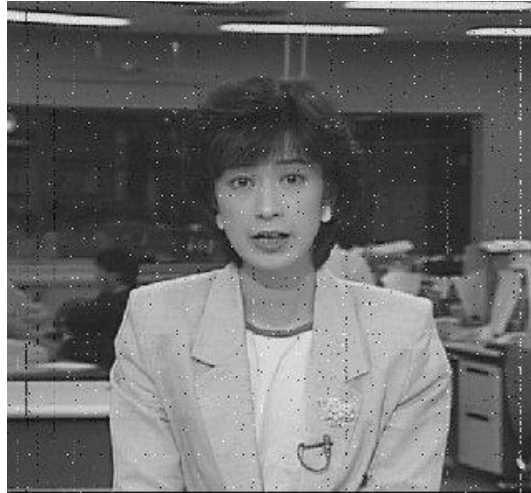
Figure 8.13 (a)
PSNR = 27.52 dB
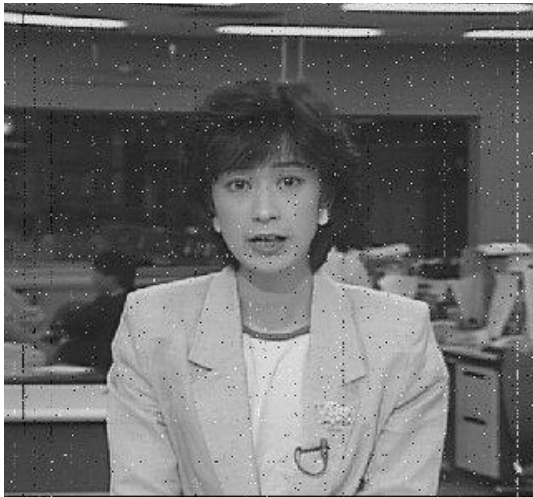
Figure 8.13 (b)
PSNR = 26.69 dB
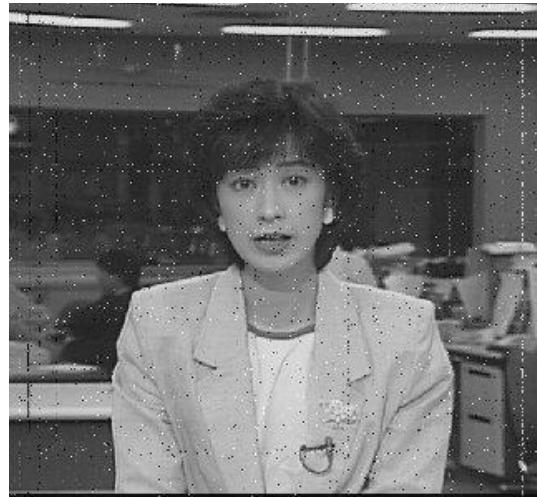
Figure 8.13 (c)
PSNR = 25.71 dB
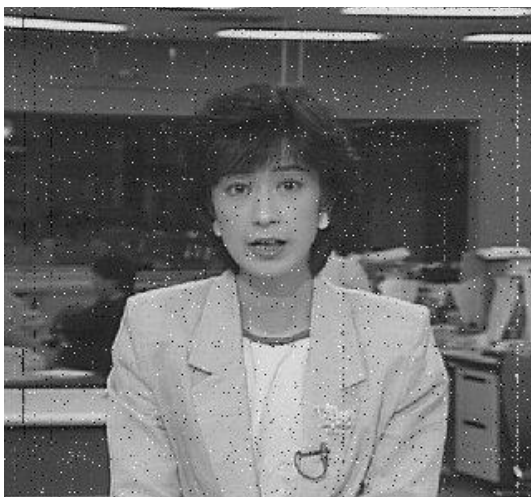
Figure 8.13 (d)
PSNR = 24.87 dB
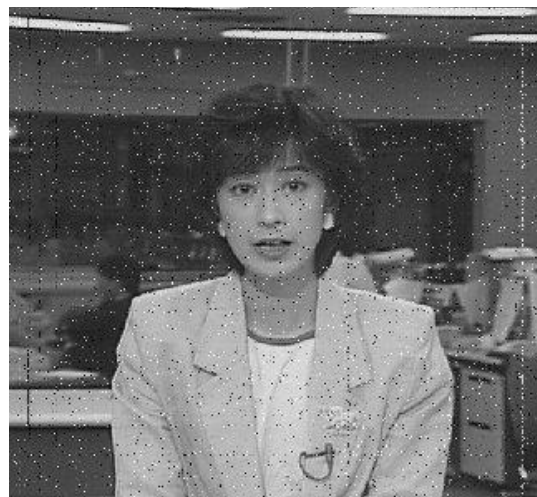
Figure 8.13 (e)
PSNR = 23.62 dB

Figure 8.13 Image "Announcer" subjected to Vehicular Environment Parameter
(a) 20 km/h Vehicular B (b) 40 km/h Vehicular B
(c) 60 km/h Vehicular B (d) 80 km/h Vehicular B (e) 100 km/h Vehicular B

The following Table summarizes the PSNR values for the various results of images "Announcer" for ease of analysis.

Velocity	Indoor A	Indoor B	Pedestrian A	Pedestrian B	Vehicular A	Vehicular B
0 km/h	40.00 dB	24.72 dB	**X**	**X**	**X**	**X**
0.5 km/h	44.66 dB	37.68 dB	**X**	**X**	**X**	**X**
1 km/h	45.53 dB	38.82 dB	**X**	**X**	**X**	**X**
1.5 km/h	45.66 dB	39.05 dB	46.97 dB	23.26 dB	**X**	**X**
3 km/h	**X**	**X**	46.08 dB	23.34 dB	**X**	**X**
10 km/h	**X**	**X**	32.14 dB	22.89 dB	**X**	**X**
20 km/h	**X**	**X**	29.85 dB	22.51 dB	24.07 dB	27.52 dB
40 km/h	**X**	**X**	**X**	**X**	23.56 dB	26.69 dB
60 km/h	**X**	**X**	**X**	**X**	23.04 dB	25.71 dB
80 km/h	**X**	**X**	**X**	**X**	22.44 dB	24.87 dB
100 km/h	**X**	**X**	**X**	**X**	21.66 dB	23.62 dB

Table 8.3 PSNR Table Summary for Varying Environment Parameter and Velocity

In these tests, indoor conditionals are only tested for extremely low velocity, as it is unlikely that indoor users will be walking at higher velocity. The same approach is applied for the pedestrian environment, as walking and jogging pedestrians are unlikely to reach speeds higher than 20 km/h or lower than 3 km/h. Similarly, moving vehicle mode as considered by vehicular parameter seldom reaches a speed below 10 km/h. Even if the user vehicle reaches such a speed, it is more logical to consider it to be in the pedestrian or indoor environment. Note from the Table that low speed testing done upon the vehicular mode, is showing a slight inconsistency as vehicular mode is really a design for higher velocity.

From the result, the varying differences in PSNR of images subjected to different modes of indoor, pedestrian and vehicular are particularly notable. The large difference is due to varying considerations upon Doppler effect, channel delay and power loses. The result reflects this point and is consistent with expected outcomes. Furthermore, the difference between mode A and mode B gives a slight range difference inside the same environment factor. This is achieved via tiny delay and multi-path power differences and is correctly reflected in the result.

In the suitable range, pedestrian and vehicular modes show degrading quality relative to increasing velocity. The indoor mode appears inconsistent in this aspect, as higher velocity yields lower drop in image quality. This phenomenon is explainable as the indoor environment uses a flat Doppler spectrum and is therefore not as reflective of velocity changes. Furthermore, the change in velocity is small compared to the range tested upon other environment parameters. Given that the change in quality is also small, this can be further explained by changes applied by the dynamic error injection. As shown, although the indoor environment is not effective to be used for testing of changing velocity, it is still consistent in reflecting the indoor environment.

The next sets of results shown are for another test image "Football".

Figure 8.14 (a)

Figure 8.14 (b)
PSNR = 39.84 dB

Figure 8.14 (c)
PSNR = 24.43 dB

Figure 8.14 Image "Football" subjected to Indoor Environment Parameter
(a) Original (b) 0 km/h Indoor A (c) 0.5 km/h Indoor A

Figure 8.15 (a)
PSNR = 43.52 dB

Figure 8.15 (d)
PSNR = 36.56 dB

Figure 8.15 (b)
PSNR = 42.73 dB

Figure 8.15 (e)
PSNR = 37.22 dB

Figure 8.15 (c)
PSNR = 43.78 dB

Figure 8.15 (f)
PSNR = 37.78 dB

Figure 8.15 Image "Football" subjected to Indoor Environment Parameter
(a)   1 km/h Indoor A (b) 1.5 km/h Indoor A
(c) 0 km/h Indoor B   (d) 0.5 km/h Indoor B (e) 1 km/h Indoor B (f) 1.5 km/h Indoor B

Figure 8.16 (a)
PSNR = 45.15 dB

Figure 8.16 (e)
PSNR = 22.88 dB

Figure 8.16 (b)
PSNR = 44.57 dB

Figure 8.16 (f)
PSNR = 22.96 dB

Figure 8.16 (c)
PSNR = 32.54 dB

Figure 8.16 (g)
PSNR = 22.54 dB
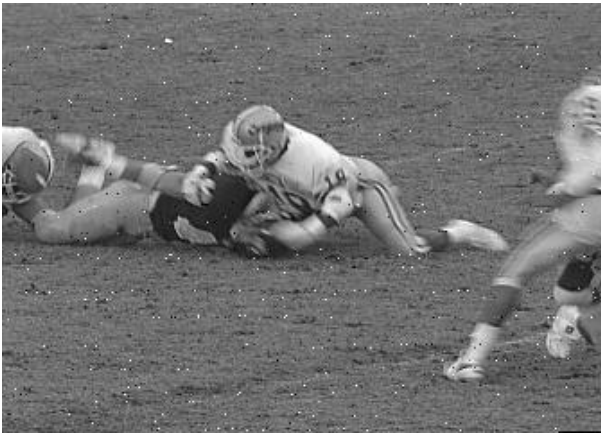
Figure 8.16 (d)
PSNR = 29.96 dB
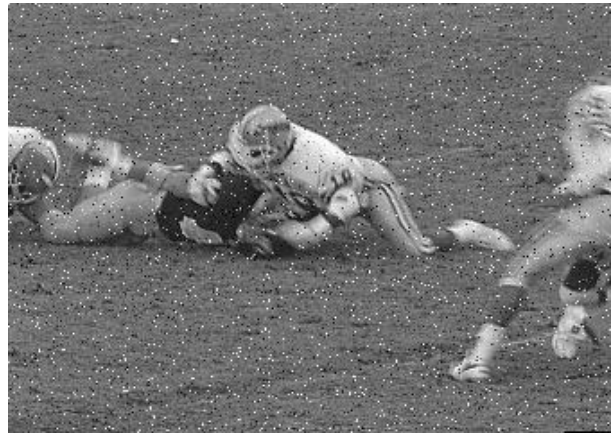
Figure 8.16 (h)
PSNR = 22.13 dB

Figure 8.16 Image "Football" subjected to Pedestrian Environment Parameter

(a) 1.5 km/h Pedestrian A (b) 3 km/h Pedestrian A (c) 10 km/h Pedestrian A
(d) 20 km/h Pedestrian A (e) 1.5 km/h Pedestrian B (f) 3 km/h Pedestrian B
(g) 10 km/h Pedestrian B (h) 20 km/h Pedestrian B

Figure 8.17 (a)
PSNR = 23.85 dB
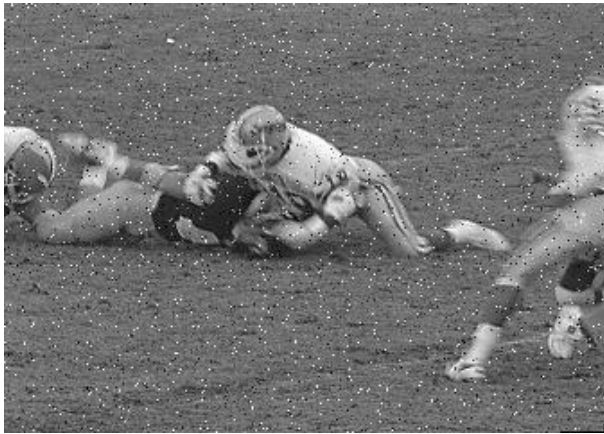
Figure 8.17 (b)
PSNR = 23.33 dB

Figure 8.17 (c)
PSNR = 23.03 dB

Figure 8.17 (d)
PSNR = 22.41 dB
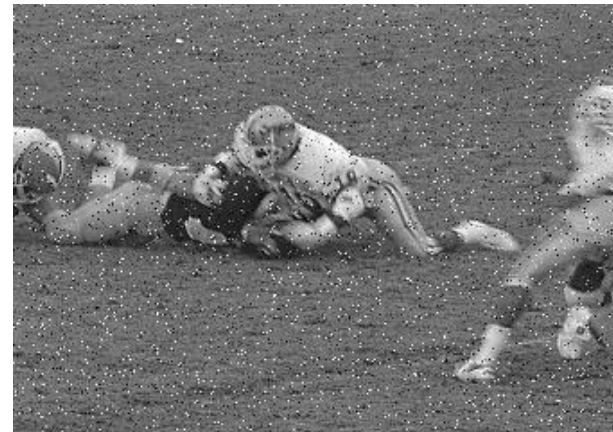
Figure 8.17 (e)
PSNR = 21.55 dB

Figure 8.17 Image "Football" subjected to Vehicular Environment Parameter

(a) 20 km/h Vehicular A (b) 40 km/h Vehicular A
(c) 60 km/h Vehicular A   (d) 80 km/h Vehicular A (e) 100 km/h Vehicular A

Figure 8.18 (a)
PSNR = 27.48 dB
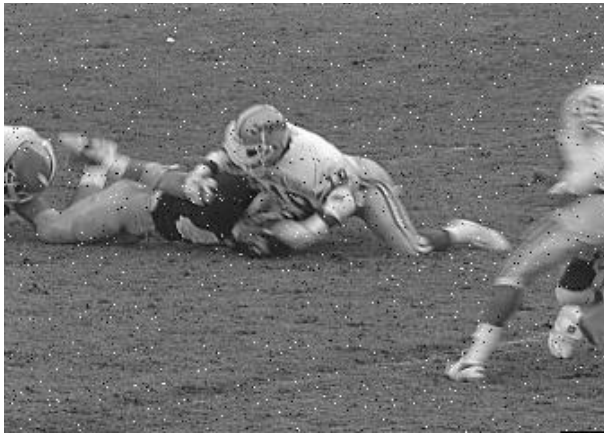
Figure 8.18 (b)
PSNR = 26.50 dB
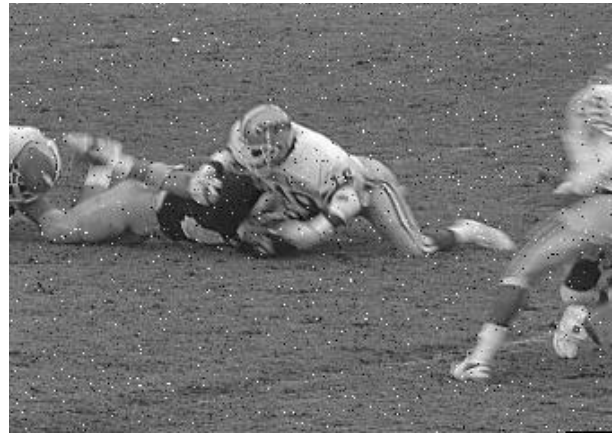
Figure 8.18 (c)
PSNR = 25.04 dB

Figure 8.18 (d)
PSNR = 24.97 dB

Figure 8.18 (e)
PSNR = 23.57 dB

Figure 8.18 Image "Football" subjected to Vehicular Environment Parameter

(a) 20 km/h Vehicular B (b) 40 km/h Vehicular B
(c) 60 km/h Vehicular B   (d) 80 km/h Vehicular B (e) 100 km/h Vehicular B

"Football" PSNR

Velocity	Indoor A	Indoor B	Pedestrian A	Pedestrian B	Vehicular A	Vehicular B
0 km/h	39.84 dB	24.43 dB	**X**	**X**	**X**	**X**
0.5 km/h	43.52 dB	36.56 dB	**X**	**X**	**X**	**X**
1 km/h	42.73 dB	37.22 dB	**X**	**X**	**X**	**X**
1.5 km/h	43.78 dB	37.78 dB	45.15 dB	22.88 dB	**X**	**X**
3 km/h	**X**	**X**	44.57 dB	22.96 dB	**X**	**X**
10 km/h	**X**	**X**	32.45 dB	22.54 dB	**X**	**X**
20 km/h	**X**	**X**	29.96 dB	22.13 dB	23.85 dB	27.48 dB
40 km/h	**X**	**X**	**X**	**X**	23.33 dB	26.50 dB
60 km/h	**X**	**X**	**X**	**X**	23.03 dB	25.04 dB
80 km/h	**X**	**X**	**X**	**X**	22.41 dB	24.97 dB
100 km/h	**X**	**X**	**X**	**X**	21.55 dB	23.57 dB

Table 8.4 Varying Environment Parameter and Velocity System Result Summary

The shown result (in Table 8.4) reflects a pattern similar to that previously displayed for the image "Announcer". This shows that the 3G/UMTS module works independently of images while upholding the expected behavior for different channel conditions.
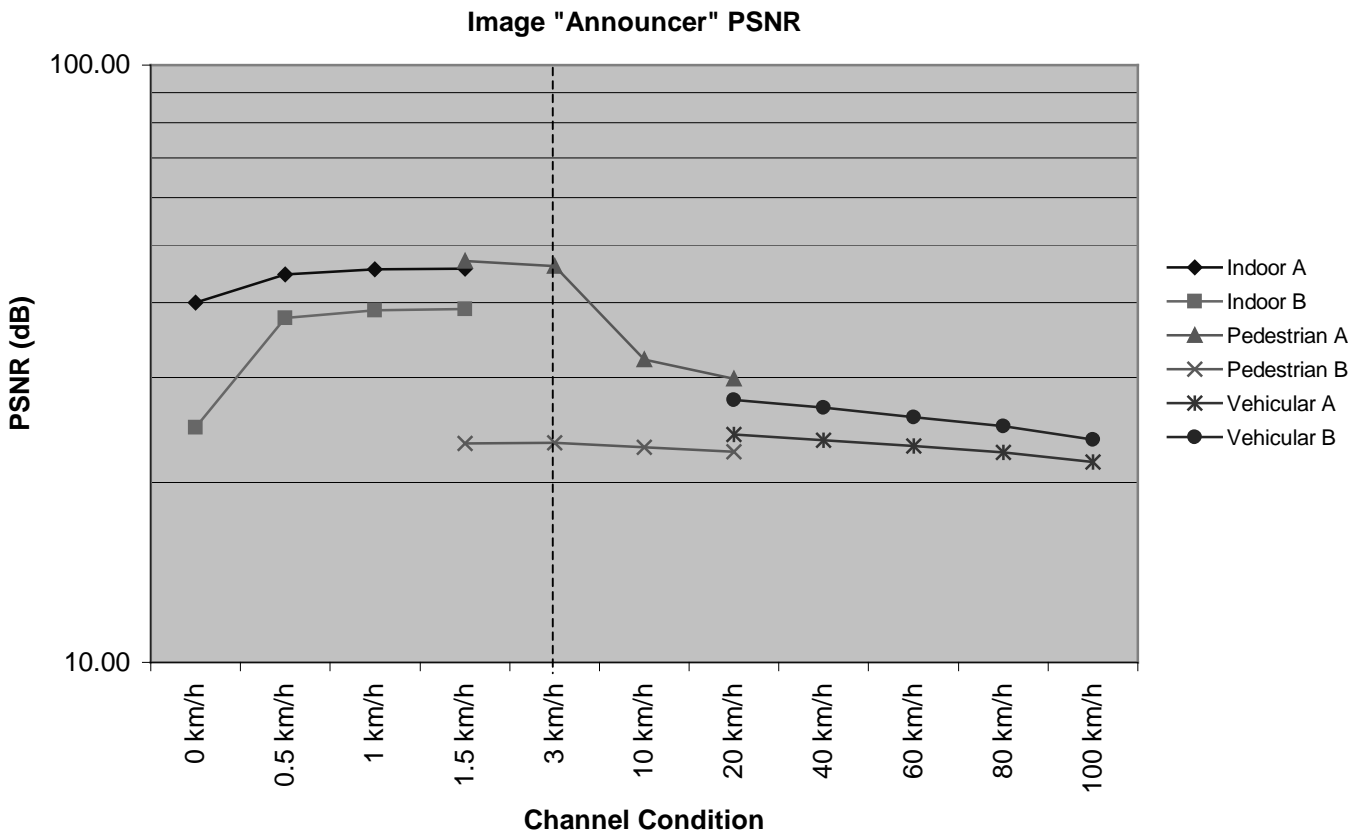
Figure 8.19 Image "Announcer" PSNR Result Plot

Image "Football" PSNR
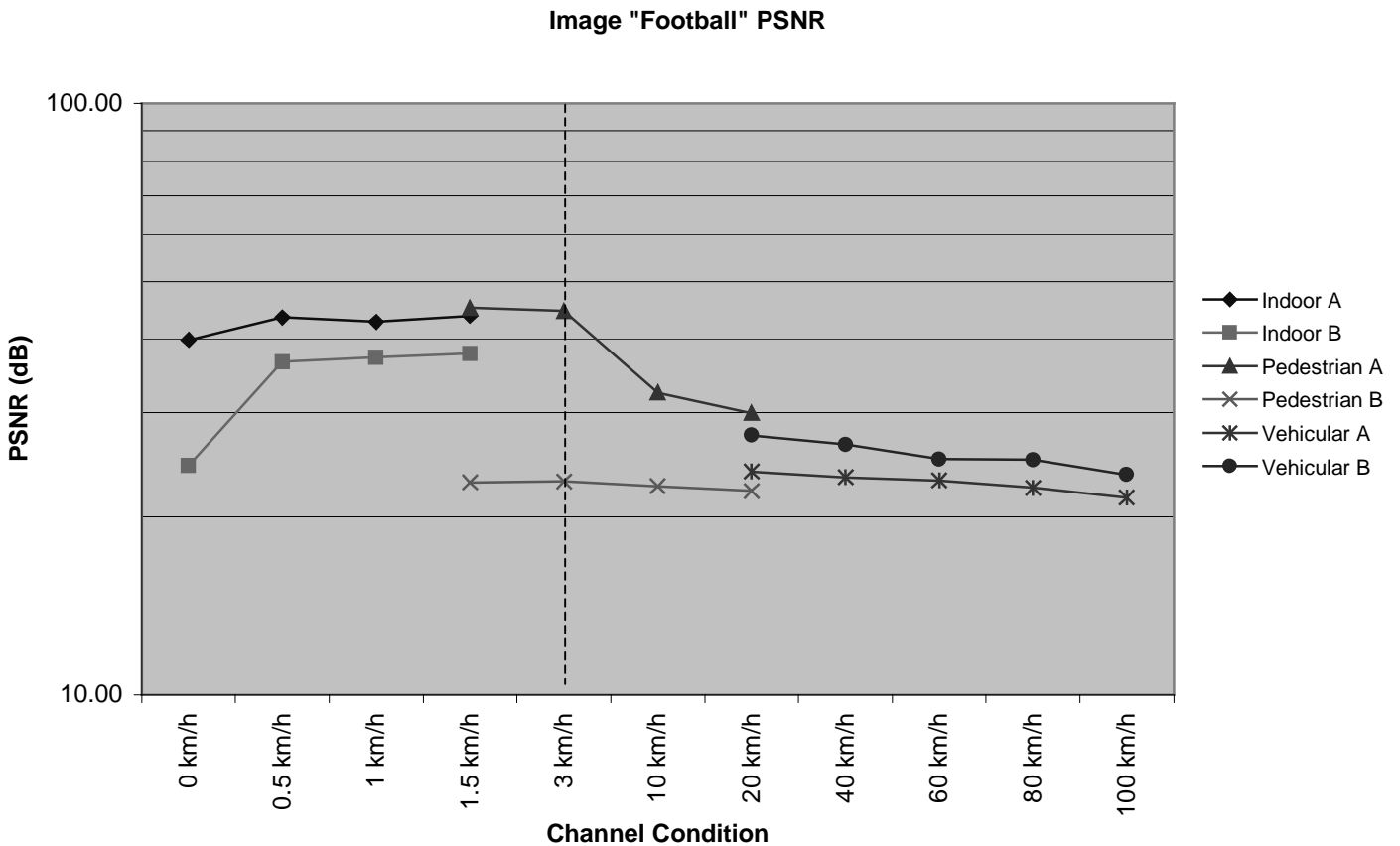
Figure 8.20 Image "Football" PSNR Result Plot

Figures 8.19 and 8.20 show the PSNR measurement graphically for the two sets of results. From the pattern displayed, one can see that channel conditions A and B cause different data loss. This is due to the designed small variation inside a major channel condition to allow simulation of a slightly different case of the same class of channel condition (the major channel condition parameters are described in Chapter 6). Note that the horizontal axis of the plot shown is not displayed in a linear manner, and shows the result in a clearer manner. A dashed line is placed in all velocity-associated graphs to visually disassociate the two horizontal linear scales.

Note that Pedestrian A quality drops sharply after 3 km/h due to its design having a stronger Doppler effect which experiences large loss at low speeds. Another anomaly lies in the result for 0 km/h as it yields a somewhat higher error than expected. This is because the system is not designed for simulating stationary conditions, and the channel condition simulator injects more errors than is intended for conditions lower than about 0.03 km/h.

This phenomenon is cause by the channel simulator (Figure 6.5) component, which was provided by ADS "as is" and cannot be modified by the user.

The remainder of results have a flat role off relative to the higher velocity, which is within expectation. Note also that in parameter A of both sets of results, the three major channel groups form an almost seamless display, showing the gradual reduction of image data quality with increasing velocity. However, this is not reflected in parameter B. This behavior can be explained by Pedestrian B channel condition taking into account more extreme environment loss factors that are not in universal conformance with parameter B of the other two groups. Furthermore, velocity 1.5 km/h shows that the Pedestrian model starts to loose convergence. This is expected as the model starts to input velocity that is lightly outside its normal lower boundary.

Selection of only 2 images for testing in the general velocity/environmental parameter section is due to the large amount of processing needed and is not within the time limit of the author. Furthermore, the two images have extremely different properties that provide a large range visual diversity for this test and in further testing later.

This section demonstrates that the 3G test bed module is able to dynamically induce a controlled level of noise onto the input image media. Subsequently, the images are exposed to channel conditioned controlled error that increases with increasing velocity and different environment parameters. Figures 8.18 and 8.19 have demonstrated that a consistent pattern of error rate is achieved with different images and different runs of the images. The range of image result has verified that the error patterns do not fixate at the same pixels, providing a rate-controlled spreading error with randomized error placing. A and B sets of parameters provide a different rate of error conditions for different considerations of channel condition.

Overall, individual environmental parameters effectively reflect the environment condition it emulates. When used in the proper range, the changing velocity yielded expected drop in quality correctly. The UTRA/3G module environment and velocity variable is working and is consistent with expected outcomes.

8.1.3 Image Subjected to Variable Arriving Angle

This section presents the result of varying channel path arriving angle. The environmen-tal

parameters are fixed at 3 km/h at Pedestrian A. The results are presented below.

Figure 8.21 (a)

Figure 8.21 (b)

Figure 8.21 (c)

Figure 8.21 (d)

Figure 8.21 (e)

Figure 8.21 Image "Announcer" Subjected to Different Arriving Angle

(a) "75.0 45.0 15.0 –15.0 –45.0 –75.0"   (b) "75.0 30.0 15.0 –15.0 –30.0 –75.0" (c) "60.0 30.0 15.0 –15.0 –30.0 –60.0"
(d) "50.0, 30.0, 10.0, -10.0, -30.0, -50.0" (e) "80.0, 40.0, 20.0, -20.0, -40.0, -80.0"

Arriving Angle	3 km/h pedestrian A
"75.0 45.0 15.0 –15.0 –45.0 –75.0"	46.08 dB
"75.0 30.0 15.0 –15.0 –30.0 –75.0"	46.08 dB
"60.0 30.0 15.0 –15.0 –30.0 –60.0"	46.08 dB
"50.0, 30.0, 10.0, -10.0, -30.0, -50.0"	46.08 dB
"80.0, 40.0, 20.0, -20.0, -40.0, -80.0"	46.08 dB

Table 8.5 Result Summary for Image "Announcer" Subjected to Varying Arriving Angle

Figure 8.22 (a)

Figure 8.22 (b)

Figure 8.22 (c)

Figure 8.22 (d)

Figure 8.22 (e)
Figure 8.22 Image "Football" Subjected to Different Arriving Angle

(a) "75.0 45.0 15.0 –15.0 –45.0 –75.0" (b) "75.0 30.0 15.0 –15.0 –30.0 –75.0" (c) "60.0 30.0 15.0 –15.0 –30.0 –60.0"
(d) "50.0, 30.0, 10.0, -10.0, -30.0, -50.0" (e) "80.0, 40.0, 20.0, -20.0, -40.0, -80.0"

Arriving Angle	3 km/h pedestrian A
"75.0 45.0 15.0 –15.0 –45.0 –75.0"	44.57 dB
"75.0 30.0 15.0 –15.0 –30.0 –75.0"	44.57 dB
"60.0 30.0 15.0 –15.0 –30.0 –60.0"	44.57 dB
"50.0, 30.0, 10.0, -10.0, -30.0, -50.0"	44.57 dB
"80.0, 40.0, 20.0, -20.0, -40.0, -80.0"	44.57 dB

Table 8.6 Result Summary for Image "Football" Subjected to Varying Arriving Angle

The result shows a minimal change in image quality yield by changes in the arriving angle. This is within expectations, as the internal Rake receiver in UE compensates for distortion brought about by the change in arriving angles. The varied error rate in the image "Announcer" is accountable by the dynamic variation of the losses in the component that simulates the physical channel condition. Note that although subjected to the same condition, both images show slightly different PSNR results. This is expected, as dynamic error rate conditioning is applied. Arriving angles (e.g. "75.0 45.0 15.0 –15.0 –45.0 –75.0") described here are elevation and azimuth angles of multi-path echo, for calculating directive gain of receiving linear antenna array. This is the ADS approach to simulate an antenna array of a receiving device [74]. The channel simulator produces variation in results relative to changes in the parameters. However the difference is too small to be reflected in the result pictures and quality measurements shown. These results are directly influenced by the method of calculating antenna directive gain in the channel simulator, which is rigid and unchangeable by the user as mentioned previously.

This ends the section on varying arriving angle testing and also ends the section on individual testing of the UTRA/3G test bed module. In summary, the UTRA/3G test bed is shown to be working and produces results that are logically consistent with usage within the proper parameter range. Testing presented has affirmed the nature of this module to simulate 3G channel condition multiple environmental parameter changes, with the important control over velocity and physical environment selection of Indoor, Pedestrian and Outdoor. Various images being tested show no evidence of repeated error spread pattern, suggesting that this module treats input media as a data stream and this makes the module versatile for any media. A controlled error rate pattern has been obtained, where stable behavior has been observed.

With the working UTRa/3G test bed module, systematic degradation of input media is assured and an important part of the objective has been achieved. The next two sections concentrate on testing of the image quality metrics.

8.2 Image Quality Metric: HVS-Based Fidelity Test Bed Module System Testing

This section presents testing of the HVS-based image fidelity system. Various images are presented with its quality degraded pair to produce PDM which is comparable with the actual pixel errors. Image impairment is produced by compression using JPEG in Adobe Photoshop 5.5 at level 5 (medium) quality. Figure 8.23 to 8.29 present the results with the figure divided into four parts, original, coded, PDM and square error. The original is the original picture while the coded is the JPEG impaired picture. The PDM is the Perceptual Distortion Map showing the distribution of perceptual error and the square error is the squared value of the actual physical error.

Figure 8.23 (a)

Figure 8.23 (b)
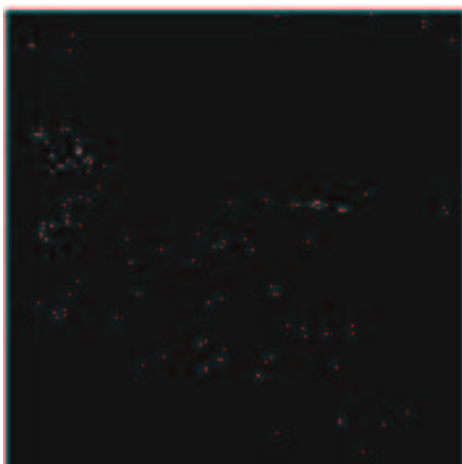
Figure 8.23 (c)
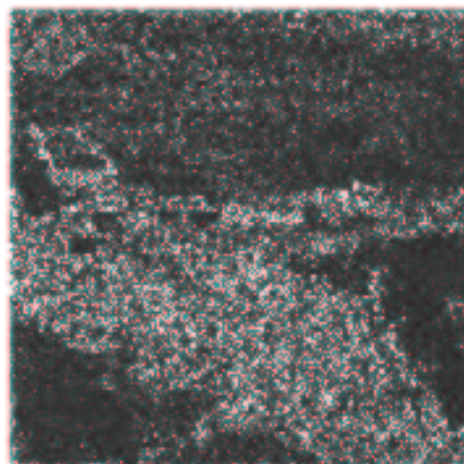
Figure 8.23 (d)

Figure 8.23 Image "Airplane"
(a) Original (b) Coded (c) PDM (d) Square Error

115

Figure 8.23 shows the result for the image "Airplane". Image "Airplane" is chosen for testing in the system for its visual property for having an object in the centre of the screen while having with a natural scene background. MSE for this result is found to be 9.50 while the PQR (using beta of 3 for accurate evaluation) is 3.89. The square error result shows the distribution of the actual error. Although the square error seems large, the PDM detects the HVS-based perceptual noticeable difference is minute. This phenomenon is within expectations and is particularly notable by comparing the coded and original images. The following images also reflect the same conditions.

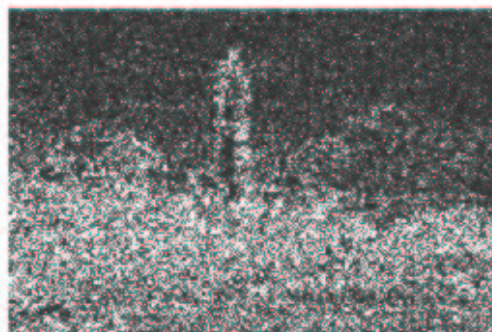**Figure 8.24 (a)**

Figure 8.24 (b)
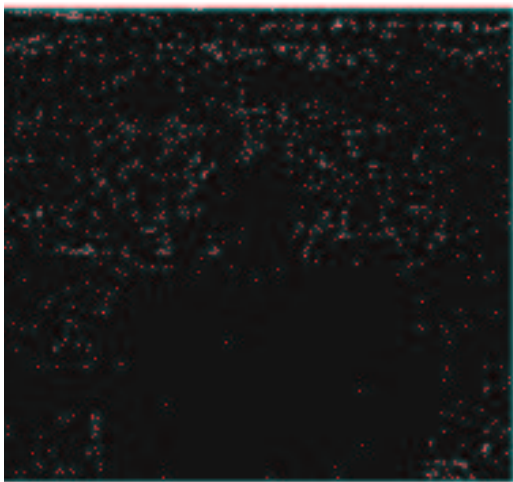
Figure 8.24 (c)
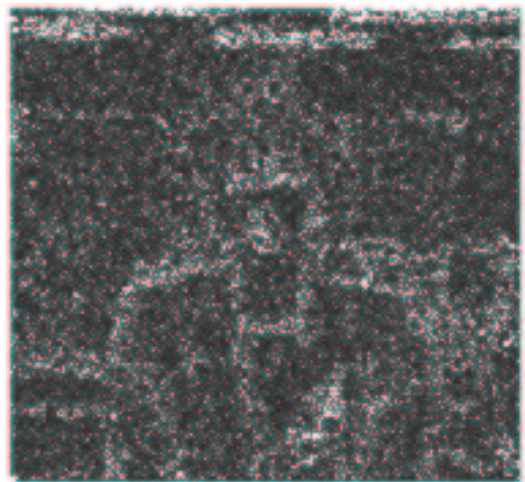
Figure 8.24 (d)

Figure 8.24 Image "Announcer"

(a) Original (b) Coded (c) PDM (d) Square Error

Figure 8.24 shows the result for the image "Announcer" image. "Announcer" is chosen for testing in the system for its visual property of reflecting the common media of "news", having a human subject as the main visual attractor. MSE for this result is found to be 8.32 while the PQR is 3.48.

Figure 8.25 (a)

Figure 8.25 (b)
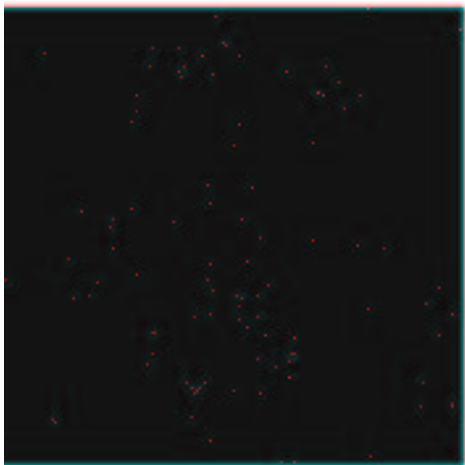
Figure 8.25 (c)
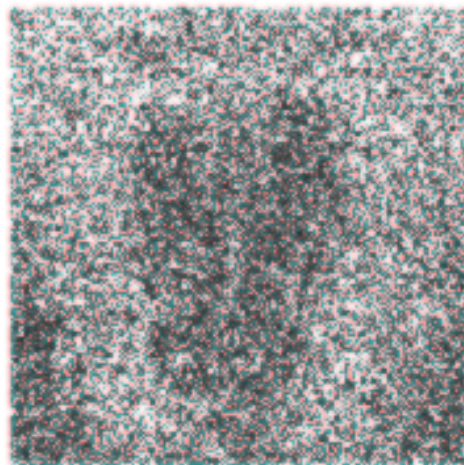
Figure 8.25 (d)

Figure 8.25 Image "Baboon"

(a) Original (b) Coded (c) PDM (d) Square Error

Figure 8.25 shows the result for the image "Baboon". Image "Baboon" is chosen for its visual property of having both a uniform texture (nose) as well as non-texture (fur) surface in the same image. Note that the PDM reflects the error in the nose error but has less error within the fur area, which is consistent with the design. MSE for this result is found to be 42.65 while the PQR is 3.89. Note that the MSE is much higher than the corresponding value in "announcer", but both results have the same PQR value. This confirms the expected condition that MSE does not directly correspond to the PQR value.

Figure 8.26 (a)

Figure 8.26 (b)
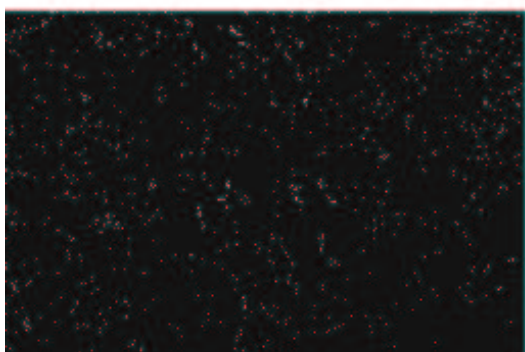
Figure 8.26 (c)
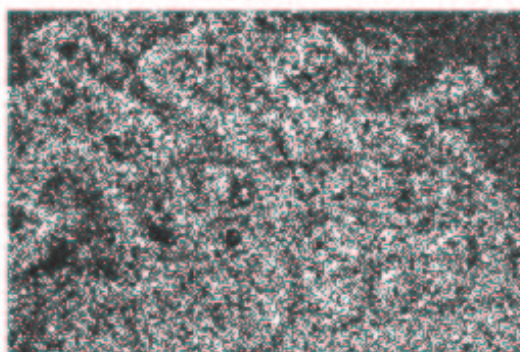
Figure 8.26 (d)

Figure 8.26 Image "Bike"
(a) Original (b) Coded (c) PDM (d) Square Error

Figure 8.26 shows the result for the image "Bike". Image "Bike" is chosen for testing in the system for its visual property for having multiple mechanical objects. MSE for this result is found to be 26.29 while the PQR is 3.58.

Figure 8.27 (a)

Figure 8.27 (b)

Figure 8.27 (c)

Figure 8.27 Image "Light House"

Figure 8.27 (d)

(a) Original (b) Coded (c) PDM (d) Square Error

Figure 8.27 shows the result for the image "Light House". Image "Light House" is chosen for its visual property of having both several small and one large visual object. MSE for this result is found to be 20.45 while the PQR is 3.75.
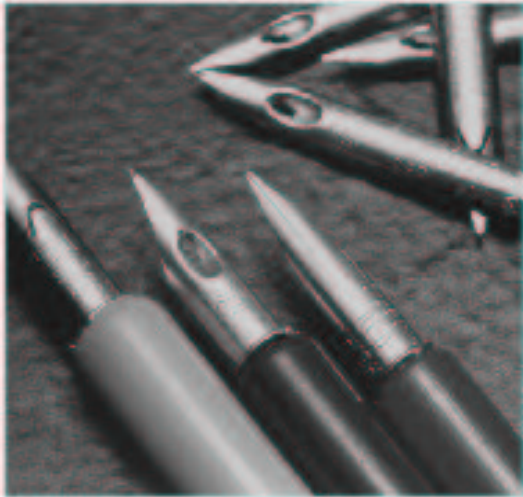

Figure 8.28 (a)	**Figure 8.28 (b)**
Figure 8.28 (c)	**Figure 8.28 (d)**
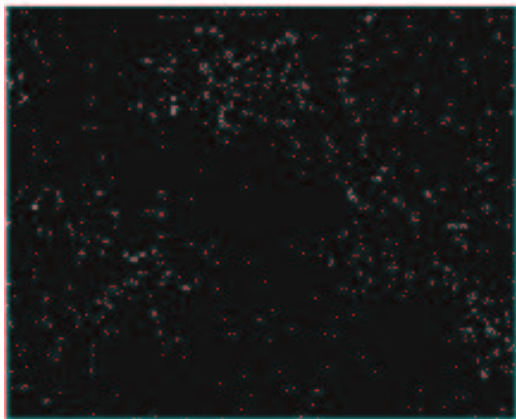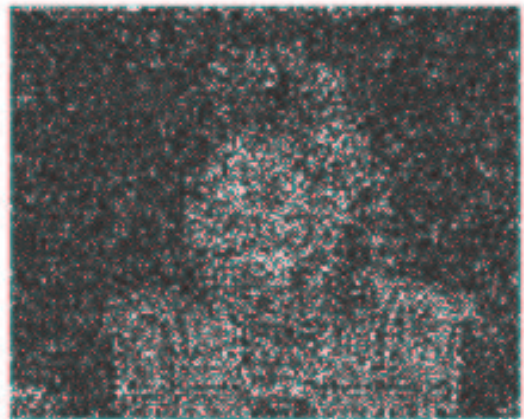
Figure 8.28 Image "Miss America"
(a) Original (b) Coded (c) PDM (d) Square Error

Figure 8.28 shows the result for the image "Miss America". Image "Miss America" is chosen for its visual property of having a human subject as the main visual object while having a uniform background. MSE for this result is found to be 7.75 while the PQR is 3.53.

Figure 8.29 shows the result for the image "Pens". Image "Pen" is chosen for its visual property of having several irregular shaped visual objects. MSE for this result is found to be 7.49 while the PQR is 3.56.

Figure 8.29 (a)

Figure 8.29 (b)
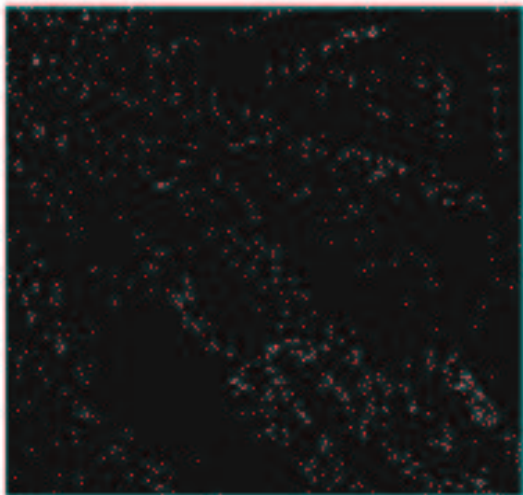
Figure 8.29 (c)
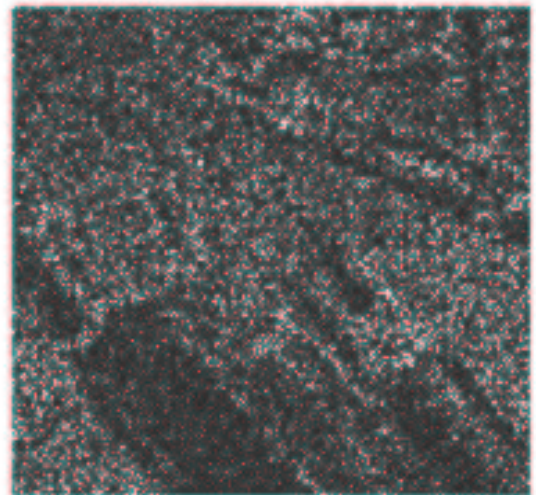
Figure 8.29 (d)

Figure 8.29 Image "Pens"

(a) Original (b) Coded (c) PDM (d) Square Error

The sets of result shown reflect closely the HVS-based fidelity system's design, with results corresponding closely with spatial frequency rather than physical error. This module is shown to be working and producing results within expectations. Note that in all results, the modules use HVS properties to break down available errors and emphasize those that are especially attractive to human vision, particularly where contrast differs beyond the detection threshold. The working module quantifies HVS correlative error on the areas of an image, allowing the image quality metric to form an image error fidelity map. The other portion of the image quality metric is the IM module, which is examined in the next section.

8.3 Image Quality Metric: Importance Map Test Bed Module System Testing

This section presents the importance map results for the same set of images as in the previous section. Note that 7 images are presented for each set of results including the original. The others are background/foreground (border) importance; centre importance; contrast importance, shape importance, size importance and the final importance map. Note that lighter/brighter areas imply higher importance.
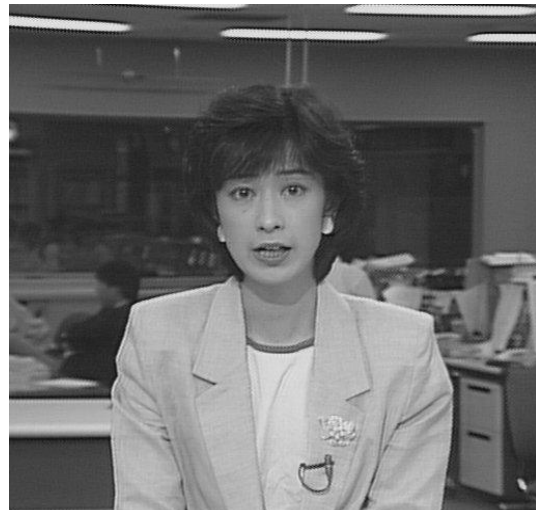

Figure 8.30 (a) "Airplane"

Figure 8.30 (b) "Announcer"
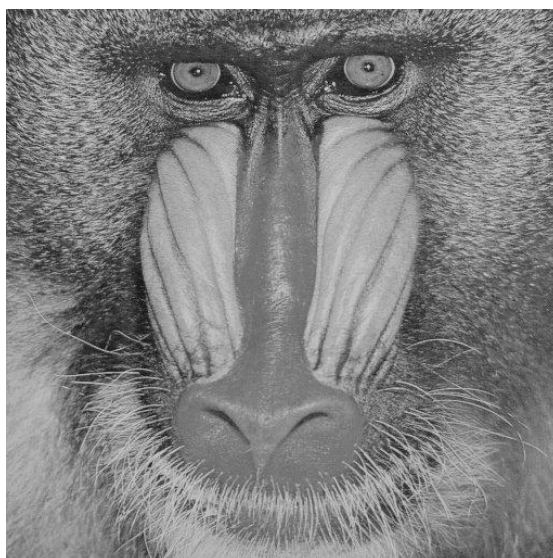
Figure 8.30 (c) "Baboon"

Figure 8.30 Original Images Part I

Figure 8.31 (a) "Bike"

Figure 8.31 (b) "Light House"

Figure 8.31 (c) "Miss America"   **Figure 8.31 (d) "Pens"**

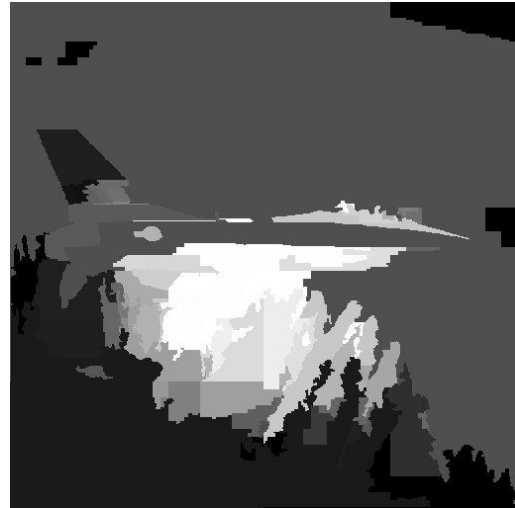**Figure 8.31 Original Images Part II**

Figure 8.32 (a)

Figure 8.32 (b)
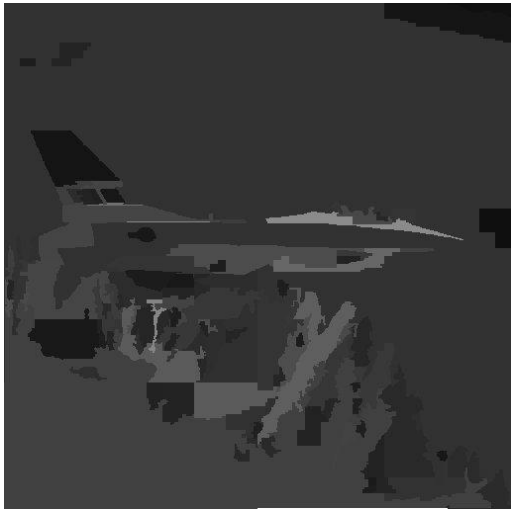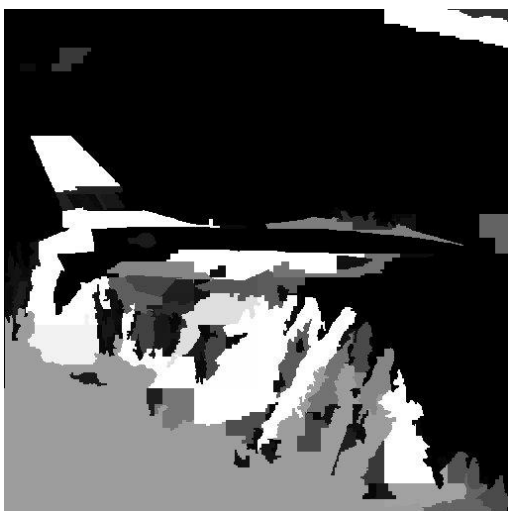

Figure 8.32 (c)

Figure 8.32 (d)

Figure 8.32 (e)

Figure 8.32 (f)

Figure 8.32 Image "Airplane"

(a) Border (b) Centre (c) Contrast (d) Shape (e) Size (f) Summation IM

Figure 8.33 (a)

Figure 8.33 (b)

Figure 8.33 (c)

Figure 8.33 (d)

Figure 8.33 (e)

Figure 8.33 (f)

Figure 8.33 Image "Announcer"

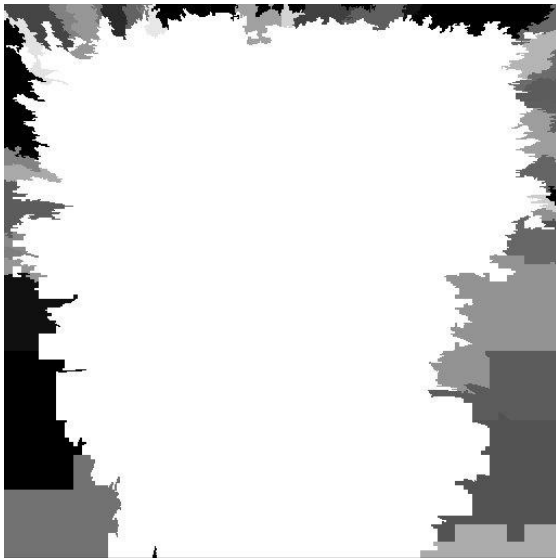**(a) Border (b) Centre (c) Contrast (d) Shape (e) Size (f) Importance Map**

Figure 8.34 (a)

Figure 8.34 (b)

Figure 8.34 (c)

Figure 8.34 (d)

Figure 8.34 (e)

Figure 8.34 (f)

Figure 8.34 Image "Baboon"

(a) Border (b) Centre (c) Contrast (d) Shape (e) Size (f) Summation IM

<div align="center">

Figure 8.35 (a)   **Figure 8.35 (b)**

</div>

<div align="center">
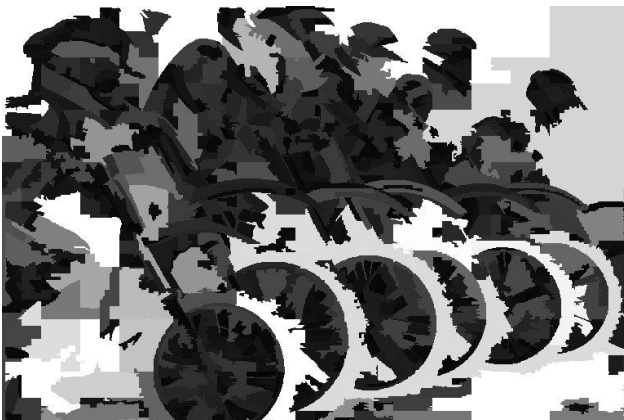
Figure 8.35 (c)   **Figure 8.35 (d)**

</div>

<div align="center">

Figure 8.35 (e)   **Figure 8.35 (f)**

Figure 8.35 Image "Bike"

(a) Border (b) Centre (c) Contrast (d) Shape (e) Size (f) Importance Map

</div>

<div align="center">**Figure 8.36 (a)**</div>

<div align="right">**Figure 8.36 (b)**</div>

<div align="center">**Figure 8.36 (c)**</div>

<div align="right">**Figure 8.36 (d)**</div>

<div align="center">**Figure 8.36 (e)**</div>
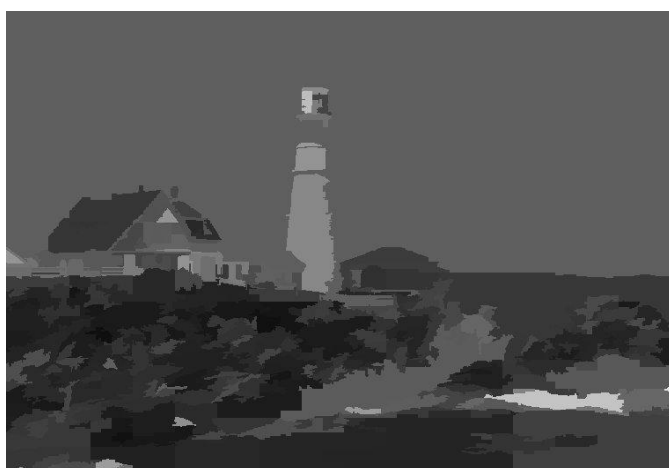
<div align="right">**Figure 8.36 (f)**</div>

<div align="center">**Figure 8.36 Image "Light House"**</div>

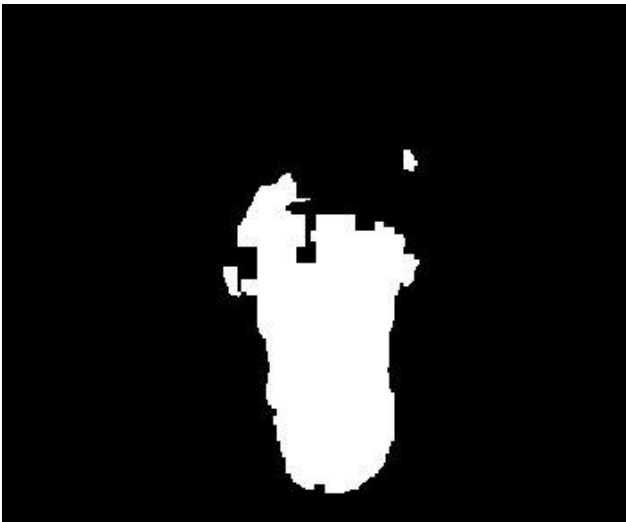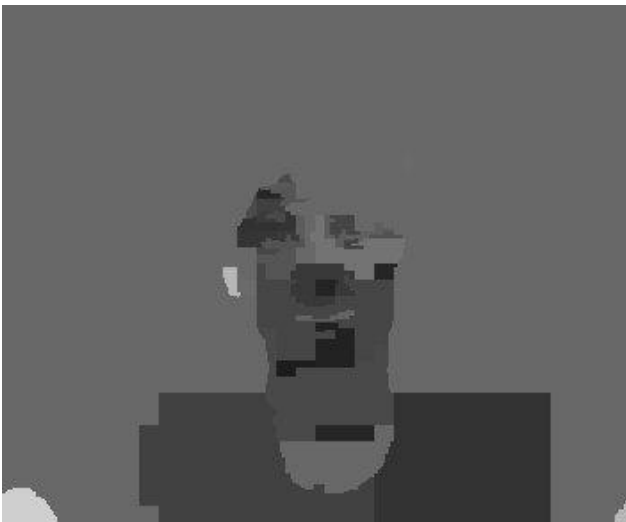<div align="center">**(a) Border (b) Centre (c) Contrast (d) Shape (e) Size (f) Summation IM**</div>
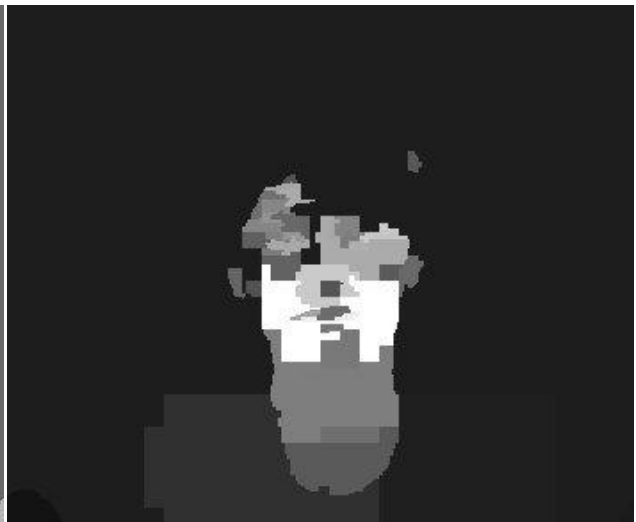
Figure 8.37 (a)

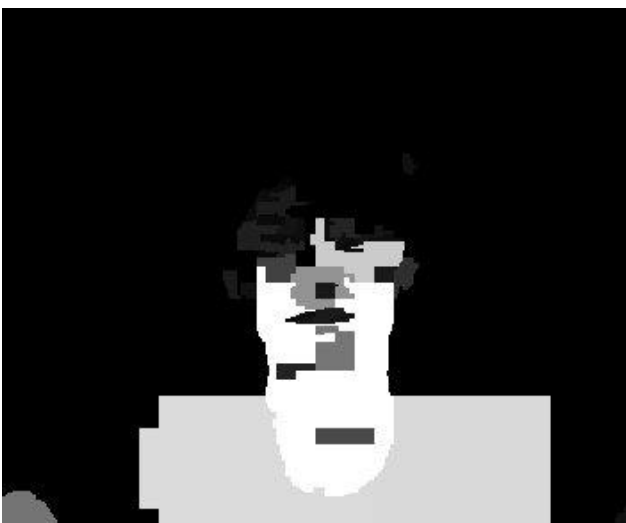**Figure 8.37 (b)**

Figure 8.37 (c)

Figure 8.37 (d)

Figure 8.37 (e)

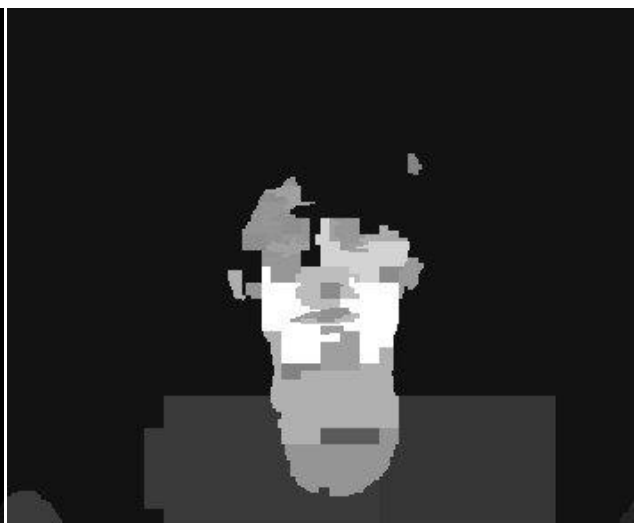**Figure 8.37 (f)**

Figure 8.37 Image "Miss America"
(a) Border (b) Centre (c) Contrast (d) Shape (e) Size (f) Summation IM
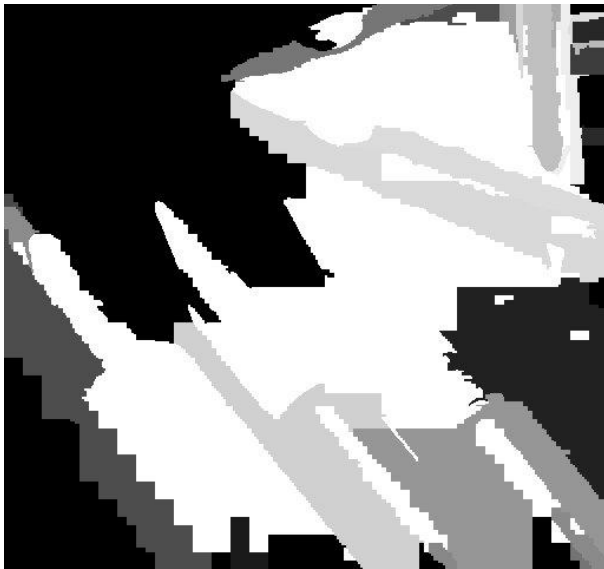
Figure 8.38 (a)

Figure 8.38 (b)

Figure 8.38 (c)

Figure 8.38 (d)

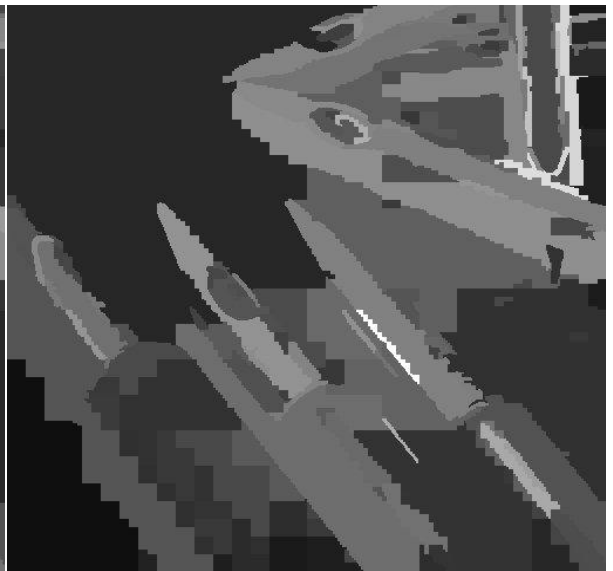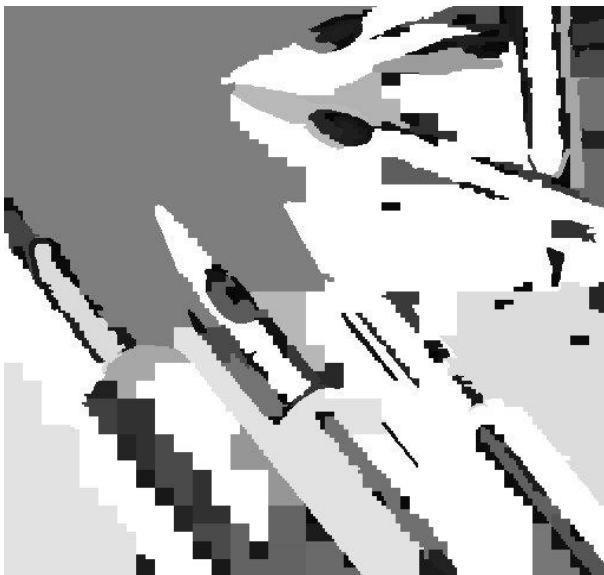**Figure 8.38 (e)**

Figure 8.38 (f)

Figure 8.38 Image "Pens"
(a) Original (b) Border (c) Centre (d) Contrast (e) Shape (f) Size (g) Importance Map

This ends the section on the individual testing system of the importance map. As shown, the system is working and the result is consistent with system design. Individual results are in direct correspondence to the importance factors of border, centre, contrast, shape and size as tested by visual inspection. All importance maps correspond reasonably well with theories outlined in Chapter 4.

Special note is taken here with the IM for contrast and shape factors, where its correspondence to the stated factors is not as clearly visible as the other 3 factors. Note from the contrast IM that the spread of the importance representation is relatively low, as the majority of the image is in dark gray scale. Note that contrast is an important calculation, for a region is based on the difference in average contrast of a region to its neighboring region, then this is relatively scaled to form the IM. Hence, in each contrast of the IMs shown, the lightest color patch represents the region with the highest contrast importance, and this is followed through to the darkest color which represents the lowest relative importance. The contrast IMs have relatively lower importance distributions, this phenomenon is caused by the few high contrast areas with values that are higher than the rest. This explanation is also applicable to shape importance, where the majority of an image region's shape importance rating is lower than average as brought down by the region with a high peak importance.

Illustrated here is a diversity of image importance maps, where different factors in different images construct a range of very different IMs. The influencing factors are illustrated individually with summation into the final IM for usage in the final system. This module has shown efficient properties of identifying and ranking areas of visual importance, giving identification of different rate of importance attraction across an image. This will combine with the HVS fidelity module in the next chapter to form a unison image quality metric.

This ends the chapter on individual system testing. Both modules are working within design specifications, as shown by the results. Furthermore, the testing of individual modules has now finished and each of the modules are in working order. The next Chapter enforces verification testing of the overall system, together with visual media quality analysis over the 3G radio interface.

Chapter 9. Integrated system testing

This section aims to test the overall system. The system is divided into two sections, with the system result section illustrating six sets of overall results for the entire test bed, and the second section listing the result summary for various system results to provide analysis. As with before, PGM file format is used.

9.1 System Result

Five images are presented per set of results in section 9.1, which is original; Received image from UTRA/3G test bed; the IM of the original image; the PDM and the IPDM of the received image. All images are subjected to Vehicular A environment parameter with 2 varying speeds of 20 and 50 km/h. Figures 9.1 to 9.7 illustrate the results.
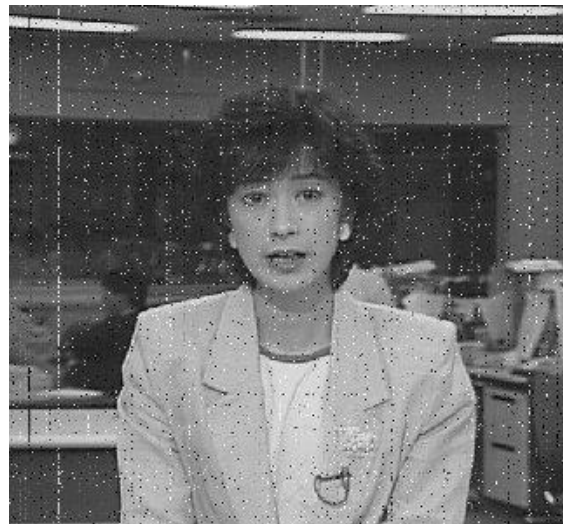

Figure 9.1 (a)

Figure 9.1 (b)

Figure 9.1 (c)
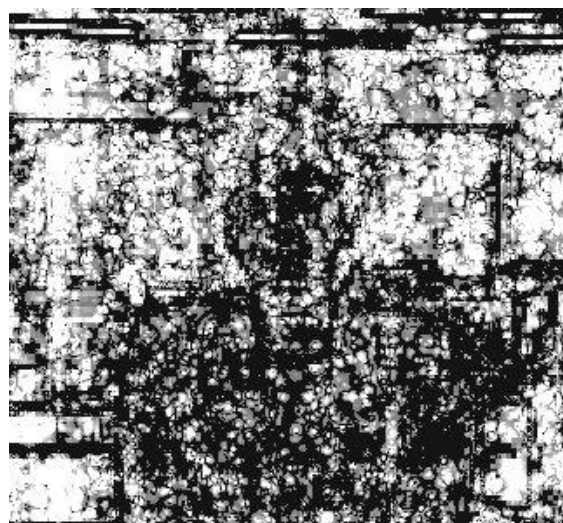
Figure 9.1 (d)
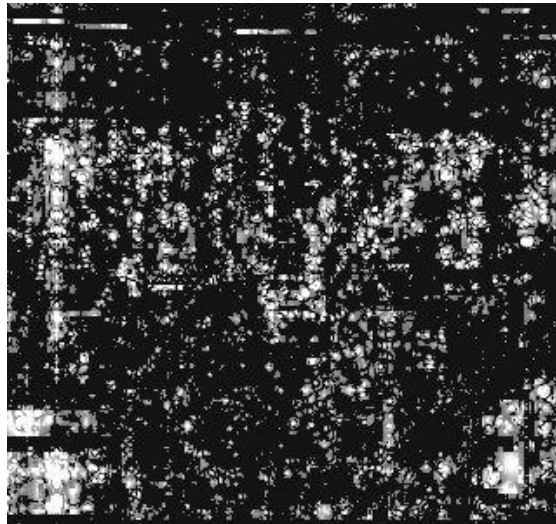
Figure 9.1 (e)
Figure 9.1 Image "Announcer"
(a) Original (b) Received (c) Importance Map (d) PDM (e) IPDM

Figure 9.1 illustrates the image "Announcer" which has been analyzed before in this thesis. This time, the image is subjected to a 50 km/h physical channel. The overall system is used to process the original, producing the received image, which is then analyzed to produce the PDM and IPDM. Note that corresponding to the IM, PDM error spread is significantly reduced to produce IPDM. IPQR is then produced and is presented in the next section. The following results follow the same presentation format.
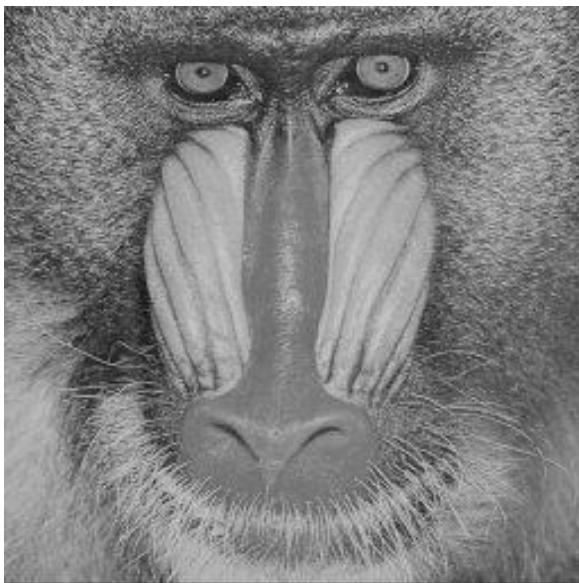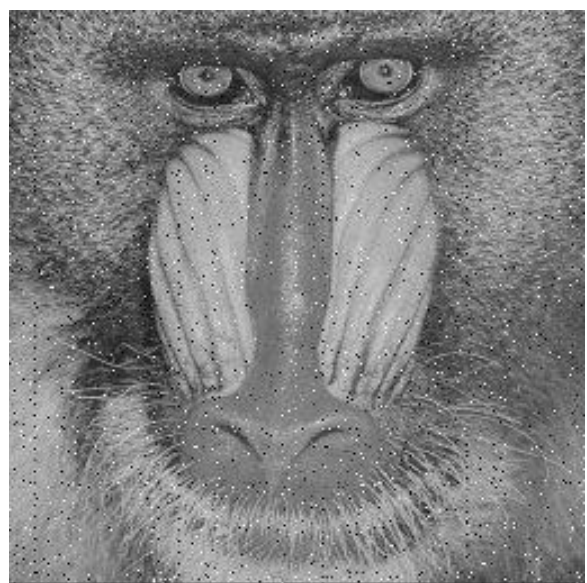
Figure 9.2 (a)   **Figure 9.2 (b)**

Figure 9.2 (c)

Figure 9.2 (d)

Figure 9.2 (e)

Figure 9.2 Image "Baboon"

(a) Original (b) Received (c) Importance Map (d) PDM (e) IPDM

Figure 9.2 presents the result for the image "Baboon", which is subjected to the physical channel of 20 km/h.

Figure 9. 3 (a)

Figure 9. 3 (b)
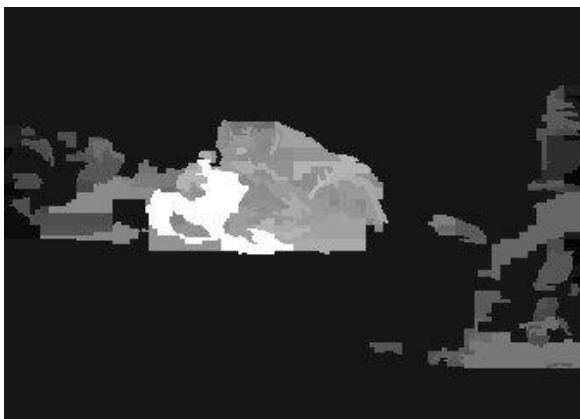
Figure 9. 3 (c)
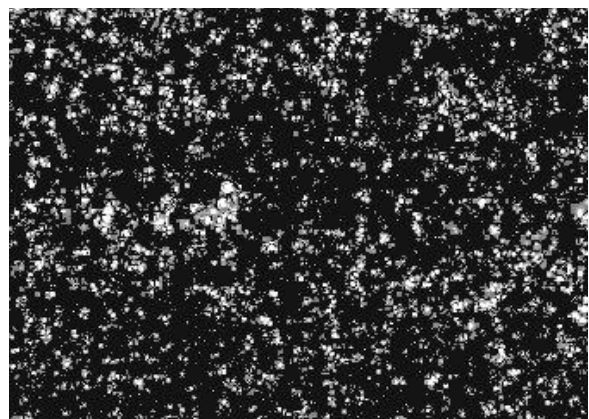
Figure 9. 3 (d)

Figure 9. 3 (e)

Figure 9.3 Image "Football"

(a) Original (b) Received (c) Importance Map (d) PDM (e) IPDM

Figure 9.3 presents the result for image "Football", which is subjected to channel velocity of 20km/h. It is chosen as test image as it represents the media service format "sports". Furthermore this image is a segment from a MPEG sequence, so the temporal factors produce the "blurring" effect that can be used to test the system further. The system appears to handle this factor in the proper manner.

Figure 9. 4 (a)

Figure 9. 4 (b)

Figure 9. 4 (c)
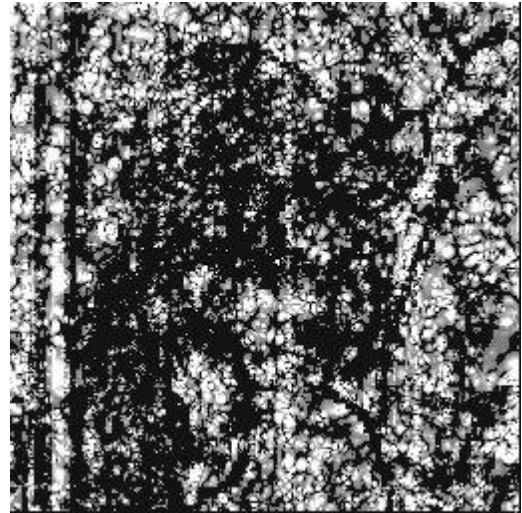
Figure 9. 4 (d)

Figure 9. 4 (e)

Figure 9.4 Image "Lena"

(a) Original (b) Received (c) Importance Map (d) PDM (e) IPDM

Figure 9.4 presents the result for image "Lena", subject to a physical channel of 50 km/h. The image is chosen as a test image as it gives a close up shot of a human subject, exposing the smooth texture and irregular surface of the human face. The test bed appears to handle it in accordance to system design.
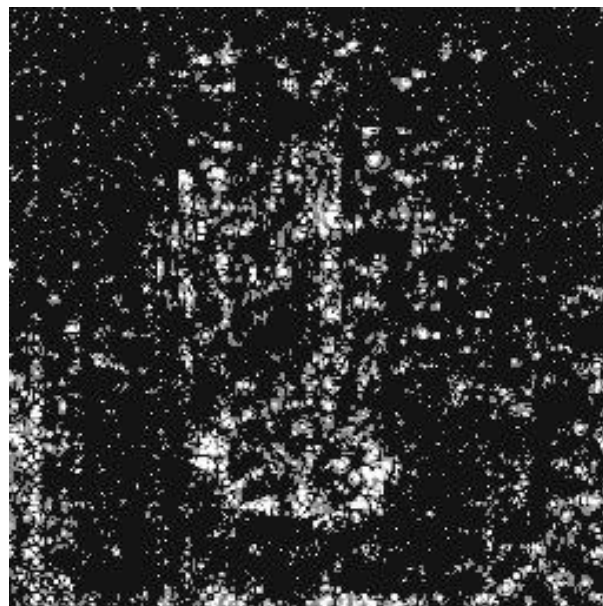

Figure 9.5 (a)

Figure 9.5 (b)

Figure 9.5 (c)
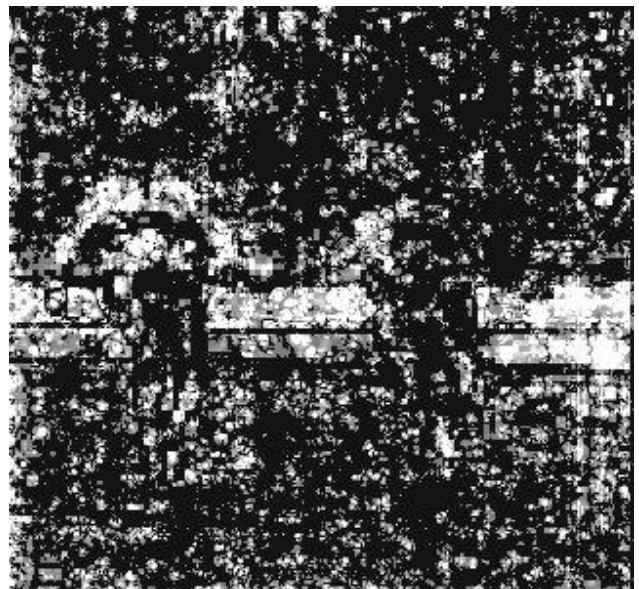
Figure 9.5 (d)
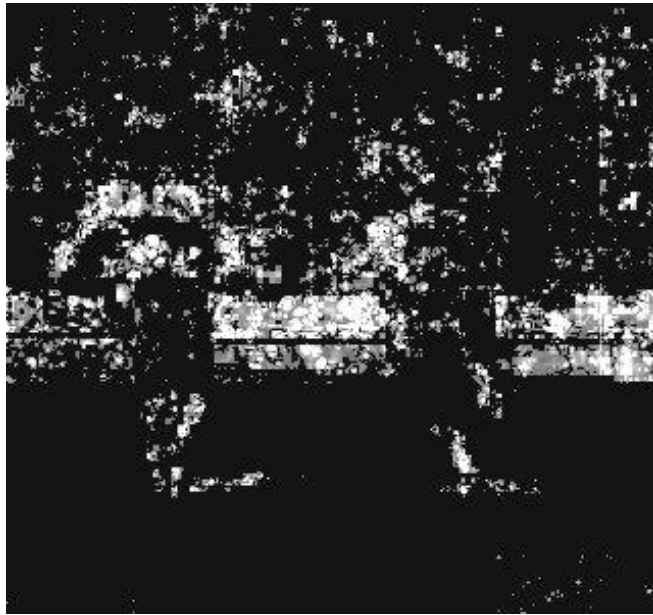
Figure 9.5 (e)

Figure 9.5 Image "Soccer"

(a) Original (b) Received (c) Importance Map (d) PDM (e) IPDM

Image "soccer" is selected as it presents two human subjects and a highly complex background. Illustrated in Figure 9.5, it is subjected to a 50 km/h physical channel.

Following are two images of "Bike" and "Light House". "Bike" is selected as it presents multiple mechanical objects while "Light House" represents a clear landscape of a building and a natural scene. Illustrated in Figure 9.6 and 9.7, it is subjected to a 50 km/h and 20 km/h physical channel respectively.

Figure 9.6 (a)   **Figure 9.6 (b)**

**Figure 9.6 (c)**   **Figure 9.6 (d)**

Figure 9.6 (e)

Figure 9.6 Image "Bike"

(a) Original (b) Received (c) Importance Map (d) PDM (e) IPDM

Figure 9.7 (a)   **Figure 9.7 (b)**
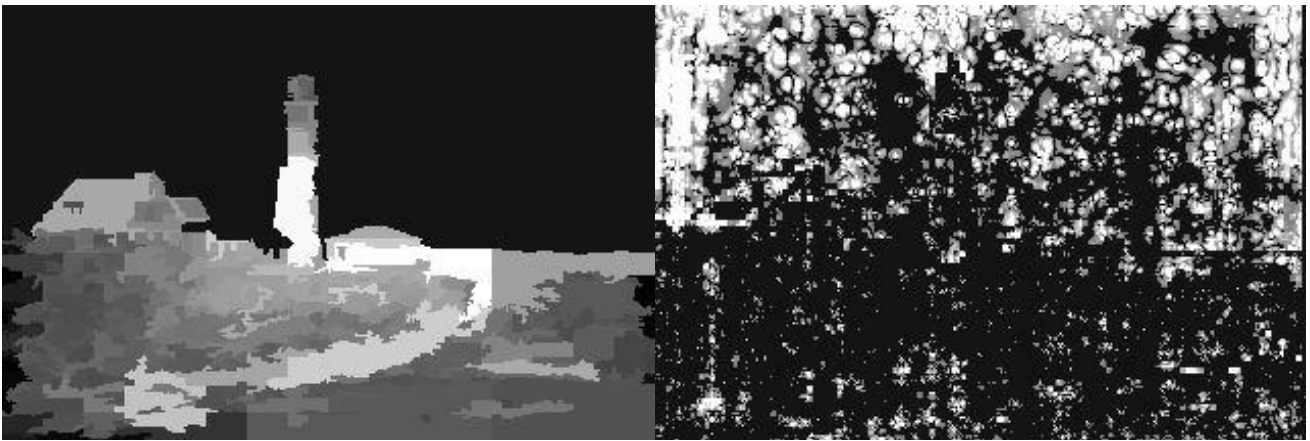
Figure 9.7 (c)   **Figure 9.7 (d)**
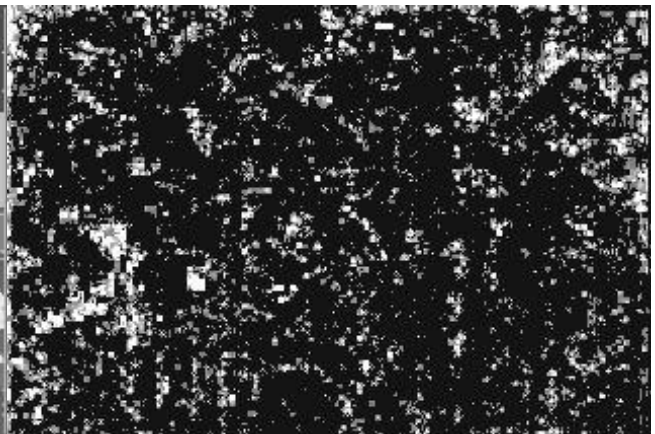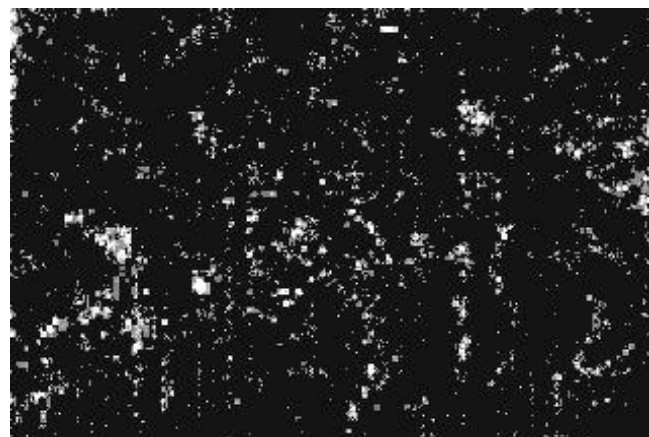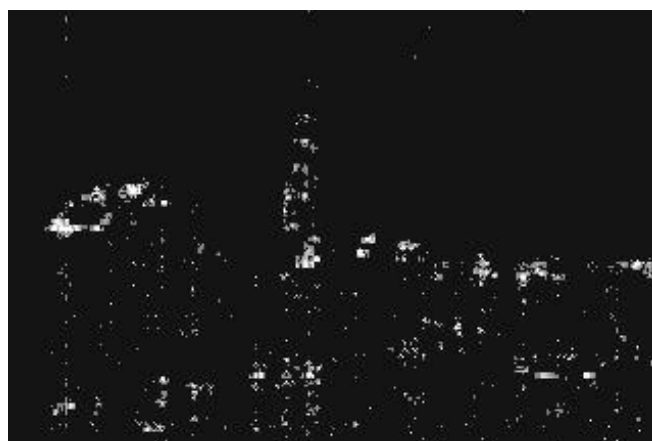

Figure 9.7 (e)

Figure 9.7 Image "Light House"

(a) Original (b) Received (c) Importance Map (d) PDM (e) IPDM

The PDM here is produced from the HVS fidelity module while the IM is from the IM module. As shown, combination of both to form a seamless image quality metric, where HVS perceptible fidelity error is subject to importance scaling to produce the IPDM. This gives a more accurate plot of the error as HVS perceptible fidelity is not area discriminatory, while different areas of images may give rise to a very different attention, thus a different rate of importance. Note from all results that the IPDM is significantly different from the PDM, which explains that the enforcement of IM is in order. By fusing both modules into the final system, an efficient error map can be generated, producing better quantification of HVS perceptible error in received images. The results further show that the overall system integrated seamlessly with individual areas and the salt and pepper noise presented by the 3G/UTRA module is within detectable capability of the HVS image quality metric. The system is tested to be seamless and in working order. The next section will analyze various results in IPQR.

9.2 System Result Summary

This section summarizes the system test results from section 9.1 and also the final system results from section 8.1. The result from section 8.1 is further processed to produce the overall system result. Table 9.1 illustrates the result details from section 9.1 where IPDM is summed to produce IPQR. Note that all Environment parameters here are all set to vehicular A.

	"Announcer"	"Baboon"	"Football"	"Lena"	"Soccer"	"Bike"	"Light House"
Vehicular velocity	50 km/h	20 km/h	20km/h	50km/h	50 km/h	50km/h	20km/h
Mean Square Error (MSE)	312.58	260.83	267.97	336.56	315.82	315.77	265.06
Perceptual Signal-to-Noise Ratio (PSNR)	23.18 dB	24.00 dB	23.85 dB	22.86 dB	23.14 dB	23.14 dB	23.90
PQR (1-5)	1.16	2.30	2.09	1.70	1.61	1.86	1.69
IPQR (1-5)	2.24	2.69	3.09	2.39	1.93	2.44	2.97

Table 9.1 System Result Summary

The MSE range is consistent with the velocity of the physical channel that the images are subjected to. Alternately the PQR value also reflects this, although there is a notable difference between the PQR values of images within the same velocity range, even if the MSE and PSNR values are relatively similar. This phenomenon is expected as the HVS-based perceptual differences takes in error differently in accordance to image properties. IM enhanced PQR processed into IPQR reflects the designated property of refining perceptual damages in accordance to image area importance. This is clearly shown by comparing PQR with IPQR and PDM with IPDM from the listed results. Overall, the results show that the test bed is working and the result is consistent with intended outcomes.

Tables 9.2 and 9.3 show the IPQR (total system output) of the testing done in section 8.1 for image "Announcer" and Table 9.4 and 9.5 for image "Football" to further illustrate the workings of the total test bed system. These results are visualized in Figures 9.7 and 9.8 respectively. As expected, the change in IPQR values corresponds with the pattern with PQR values shown in section 8.1, with increasing velocity resulting in higher quality loses.

Image "Announcer" IPQR Values

	Indoor A	Indoor B	Pedestrian A	Pedestrian B	Vehicular A	Vehicular B
0 km/h	3.90	2.46	**X**	**X**	**X**	**X**
0.5 km/h	4.32	3.78	**X**	**X**	**X**	**X**
1 km/h	4.33	3.82	**X**	**X**	**X**	**X**
1.5 km/h	4.38	3.81	4.42	2.21	**X**	**X**
3 km/h	**X**	**X**	4.43	2.21	**X**	**X**
10 km/h	**X**	**X**	3.29	2.19	**X**	**X**
20 km/h	**X**	**X**	3.03	2.16	2.33	2.63
40 km/h	**X**	**X**	**X**	**X**	2.30	2.57
60 km/h	**X**	**X**	**X**	**X**	2.23	2.46
80 km/h	**X**	**X**	**X**	**X**	2.17	2.41
100 km/h	**X**	**X**	**X**	**X**	2.13	2.30

Table 9.2 Image "Announcer" Varying Environment Parameter and Velocity System Result Summary

Arriving Angle	3 km/h pedestrian A (IPQR)
"75.0 45.0 15.0 –15.0 –45.0 –75.0"	4.43
"75.0 30.0 15.0 –15.0 –30.0 –75.0	4.43
"60.0 30.0 15.0 –15.0 –30.0 –60.0	4.43
"50.0, 30.0, 10.0, -10.0, -30.0, -50.0"	4.43
"80.0, 40.0, 20.0, -20.0, -40.0, -80.0"	4.43

Table 9.3 "Announcer" Arriving Angle System Result Summary
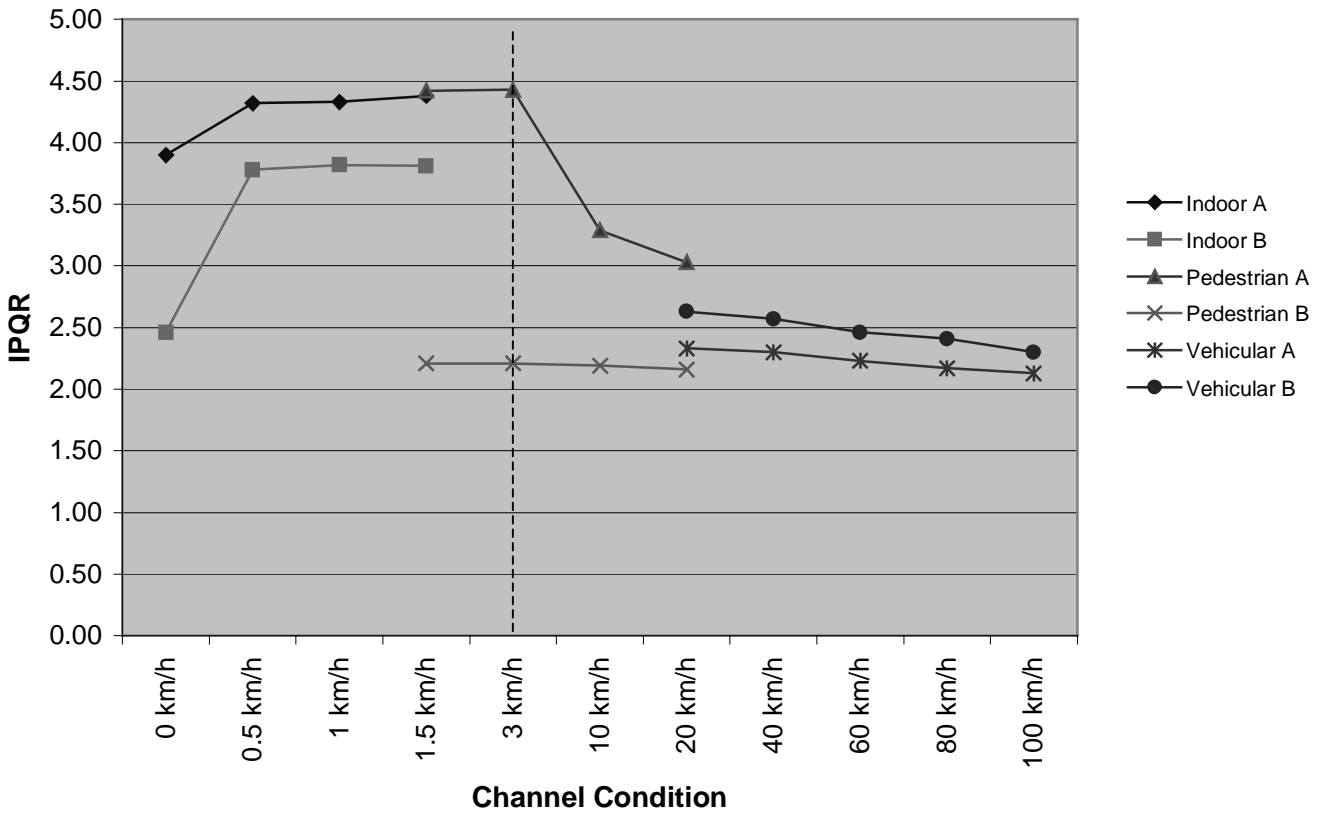
Figure 9.8 Image "Announcer" IPQR Result Plot

Image "Football" IPQR Values

	Indoor A	Indoor B	Pedestrian A	Pedestrian B	Vehicular A	Vehicular B
0 km/h	4.27	2.74	**X**	**X**	**X**	**X**
0.5 km/h	4.78	4.53	**X**	**X**	**X**	**X**
1 km/h	4.79	4.53	**X**	**X**	**X**	**X**
1.5 km/h	4.78	4.53	4.79	2.67	**X**	**X**
3 km/h	**X**	**X**	4.80	2.68	**X**	**X**
10 km/h	**X**	**X**	3.36	2.66	**X**	**X**
20 km/h	**X**	**X**	3.55	2.62	3.09	3.29
40 km/h	**X**	**X**	**X**	**X**	2.84	3.18
60 km/h	**X**	**X**	**X**	**X**	2.75	3.01
80 km/h	**X**	**X**	**X**	**X**	2.78	2.88
100 km/h	**X**	**X**	**X**	**X**	2.47	2.86

Table 9.4 Image "Football" Varying Environment Parameter and

Velocity System Result Summary

Arriving Angle	3 km/h pedestrian A (IPQR)
"75.0 45.0 15.0 –15.0 –45.0 –75.0"	4.80
"75.0 30.0 15.0 –15.0 –30.0 –75.0	4.80
"60.0 30.0 15.0 –15.0 –30.0 –60.0	4.80
"50.0, 30.0, 10.0, -10.0, -30.0, -50.0"	4.80
"80.0, 40.0, 20.0, -20.0, -40.0, -80.0"	4.80

Table 9.5 "Football" Arriving Angle System Result Summary

Image "Football" IPQR
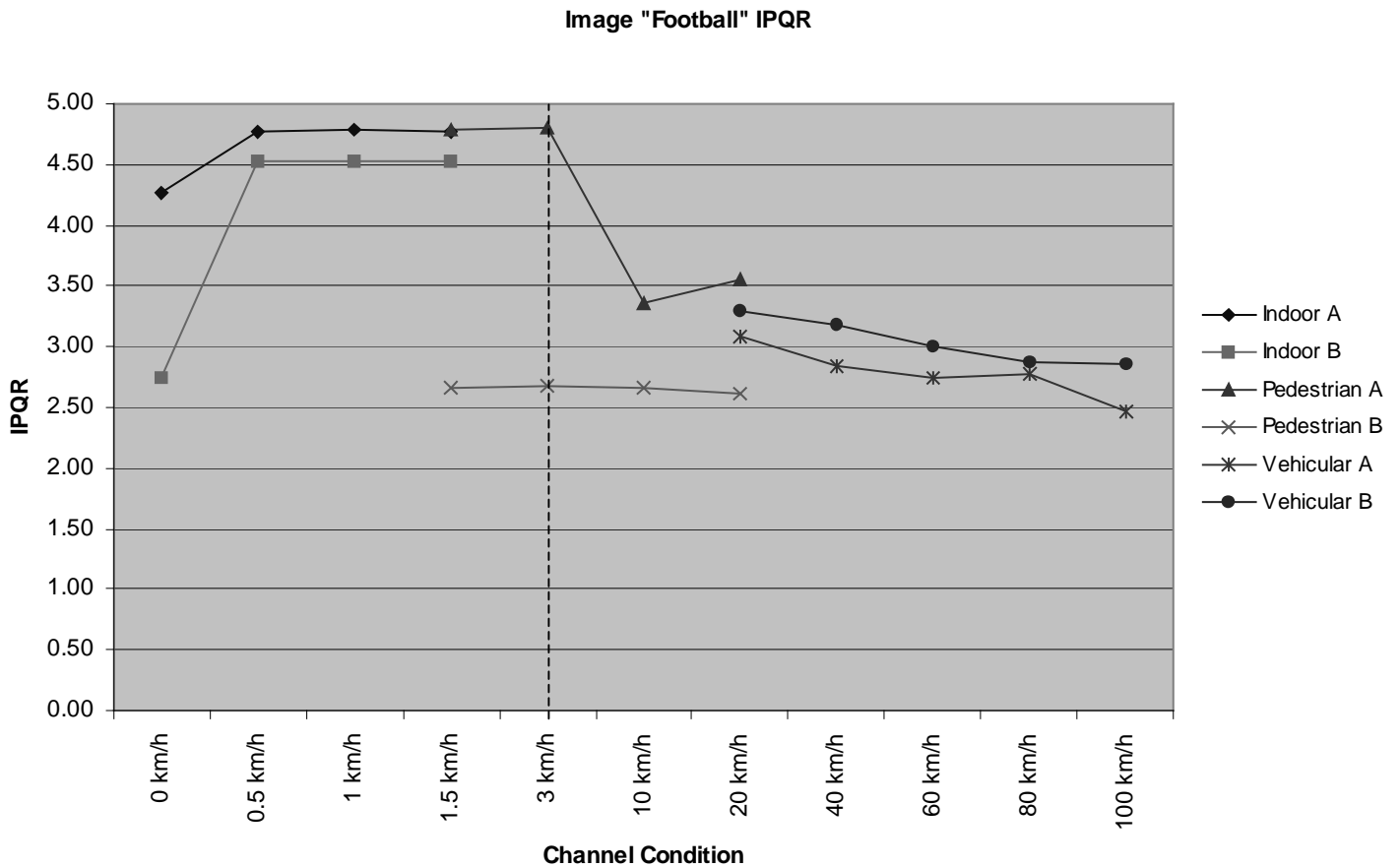
Figure 9.9 Image "Football" IPQR Result Plot

Note from Tables 9.3 and 9.5 that the IPQR reflects the pattern exhibited for the results in the PSNR domain, as with Tables 9.2 and 9.4. Visualization using Figures 9.8 and 9.9 shows a similar tracing pattern of the plots illustrated in Figures 8.19 and 8.20. Minimal pattern differences can be spotted for the results in Indoor mode. The difference starts to emerge in Pedestrian mode results of Figure 9.9. Comparing Figure 9.9's Pedestrian A index graph pattern to that of Figure 8.20, one sees that the drop in image PSNR did not result in a lower IPQR by default. This becomes more apparent in Vehicular mode results in both Figures 9.8 and 9.9, where the smooth drop in PSNR did not dictate a similar decrease in IPQR. The definition of IPQR implies that distortion in different areas of images amounts to a different quality degradation rating, thus explaining this phenomenon. The results have clearly shown that the system applies controlled but dynamic and randomized distortion upon an input multimedia data stream while providing an ergonomic quality rating.

The rating weights induced error is dependent on the area of image being distorted instead of purely measuring the physical error. Although patterns between the two graphs can be visually observed, the IPQR values between the two sets of results are quite different. This is because both test images have a very different Importance Map and also different HVS fidelity errors, which derive a very different IPQR although the average difference of their physical errors is relatively small. The following presents results across different images subjected to 3 different velocities as in IPQR, continuing the results in Table 8.1 and Figure 8.7.

Image	Velocity	IPQR
"Baboon"	20 km/h	2.69
	50 km/h	2.63
	80 km/h	2.57
"Bike"	20km/h	2.60
	50 km/h	2.44
	80 km/h	2.39
"Football"	20 km/h	2.96
	50 km/h	2.73
	80 km/h	2.78
"Lena"	20 km/h	2.53
	50 km/h	2.39
	80 km/h	2.36
"Light House"	20 km/h	2.98
	50 km/h	2.87
	80 km/h	2.82
"Soccer"	20 km/h	1.96
	50 km/h	1.93
	80 km/h	1.83

Table 9.6 Multiple images with Varying Velocity System Result Summary
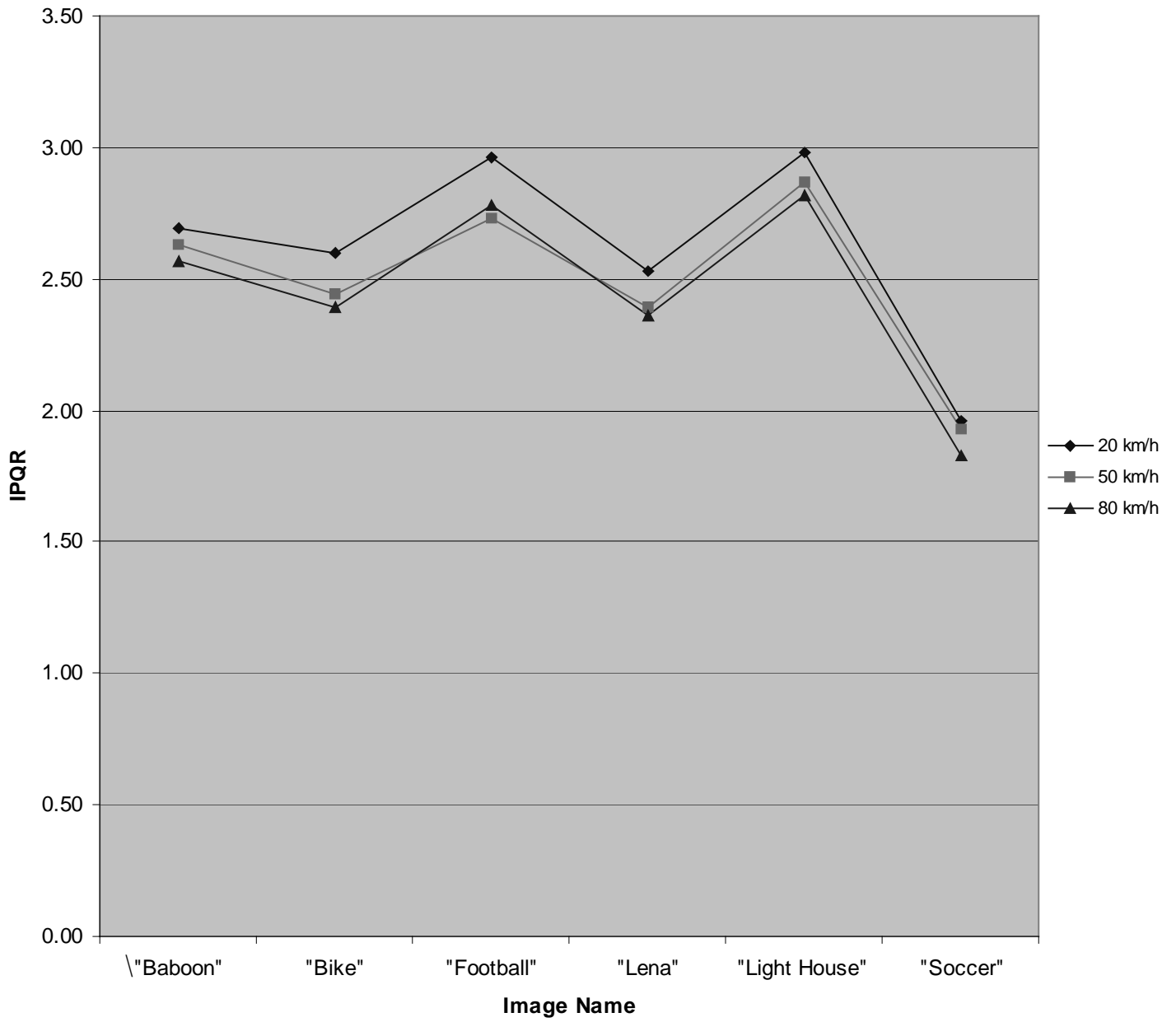
Image IPQR

Figure 9.10 Multiple images with Varying Velocity System Result Summary Plot

Figure 9.10 shows results of six images in terms of IPQR, further extending those presented in Figure 8.7 where results are presented in MSE. Note that the smooth pattern as presented in Figure 8.7 is not reflected in Figure 9.10. In the distinct case of the image "Football", the image subjected to 50 km/h attracts higher damage than 80 km/h while MSE results show otherwise. In the case of image "Soccer", the quality gets a much lower rating overall in IPQR, where the MSE results shows near uniform pattern with the rest of the images. Across the different images, IPQR diversifies greatly although most results have higher velocities reflecting lower IPQR. This contradicts the much smoother pattern appearing in Figure 8.7. Note also that IPQR is in linear scale while PSNR is in logarithmic scale. That is why only relative visual reference is used. This further illustrates the earlier analysis by which the system effectively rates the distortion of the images using HVS properties.

IPQR takes IPDM and summarizes the error map into a single number ranged from 1.0 to 5.0 for ease of reference. Close comparison of Figure 8.7 and Figure 9.10 shows that a image of the same error rate produces a significantly different pattern of quality quantification. This shows the unique properties of the HVS image quality metric, where physical image errors are translated into the HVS domain, then further applied onto a visual attention model. Across the images subjected to the same velocity and having very similar PSNR, diverse IPQR has been produced due to the impact area of the errors on the images. This is very obverse in image "Lena" and "Football", where one has very close IPQR between images with very different PSNR while the other has a higher IPQR where lower PSNR is presented. From this phenomenon produced by the system, images subjected to the same channel data error can show significantly different human perceptual qualities. Now, one can see that this system produces a different yet efficient image quality testing and measurements that have impact on content-based multimedia delivery.

This ends the section on system result summary and also on system testing. In summary, the total system has integrated the individual system with minimal problems and has demonstrated its proper workings. All illustrated, behavior is within expectations in accordance to the design prospect, and the test bed methodology has been accurately implemented. The next chapter continues the discussion on the presented results and brings conclusion to the entire work.

Chapter 10. Discussion and Conclusion

In the preceding chapters, this thesis has presented an implementation of a 3G software test bed with the capability to analyze quality degradation of images in multimedia data transmitted over the 3G radio/wireless interface. This test bed consists of two major modules, the UTRA/3G test bed module and the HVS-based image quality metric. The UTRA/3G test bed module emulates the operation of processing UMTS transport layer channel DCH into a physical signal and subjects it to a 3G physical channel model followed by receiving and reverse processing to produce the received DCH on the receiver side. Upon recovering the images from the received channel, the HVS-based image quality metric compares it with the original to provide a quality rating, based on human vision perception. This system illustrates a new yet different approach to quality measurement for a multimedia stream over the mobile wireless interface. Therefore, it is useful in providing a versatile platform for performing media protection research and analysis. For example, using the system to test the effectiveness of a protective protocol for the physical structure of the data, the image quality metric provides an efficient way of representing the effectiveness of the protocol to protect image quality.

This work concentrates on system development. Both the UTRA/3G test bed module and the HVS-based image quality metric have been built and tested extensively. Various calibration tests that have been done are not included in this thesis as they are of little relation to the actual methodology of the test bed. The result presented in Chapters 8 and 9 has effectively verified the various system functionalities by illustrating working results of multiple varied parameters of the UTRA/3G test bed module and the various functionalities of the image quality metric.

In Chapter 8, the system has successfully shown the emulated 3G condition is free of image dependency and is able to process any type of image. Together with this, the results of the image quality metric clearly illustrate HVS-based quality analysis is in working order. It effectively analyzes image fidelity and weighted error depending on attention importance of the image area. The integration of both modules enabled strong coupling where the inter-

processing of the 3G data and image quality are carried out seamlessly to give an overall system for media analysis, as tested and presented in Chapter 9. A seamless 3G multimedia quality analysis testing platform is constructed and analysis of degradation of visual multimedia content in terms of human oriented perception has been performed. Presented in this thesis is an ergonomic method using the human visual properties, with favorable results as backing. The novelty of this work builds on the successfully showing of another method of analyzing visual multimedia degradation over high bandwidth mobile interface of 3G/UMTS, as against QoS, physical data measurements or even image level physical data measurements. As shown in Chapter 9, image difference rates of environmental parameter controlled error are being tested to produce HVS domain quantity quantification results. The results deliver a non-linear correlation with image level physical data measurement as obtained in Chapter 8. While producing a significantly different outcome, the IPQR results demonstrate consistency with background theory and deliver a consistent system of quality measurement. The novelty of this work is fulfilled.

Using this 3G test bed that incorporates HVS correlative error measuring technique, a much more accurate and effective quantification of error impact on the visual properties in multimedia contents are produced. It will prove extremely useful by applying the concept developed in this work to other related topics, for example, development of dynamic multimedia protection techniques where protection of visual contents is of prime importance. This is apparent, when considering that the purpose of multimedia protection is to minimize user perception of quality losses.

While verification is shown by logically compare system results with expected outcome from the design, validation is the other process of most system development projects. The author has to report that proper validation has not been fully and extensively done, due to limited time and the absence of resources. The UTRA/3G test bed can be validated in accordance to 3G standards by comparing it to a known test bed or subject it to a specifically designed test that is approved by 3G or a related telecommunication body. The image quality metric can be properly validated by either comparing it to the system documented by [62] or evaluating it with a subjective human observation test as described in [42]. This process produces objective data for close analysis as compared to subjective analysis provided in this thesis. Unfortunately, both of these options are not within the resource boundaries of the author.

Although useful on its own, this test bed is built as the foundation of an extendable system. Three main areas exist for extending the test bed, as described below.

- *Extension to channel condition simulator.* The ADS channel condition simulator component used in the test bed can be replaced with a custom Matlab module. This extension should provide a more controllable channel condition simulator, relative to the rigid environment of ADS. Two shortcomings of the ADS component, as mentioned in section 8.1.2 and 8.1.3, should also be addressed in this new development. Addition of advance radio channel analytical models should also be considered, to more accurately model behaviors of 3G physical channels. An example architecture for this custom component is presented in the hardware experiment of [75].

- *Extension to traffic modeling.* This option extends the test bed to cover network and data link levels of 3G/UMTS, by incorporating the present system with the modeling of UMTS network behavior. The progress to date has been on the physical layer infrastructure, where the next step is to consider the likely network condition to which the data stream is subjected. Two modeling scenarios within immediate consideration are the UMTS network level services traffic and the inter-network traffic volume which arise from connection with HiperLAN2. The OPNET package is a favorable implementation tool, where mock traffic sources are introduced with the primary source at the network level.

- *Extension to the HVS based quality metric.* This extension requires inclusion of temporal consideration between images together with spatial channels. The image importance area can be better determined by considering the temporal changes between two images. By taking into account motion factors between images, this extension feature enables the test bed to better measure quality of video sequences as a series of images.

The potential application of the final system is for it to be used as a base system and further developed into a dynamic media quality adaptation protocol and deployment system. This system can also be used for routing multi-media service components over rapidly changing

wireless channel conditions that greatly impair available channel traffic capacity. Designed to be versatile and having a different approach to quality quantification, the system is useable in many situations.

Overall, the implemented test bed is working and the result provided is within expectations. Reflecting on the objectives defined in the introduction, the conclusion can be drawn that the aims of the work have been achieved and the objective of the work has been satisfactorily completed.

Bibliography

[1]   G. Eneroth, G. Fodor, G. Leijonhufvud, A. Racz, and I. Szabo, "Applying ATM/AAL2 as a Switching Technology in Third-Generation Mobile Access Networks," in *IEEE Communmications Magazine*, vol. 37, 1999, pp. 112-123.

[2]   M. Zeng, A. Annamalai, and V. K. Bhargava, "Recent Advances in Cellular Wireless Communications," in *IEEE Communications Magazine*, vol. 37, 1999, pp. 128-138.

[3]   J. F. Huber, D. Weiler, and H. Brand, "UMTS, the Mobile Multimedia Vision for IMT-2000: A Focus on Standardization," in *IEEE Communications Magazine*, vol. 38, 2000, pp. 129-136.

[4]   V. Sundaramurthy and J. Cavallaro, "A Software Simulation Testbed for Third Generation CDMA Wireless Systems," presented at IEEE Conference on Signals, Systems and Computers, 2, pp. 1680-1684, 1999.

[5]   Y. Mohasseb and M. P. Fitz, "A 3D Spatio-Temporal Simulation Model for Wireless Channels," presented at IEEE International Conference on Communications, 2001., 6, pp. 1711-1717, 2001.

[6]   Q. Zhang, W. Zhu, and Y. Zhang, "Network-adaptive Scalable Video Streaming Over 3G Wireless Network," *Proceedings of the International conference on Image Processing 2001*, vol. 3, pp. 579-582, 2001.

[7]   M. Patzold, U. Killat, Y. Li, and F. Laue, "Modeling, Analysis, and simulation of Nonfrequency-Selective Mobile Radio Channels with Asymmetrical Doppler Power Spectral Density Shapes," *IEEE Transactions on Vehicular Technology*, vol. 46, pp. 494-507, 1997.

[8] K. Tan and T. Wysocki, "A 7 rays Empirical-based Model of an indoor Microwave Wirelss Mobile Channel with Randomized Distortions," presented at IEEE 47th Vehicular Technology Conference, 2, pp. 1128-1132, 1997.

[9] G. Boggia and P. Camarda, "Modeling Dynamic Channel Allocation in Multicellular Communication Networks," *IEEE Journal on Selected Areas in Communications*, vol. 19, pp. 2233-2242, 2001.

[10] D. Grace, T. C. Tozer, and G. Burr, "Simulation of a Wireless Communications Network which Employs Distributed Dynamic Channel Assignment," presented at International Conference on SIMULATION, Conf. Publ. No. 457., pp. 432-437, 1998.

[11] 3GPP, "Spreading and modulation (FDD)," 3GPP, Volbonne, Technical Specification TS 25.213 v4.2.0, 2001.

[12] 3GPP, "Physical layer - General description," 3GPP, Volbonne, Technical Specification TS 25.201 v4.1.0, 2001.

[13] R. Koodli and M. Puuskari, "Supporting Packet-Data QoS in Next-Generation Cellular Networks," in *IEEE Communications Magazine*, vol. 39, 2001, pp. 180-188.

[14] T. Warabino, S. Ota, D. Morikawa, and M. Ohshi, "Video Transcoding Proxy for 3Gwireless Mobile Internet Access," in *IEEE Communications Magazine*, vol. 38, 2000, pp. 66-71.

[15] ITU-T, "Framework Recommendation for Multimedia Services," Audiovisual Services 2001.

[16] 3GPP, "QoS Concept and Architecture," Volbonne, Technical Specification TS 23.107 V5.0.0, 2001.

[17] Nortel Networks., "QoS Performance Requirements for UMTS," 3GPP, Copenhagen 1999.

[18] S. Worrall, A. H. Sadka, P. Seeney, and A. M. Kondoz, "Prioritisation of Data Partitioned MPEG-4 Video Over Mobile Networks," *ETT-European Transactions on Telecommunications*, vol. 12, 2001.

[19] W. Schonfeld, R. Steinmetz, N. Berier, and L. Wolf, "QoS in Mobile Multimedia Networks," presented at Proceedings of International Conference on Communication 2000, 1, pp. 791-796, 2000.

[20] R. Fantacci and S. Nannicini, "Multiple Access Protocol for Integration of Variable Bit Rate Multimedia Traffic in UMTS/IMT-2000 Based on Wideband CDMA," *IEEE Journal on Selected Areas in Communications*, vol. 18, pp. 1441-1454, 2000.

[21] Q. Zhang, W. Zhu, and Y. Zhang, "QoS-Adaptive Multimedia Streaming over 3G Wireless Channels," presented at Second International Symposium on Mobile Multimedia Systems & Applications (MMSIA), Delft, Netherlands., 2000.

[22] L. Hanzo, C. H. Wong, and P. Cherriman, "Channel-Adaptive Wideband Wireless Video Telephony," in *IEEE Signal Processing Magazine*, vol. 17, 2000, pp. 10-30.

[23] D. Wu, Y. T. Hou, and Y. Zhang, "Scalable Video Coding and Transport over Broad-Band Wireless Networks," *Proceedings of The IEEE*, vol. 89, pp. 6-20, 2001.

[24] ETSI, "Broadband Radio Access Networks (BRAN); HIPERLAN Type 2; TS 101 493-1,", 2000.

[25] M. Johnsson, "HiperLAN/2 - The Broadband Radio Transmission Technology Operating in the 5GHz Frequency Band," HiperLAN/2 Global Forum 1999.

[26] P. Chaudhury, W. Mohr, and S. Onoe, "The 3GPP Proposal for IMT-2000," *IEEE Communications Magazine*, pp. 72-81, 1999.

[27]   K. Yen and K. Hanzo, "Third-Generation Wireless Systems," in *Mobile Radio Communications 2nd edition*, R. H. Steele, Lajos., Ed.: John Wiley & Son LTD, 1999, pp. 897-963.

[28]   W. Stalling, *Data & Computer Communications*, 6th ed. New Jersey: Prentice Hall, 2000.

[29]   V. K. Garg and O. T. W. Yu, "Integrated QoS Support in 3G UMTS Networks," presented at Wireless Communications and Networking Conference 2002, 3, pp. 1187-1192, 2000.

[30]   3GPP, "Network Architecture," 3GPP, Volbonne, Technical Specification TS 25.212 v4.2.0, 2001.

[31]   M. Zeng, A. Annamalai, and V. K. Bhargava, "Harmonization of Global Third-Generation Mobile Systems," in *IEEE Communications Magazine*, vol. 38, 2000, pp. 94-104.

[32]   T. Ojanpera, "WCDMA," in *Third Generation Mobile Communication Systems*, R. Prasad, W. Mohr, and W. Konhauser, Eds. Boston: Artech House, 2000, pp. 73-90.

[33]   3GPP, "Spreading and modulation (TDD)," 3GPP, Volbonne, Technical Specification TS 25.223 v4.3.0, 2001.

[34]   R. N. Williams, "A Painless Guide to CRC Error Detection Algorithms," vol. 2002: University of Adelaide, 1993.

[35]   3GPP, "Multiplexing and channel coding (FDD)," 3GPP, Volbonne, Technical Specification TS 25.212 v4.2.0, 2001.

[36]   J. G. Proakis, *Digital Communications*, 4th ed. Boston: McGraw-Hill, 2001.

[37]   A. Burr, *Modulation and Coding: for Wireless Communications*. Harlow: Prentice Hall, 2001.

[38]   G. L. Stuber, "Modulation Methods," in *Mobile Communications Handbook*, J. D. Gibson, Ed., 2nd ed: CRC Press, 1999, pp. 16-1:16-14.

[39]   D. K. Imbeni, Magnus., "Quality of Service Management of Mixed Services in WCDMA," presented at IEEE VTS-Fall VTC 2000 52nd, 2, pp. 565-572, 2000.

[40]   S. Winkler, A. Charma, and D. McNally, "perceptual Video Quality and Blockiness Metrics for Multimedia Streaming Applications," presented at Procedings of the 4th International Symposium on Wireless Personal Multimedia communications, Aalborg, Denmark, pp. 553-556, 2001.

[41]   "Methodology for the subjective assessment of the quality of television pictures.," in *ITU-R Recommendation 500-6*, 1994.

[42]   W. Osberger, "Perceptual Vision Models for Picture Quality Assessment and Compression Applications," PHD Dissertation. Brisbane: Queensland University of Technology, 1999.

[43]   E. Peli, "Contrast of Slightly Complex Patterns: Computing the Perceived Contrast of Gabor Patches," presented at Proceedings of the SPIE: Human Vision and Electronic Imaging, San Jose, USA, 2657, pp. 166-174, 1996.

[44]   A. B. Watson, "The Cortex Transform: Rapid Computation of Simulated Neural Images," *Computer Vision, Graphics and Image Processing*, vol. 39, pp. 311-327, 1987.

[45]   A. B. Watson and J. A. Solomon, "A Model of Visual Contrast Gain Control and Pattern Masking," *Journal of the Optical Society of America A*, vol. 14, pp. 2379-2391, 1997.

[46]   A. B. Watson, "Toward a Perceptual Video Quality Metric," presented at SPIE Conference on Human Vision and Electronic Imaging III, San Jose, 3299, pp. 139-147, 1998.

[47]   R. C. Gonzalez and R. E. Woods, *Digital Image Processing*. Reading: Addison-Wesley, 1992.

[48]   E. Peli, "Contrast in complex images," *Journal of the Optical Society of America A*, vol. 7, pp. 2032-2040, 1990.

[49]   J. M. Foley and G. M. Boynton, "A New Model of Human Luminance Pattern Vision Mechanisms: analysis of the effects of pattern orientation, spatial phase and temporal frequency.," presented at Proceedings of the SPIE - Computational Vision Based on Neurobiology, 2054, pp. 32-42, 1994.

[50]   S. Daly, "The Visible Difference Predictor: An Algorithm for the Assessment of Image Fidelity," in *Digital Images and Huma Vision*, A. B. Watson, Ed. Cambridge: MIT Press, 1993, pp. 179-206.

[51]   S. A. Karunasekera and N. G. Kingsbury, "Perceptual characterisation of Images Degraded by Blur and Noise: experiments.," *Journal of the Optical Society of America A*, vol. 13, pp. 1166-1177, 1996.

[52]   J. Lubin, "The Use of Psychophysical Data and Models in the Analysis of Display System Performance," in *Digital Images and Human Vision*, A. B. Watson, Ed. Cambridge,: MIT Press, 1993, pp. 163-178.

[53]   P. C. Teo and D. J. Heeger, "Perceptual Image Distortion," *Proceedings of the SPIE - Human Vision, Visual Processing and Digital Disply V,*, vol. 2179, pp. 127-141, 1994.

[54]   W. Osberger and A. Maeder, "Automatic Identification of Perceptually Important Regions in an Image," presented at 14th International Conference on Pattern Recognition, Brisbane, Australia., pp. 701-704, 1998.

[55]   V. I. S. R. Group., "Sarnoff JND Vision Model Algorithm Description and Testing," Sarnoff Corporation, Princeton 1997.

[56]   A. B. Watson and L. Kreslake, "Measurement of Visual Impairment Scales for Digital Video," presented at Human Vision and Electronic IMaging VI, San Jose, 2, 2001.

[57]   E. Peli, L. E. Arend, and G. M. Young, "Contrast Sensitivity to Patch Stimuli: Effects of Spatial Bandwidth and Temporal Presentation.," *Spatial Vision*, vol. 7, pp. 1-14, 1993.

[58]   O. Luntinen, J. Rovamo, and R. Nasanen, "Modelling the increase of Contrast Sensitivity with Granting Area and Exposure Time.," *Vision Research*, vol. 35, pp. 2339-2346, 1995.

[59]   O. Luntinen, J. Rovamo, and R. Nasanen, "The Effects of Granting Area and Spatial Frequency on Contrast Sensitivity as a Function of LIght Level," *Vision Research*, vol. 33, pp. 2065-2072, 1993.

[60]   O. Luntinen, J. Rovamo, and R. Nasanen, "Modelling the Dependence of Contrast Sensitivity on Grating Area and Spatial Frequency," *Vision Research*, vol. 33, pp. 2773-2788, 1993.

[61]   O. Luntinen, J. Rovamo, and R. Nasanen, "Modelling Contrast Sensitivity as a Function of Retinal Illuminance and Grating Area," *Vision Research*, vol. 34, pp. 1301-1314, 1994.

[62]   W. Osberger, "Automatic detection of regions of interest in complex video sequences," presented at Human Vision and Electronic Imaging VI, 4299, pp. 261-372, 2001.

[63]   A. Maeder, "Human Understanding Limits in Visualization," in *Spatial Computing: Issues in Vision, Multimedia and Visualization Technologies*, T. Caelli, P. Lam, and H. Bunke, Eds., 1997, pp. 229-238.

[64]   W. Osberger, "Assessing the quality of compressed pictures using a perceptual model," presented at 14th SMPTE Techincal Conference, Pasadena, pp. 495-508, 1998.

[65]   I. Sommerville, *Software Engineering*, 5th ed: Addison-Wesley Publishing Company, 1996.

[66]   3GPP, "Radio Link control (RLC) Protocol Specification," 3GPP, Volbonne, Technical Specification TS 25.322 v5.0.0, 2001.

[67]   3GPP, "Packet Data Convergence Protocol (PDCP) Specification," 3GPP, Volbonne, Technical Specification TS 25.323 v5.0.0, 2001.

[68]   J. Lundsjo and M. Rinne, "UTRA Trnasport Control Function," in *Third Generation Mobile Communication Systems*, R. Prasad, W. Mohr, and W. Konhauser, Eds. Boston: Artech House, 2000, pp. 73-90.

[69]   T. Rappaport, *Wireless Communication Principles & Practice*, 2nd ed. London: Prentice Hall, 2002.

[70]   J. G. Proakis and M. Salehi, *Communication Systems Engineering*. Englewood Cliffs: Prentice Hall, 1994.

[71]   I. Burlin, M. Fellbrink, S. Forsgren, J. Mannby, and M. Sundstrom, "Evaluation of CRTP and ROCCO," Department of Computer Science and Electrical Engineering, Lulea University of Technology 2000.

[72]   The Math Works Inc., "MATLAB," 6.1.0.450 ed: The Math Works Inc., 2001.

[73]   OPNET Technologies Inc., "OPNET Network Modeler," 2001 ed. Bethesda: OPNET Technologies Inc., 2001.

[74]   Agilent Technologies., "Advanced Design System 2001." Palo Alto: Agilent Technologies, 2001.

[75]   J. Arponen, J. Eldstahl, and A. Nasman, "FDD Demonstrator," in *Third Generation Mobile Communication Systems*, R. Prasad, W. Mohr, and W. Konhauser, Eds. Boston: Artech House, 2000, pp. 73-90.